

**EFFECT OF ORGANO-MODIFIED CLAY
ADDITION ON PROPERTIES OF POLYHYDROXY
BUTYRATE HOMO AND COPOLYMERS
NANOCOMPOSITE FILMS**

**A Thesis Submitted to
the Graduate School of Engineering and Sciences of
İzmir Institute of Technology
in Partial Fulfillment of the Requirements for the Degree of**

MASTER OF SCIENCE

in Chemical Engineering

**by
Okan AKIN**

**July 2012
İZMİR**

We approve the thesis of **Okan AKIN**

Examining Committee Members:

Prof. Dr. Funda TIHMINLIOĞLU

Department of Chemical Engineering, İzmir Institute of Technology

Prof. Dr. Devrim BALKÖSE

Department of Chemical Engineering, İzmir Institute of Technology

Assoc. Prof. Dr. Mustafa M. DEMİR

Department of Chemistry, İzmir Institute of Technology

9 July 2012

Prof. Dr. Funda TIHMINLIOĞLU

Supervisor, Department of Chemical Engineering
İzmir Institute of Technology

Prof. Dr. Mehmet POLAT

Head of the Department of Chemical Engineering

Prof. Dr. R. Tuğrul SENGER

Dean of the Graduate School of
Engineering and Sciences

ACKNOWLEDGMENT

Firstly, I would like to express my gratitude to my supervisor Prof. Dr. Funda Tihmınlıođlu for her supervision, invaluable guidance, encouragement and support throughout this study. I am also grateful to Prof. Dr. Devrim Balköse for her valuable comments and suggestions.

I am thankful to Prof. Dr. Ahmet Yemeniciođlu for giving access to texture analyzer for tensile tests and to Prof. Metin Tanođlu for giving access to Composites Center. Research assistant İskender Arcan is also acknowledged for his helps in my tensile tests. I am also thankful to Prof. Dr. Orhan Öztürk for X-Ray Diffraction analyses.

The financial support of Turkish Scientific Technical Research Organization (108M335) is gratefully acknowledged. I also present my deepest thanks to Southern Clay Products for supplying the nanoclay samples.

I express many thanks to my workmates, Hale Ođuzlu, Emre Kılıç, Ekrem Özer, Seda Güneş, and Sedef Tamburacı for their friendship and support during my thesis period. I am also grateful to Dr. Burcu Alp for her help in the laboratory and suggestions in thermal analyses.

Finally, my deepest thanks go to my family. I am grateful for their endless support. I would like to express special thanks to my parents, Aydın Akın, Aysel Akın for all their motivation, inspiration and cooperation throughout not only in this study and also in my social life. I extent my sincere appreciation to my brother Ozan Akın for his support and encouragements during my thesis study.

ABSTRACT

EFFECT OF ORGANO-MODIFIED CLAY ADDITION ON PROPERTIES OF POLYHYDROXY BUTYRATE HOMO AND COPOLYMERS NANOCOMPOSITE FILMS

As an alternative to conventional non-degradable food packaging plastics, bionanocomposites, based on bacterial biodegradable thermoplastic polyesters, poly(hydroxybutyrate) (PHB) and poly(hydroxybutyrate-covalerate) (PHBHV) polymers incorporated with commercial organomodified monmorillonite (OMMT) were prepared by solution intercalation and melt-mixing techniques. The enhancements in barrier, mechanical, thermal, surface and optical properties of resulting nanocomposite films were evaluated as effected by OMMT concentration and preparation method.

The degree of dispersion of layered silicates into polymer matrix was evaluated by X-Ray diffraction (XRD) analyses. The best level of dispersion was obtained in nanocomposites that contain 1% w/w of OMMT. However, intercalated structure was observed at higher amount of clay loaded composites. The fine delamination of OMMT in PHB and PHBHV matrix was found to be responsible for the improvements in water vapor barrier performance since more tortuous path formed for permeation of water vapor. Moreover, enhancement in mechanical and thermal properties was highly depending on the dispersion level of layered silicates which is in good accordance with structural analyses. Addition of 2% w/w of OMMT reduced the WVP of virgin films by 41.1%. Meanwhile, improvements were less significant at higher amount of clay loaded samples due to weak interaction between polymer and layered silicates. Moreover, significant improvements in mechanical properties including doubled tensile strength and 69% increase in strain at break were obtained for 2% w/w of OMMT incorporated PHB composites. In addition, significant enhancement in thermal stability, which is the major drawback of PHB films, was obtained in nanocomposites, decomposition temperature increased by 10 °C compared to pristine polymers. Moreover, addition of layered silicates into polymer matrix at low content resulted in increase in erosion rate which makes nanocomposites more eco-friendly promising alternative to conventional barrier packaging systems.

ÖZET

ORGANO MODİFİYE KİL KATKISININ POLİHİDROKSİ BÜTARAT HOMO VE KOPOLİMER NANOKOMPOZİT FİMLERİN ÖZELLİKLERİ ÜZERİNDEKİ ETKİSİ

Polihidroksibütirat (PHB) ve Polihidroksibütirat-cohidroksivalerat (PHBHV) nanokompozit filmler, mevcut geleneksel gıda ambalaj uygulamalarında kullanılan filmlere alternatif olarak çözücü interkalasyon ve eriyik karıştırma yöntemleri ile hazırlandı. Bu çalışmada organomodifiye tabakalı silikat nanokil (OMTS) miktarının, ve nanokompozit hazırlama metodunun etkisi, yapısal, bariyer mekanik termal ve optik özellikleri incelenerek belirendi. Analizler sonucu, düşük oranda kil katkıli nanokompozit filmlerde, kil tabakaların polimer zincirleri içindeki dağılımın yüksek oranda kil katkıli örneklere göre daha iyi olduğu gözlemlendi. Polimer zincirlerindeki kil dağılımın yapısına bağlı olarak, nanokompozitlerin mekanik ve bariyer özelliklerinde ki artış eksfoliyeye yapıda, interkale yapıya göre daha fazla olduğu bulundu. Bu durum eksfoliyeye yapıdaki kil polimer etkileşiminin daha güçlü olmasından kaynaklanmaktadır. Silikat tabakaların etkili biçimde açılması sonucu artan dolambaçlı difüzyon yoluna bağlı olarak nanokompozit filmlerin su buharı bariyer özelliği geliştirilmiştir. Ağırlıkça 2% OMTS içeren PHB filmin su buharı geçirgenlik değeri katkısız PHB film ile karşılaştırıldığında, % 41 oranında azalma gözlemlenmiştir. Ayrıca, nanokompozitlerin mekanik özellikler katkısız PHB filmler ile karşılaştırıldığında çekme mukavemeti 2 kat, kopmadaki uzama miktarı da 69% oranında geliştirilmiştir. Buna ilaveten, kil ilavesi ile PHB'nin en önemli problemlerinden biri olan termal bozunma sıcaklığındaki 10 °C artış ile önemli oranda iyileştirilmiştir. Düşük oranda kil ilavesi ile biyobozunma hızını artmış, böylece mevcut gıda paketlerine alternatif daha çevre dostu filmler elde edilmiştir.

TABLE OF CONTENTS

LIST OF FIGURES.....	ix
LIST OF TABLES.....	xii
CHAPTER 1. INTRODUCTION.....	1
CHAPTER 2. BIODEGRADABLE POLYMERS.....	4
2.1. Classification of Biodegradable Polymer.....	6
2.1.1. Polyhydroxyalkonates (PHAs).....	8
2.1.2. Production of Polyhydroxyalkonates (PHAs).....	9
2.1.3. Chemical Properties of Polyhydroxyalkanotes.....	11
2.1.4. Physical Properties of Polyhydroxyalkonates.....	11
2.1.5. Solubility of PHAs.....	12
2.1.6. Barrier Properties of PHAs.....	14
2.1.7. Thermal Properties of Polyhydroxyalkonates (PHAs).....	18
2.1.7.1. Crystallization Kinetic Models.....	21
2.1.8. Mechanical Properties of PHAs.....	23
2.1.9 Biodegradability of PHAs.....	24
CHAPTER 3. POLYMER NANOCPOPOSITES.....	27
3.1. Nanoparticles.....	28
3.1.1. Montmorillonite Nanoclays.....	29
3.2. Polymer Layered Silicate Nanocomposites.....	32
3.3. Characterization of Polymer Layered Nanocomposite Films.....	33
3.4. Preparation Methods of PLS Nanocomposites.....	35
3.4.1. Solution Intercalation.....	36
3.4.2. In Situ Intercalative Polymerization.....	37
3.4.3. The Melt Intercalation Method.....	38
3.5. Polyhydroxyalkonates (PHAs) Layered Silicates Nanocomposites (PHALSN).....	38
3.5.1. Barrier Properties of Layered Silicate Nanocomposites.....	38

3.5.2. Mechanical Properties of Layered Silicate Nanocomposites.....	45
3.5.3. Thermal Properties of Layered Silicate Nanocomposite Films....	46
CHAPTER 4. EXPERIMENTAL STUDY.....	50
4.1. Materials.....	50
4.2. Preparation of PHB and PHBHV Nanocomposite Films.....	50
4.3. Determination of Film Thickness.....	52
4.4. Fourier Transform Infrared (FTIR) Analysis of PHB and PHBHV nanocomposite films.....	52
4.5. X-Ray Diffraction (XRD) Analysis of PHB-PHBHV Nanocomposite Films.....	53
4.6. Water Vapor Permeability Measurements of PHB and PHBHV Nanocomposite Films.....	53
4.7. Mechanical Property Determination of PHB-PHBHV Nanocomposite Films.....	54
4.8. Thermal Stability of PHB-PHBHV Nanocomposite Films.....	55
4.8.1. Isothermal Degradation Study of PHB and PHBHV Nanocomposite Film.....	55
4.9. Non-Isothermal Crystallization Study of PHB and PHBHV Nanocomposite Films.....	55
4.10. Contact Angle Measurements of PHB-PHBHV Nanocomposite Films.....	56
4.11. Color Measurements of PHB-PHBHV Nanocomposite Films.....	56
CHAPTER 5. RESULTS AND DISCUSSION.....	58
5.1. Structural Analysis.....	58
5.1.1. X-Ray Diffraction (XRD) Analysis.....	58
5.1.2. Fourier Transform Infrared (FTIR) Analysis of PHB and PHBHV nanocomposites.....	61
5.2. Water Vapor Permeability of PHB and PHBHV Nanocomposite Films.....	65
5.2.1. Temperature Effect in WVPs of PHB-S and PHBHV-S Nanocomposites.....	70
5.3. Mechanical Properties of PHB and PHBHV Nanocomposites.....	74

5.4. Thermal Characterization of PHB and PHBHV Nanocomposites.....	78
5.4.1. Thermogravimetric Analysis (TGA).....	78
5.4.1.1. Isothermal Degradation of PHB-P and PHBHV-P Nanocomposites.....	82
5.4.2. Differential Scanning Calorimetry (DSC) Analysis of PHB and PHBHV Nanocomposites.....	85
5.4.3. Non-isothermal Crystallization Study of PHB-S Nanocomposites.....	90
5.4.3.1. Primary Nucleation Kinetics by Avrami Jeziorny, Ozawa and Lui Mo Models for Nonisothermal Crystallization.....	90
5.5. Contact Angle Measurements of PHB and PHBHV Nanocomposite Films.....	95
5.6. Biodegradation of PHB-P Nanocomposite Films.....	96
5.7. Color Changes in PHB-S and PHBHV-S Nanocomposite Film.....	100
 CHAPTER 6. CONCLUSION.....	 102
 REFERENCES.....	 105
 APPENDICES	
APPENDIX A. CHARACTERIZATION OF PHB AND PHBHV NANOCOMPOSITE FILMS.....	113
APPENDIX B. THERMAL ANALYSES OF PHB AND PHBHV NANOCOMPOSITE FILMS.....	129
APPENDIX C. CRYSTALLIZATION KINETIC OF PHB NANOCOMPOSITE FILMS.....	134

LIST OF FIGURES

<u>Figure</u>	<u>Page</u>
Figure 2.1. Partially bio-based plastics and their biodegradability.....	4
Figure 2.2. Life Cycle of biodegradable polymers	5
Figure 2.3. Biodegradable polymers and their origin based on method of production ...	7
Figure 2.4. Bacterial cell containing PHA granules imaged by scanning electron microscopy	8
Figure 2.5. A schematic representation of the biosynthesis of PHA in bacteria	10
Figure 2.6. Molecular structure of polyhydroxyalkonates (PHAs).	11
Figure 2.7. Relative water vapor transmission rates of polymers.....	16
Figure 2.8. Oxygen transmission rates of polymers	18
Figure 3.1. Structure of MMT	30
Figure 3.2. Surface modification of the aluminosilicate surface.	31
Figure 3.3. Schematic illustration of three different types of thermodynamically achievable polymer/clay nanocomposites	33
Figure 3.4. (a) EAXD patterns, and (b) TEM images of three different types of nanocomposites.....	34
Figure 3.5. FTIR spectra of various commercial clays	35
Figure 3.6. Different methods in preparation of layered silicate polymer nanocomposites.....	36
Figure 3.7. Free swelling factors, S(Black bar), and interplaner distance, d_{001} (Grey bar) determined for 2MBHT nanoclay- based suspensions in various solvents	37
Figure 3.8. Representation of the polymerization from the surface of aluminasilicate layer.....	37
Figure 3.9. a) Regular oriented b) Random oriented silicate layers in polymer matrix .	39
Figure 3.10. Relative permeability predictions based on Nielsen Model as a function of aspect ratio at different layered silicate volume fraction.....	42
Figure 4.1. Representation of water vapor transmission measurement	54
Figure 5.1. XRD Pattern of Cloisite 10A.....	59
Figure 5.2. XRD Patterns of PHB-S nanocomposites at different Cloisite 10A content	60

Figure 5.3. XRD Patterns of PHBHV-S nanocomposites at different Cloisite 10A, content	61
Figure 5.4. FTIR spectra of Cloisite 10A	62
Figure 5.5. FTIR spectra of PHB-S and its nanocomposites at different amount of Cloisite 10A in 1300-400 cm ⁻¹ region.....	63
Figure 5.6. FTIR spectra of PHB-S and its nanocomposites at different amount of Cloisite 10A in 4000-2000 cm ⁻¹ region.....	64
Figure 5.7. FTIR spectra of PHBHV-S and its nanocomposites at different amount of Cloisite 10A in 1500-400 cm ⁻¹ region	64
Figure 5.8. Water vapor permeabilities of PHB-S nanocomposites films at different clay contents.....	67
Figure 5.9. Water vapor permeabilities of PHBHV-S nanocomposites films at different clay contents	67
Figure 5.10. Water vapor permeabilities of PHBHV-P nanocomposites films at different clay contents	68
Figure 5.11. Water vapor permeabilities of PHB-P nanocomposites films at different clay contents.....	68
Figure 5.12. Permeability models fitted to experimental water vapor permeability of PHB-S nanocomposite films.....	70
Figure 5.13. Temperature dependence of WVP of PHB-S nanocomposite films	72
Figure 5.14. Temperature dependence of WVPs of PHBHV-S nanocomposite films ...	73
Figure 5.15. Sample stress-strain curves of PHBHV-S nanocomposites	75
Figure 5.16. Young's Modulus of PHB and PHBHV nanocomposites.....	76
Figure 5.17. Strain of PHB and PHBHV nanocomposites	77
Figure 5.18. Tensile strength (MPa) of PHB and PHBHV nanocomposites.....	77
Figure 5.19. TGA curves of PHB-S nanocomposite films	79
Figure 5.20. TGA curve of Cloisite 10A	80
Figure 5.21. Dependence of “k” on Cloisite 10A content and temperature of isothermal degradation of PHB-P nanocomposites	84
Figure 5.22. Dependence of “k” on Cloisite 10A content and temperature of isothermal degradation of PHBHV-P nanocomposites.....	84
Figure 5.23. First heating run of DCS analysis of PHBHV-P nanocomposites	85
Figure 5.24. Cooling run of DSC analysis of PHBHV-P nanocomposites.....	87
Figure 5.25. Weight remaining of PHB-P nanocomposites in enzymatic degradation ..	97

Figure 5.26. Rate of erosion of PHB-P nanocomposite films	98
Figure 5.27. Scanning electron microscope of PHB-P nanocomposites before and after biodegradation a) PHB-P-N before degradation b) PHB-P-N after degradation, c) PHB-P-1 before degradation d) PHB-P-1 after degradation, e) PHB-P-3 before degradation f) PHB-P-3 after degradation, g) PHB-P-5 before degradation h) PHB-P-5 after degradation, i) PHB-P-7 before degradation j) PHB-P-7 after degradation for 8 weeks.....	99

LIST OF TABLES

<u>Table</u>	<u>Page</u>
Table 2.1. Global production of biodegradable polymers by polymer type, 2000, 2005 and 2010 ('000 tonnes).....	6
Table 2.2. Effect of substrate cost and PHB yield on the production cost	10
Table 2.3. Solubility parameters and distance, ^{ij}R , of various solvents for PHB.....	13
Table 2.4. Water vapor transmission rates through PHB and PHBHV at 30 °C	17
Table 2.5. Oxygen permeability of PHB, PCL and PET at 0%RH and 24°C.....	17
Table 2.6. Thermal properties of PHAs and Polypropylene.....	19
Table 2.7. Melting Temperature (T_m) and crystallization temperature (T_c) of PHB, P(HB-co HV), and PHV	20
Table 2.8. The values of Avrami exponent n and K at different crystal growth shapes.	21
Table 2.9. Avrami Parameters and the values of $T_o(^{\circ}C)$, $T_p(^{\circ}C)$, and $T_i(^{\circ}C)$ at various cooling rates for PHB	23
Table 2.10. Mechanical Properties of PHAs.....	25
Table 3.1. Characteristics of Nanoparticles to Polymers.....	28
Table 3.2. OMMTs and their organic modifiers	31
Table 3.3. Permeability models for nanocomposites	44
Table 4.1. Properties of PHB and PHBHV polymers.....	50
Table 4.2. Properties of Cloisite 10A	50
Table 4.3. Sample codes of prepared films depending on preparation method and Cloisite 10A.....	52
Table 5.1. Slope and R^2 values of Arrhenius plot and WVP Activation energies of PHB-S nanocomposites films.....	72
Table 5.2. Slope and R^2 values of Arrhenius plot and WVP Activation energies of PHB-S nanocomposites films.....	74
Table 5.3. Thermal degradation properties of PHB and PHBHV nanocomposites.....	81
Table 5.4. Values of empirical kinetic triplets obtained by Avrami-Eroffev model	83
Table 5.5. DSC result of PHB and PHBHV nanocomposites	89
Table 5.6. Avrami Jeziorny parameter for PHB-P nanocomposite at different cooling rates	93

Table 5.7. Nonisothermal Crystallization Kinetic Paramaters at Different Degree of Crystallinity	94
Table 5.8. Static contact angles measured for PHB and PHBHV nanocomposites.....	95
Table 5.9. The total color difference (ΔE) and color parameters of prepared PHB-S and PHBHV-S nanocomposites	101

CHAPTER 1

INTRODUCTION

There has been a significant increase in the amount of plastics being used in packaging applications. Today, packaging is the largest application area for plastics and oil based plastics are the main material for the production of packaging materials. Thus, concerns over the persistence of packaging plastic materials in the environment from waste management point of view have increased the research development efforts on both natural and synthetic based biodegradable polymers such as corn zein, chitosan, polylactide (PLA) and polyhydroxyalkanoates (PHAs).

PHAs are a class of biodegradable and biocompatible thermoplastics produced by different types of microorganisms from renewable resources. PHAs, in particular, polyhydroxybutyrate and its copolymers are the most common used, are promising polymers in food packaging applications due to its similar properties to conventional synthetic plastics e.g. polypropylene as a substitute to synthetic ones. However, PHAs suffer from brittleness and poor processing temperature range that limits its application areas (Reddy et al. 2003). In order to overcome these drawbacks various approaches have been used in literature such as by blending with other biodegradable plastics (Nguyen et al. 2010; Zhang and Thomas 2011) and by addition of nanoparticles into a polymer matrix (Xu et al. 2001; Thellen et al. 2005; Oguzlu and Tihminlioglu 2010). Although there are many references to attempts to mix PHB with other polymers with the aim of improving its mechanical properties, unfortunately with only limited success up until now (Garcia-Quesada et al. 2012).

Incorporation of nanoparticles into a polymer matrix such as hydroxyapatite, layered silicates, has attracted considerable attention since addition of only a few percent of nanoparticles to polymers has greatly enhanced polymer properties such as barrier, mechanical and thermal properties by lowering the cost variance compared with other approaches and traditional composites (Platt 2006). In order to improve barrier properties of biodegradable polymer nanocomposites, layered silicates are preferred have potential to improve the barrier resistances of polymers as diffusion path in the polymer matrix increases by incorporation of layered silicates into the polymer (Cornwelle 2009). In most of the polymer nanocomposite studies, montmorillonite is

the most commonly used layered silicate used for its dispersion in nanoscale dimensions in polymer matrix that enhance polymer properties by interaction in atomic level. Therefore, not only barrier properties but also other properties such as mechanical and thermal properties are improved as well. Since the nanocomposite structure depends on the polymer-layered silicate compatibility and on the processing conditions, the enhancement in properties is highly depending on the dispersion of layered silicates in polymer matrix. The dispersion of layered silicates is mainly defined as intercalated or exfoliated structures. Exfoliated structure is the desired one where, interfacial interaction is achieved in nanometer scale. Structure of layered silicates in polymer matrix depends on the nature of the polymer (molecular weight, polarity etc.) and layered silicate (organomodification, etc). Besides, preparation method of polymer nanocomposites is also a key parameter that affects dispersion level of layered silicates in polymer matrix. There are various methods have been studied to prepare PHAs layered silicate nanocomposite films in literature. In situ polymerization (Nguyen and Baird 2006), melt extrusion(Maiti et al. 2007), solvent casting, are the common (Gunaratne and Shanks 2005) methods in preparation of layered silicate nanocomposite polymer films (LSNP) (Botana et al. 2010). Botana et al studied the effect of modified montmorillonite (Cloisite 30B-M) on thermal, mechanical and morphological properties. They concluded that even small amount of Cloisite 30B enhanced mechanical and burning properties of pristine PHB (Botana et al. 2010). Additionally, Lagaron and co workers reported the effect of layered silicate with different type of organomodifiers on barrier performance of PHB-PCL blend nanocomposites. They concluded that, oxygen barrier performance increased tremendously compared with pristine PHB-PCL blend. Moreover, the importance of organomodification was also revealed by testing oxygen transmission rate using various types of modifiers (Lagaron et al. 2008).

Although there are various studies in literature related to Cloisite 20A, 25A and 30B incorporated PHB nanocomposites, to our knowledge there is no study related to Cloisite 10A layered silicate in PHB matrix. Therefore, in this study, Polyhydroxybutyrate (PHB) and Polyhydroxyvalerate (PHBHV) nanocomposite films were prepared using solvent casting and melt extrusion methods by introducing Cloisite 10 A organically modified montmorillonite (OMMT) in polymer matrix. The effects of OMMT amount and valerate content on barrier, mechanical and thermal properties of PHB nanocomposite films were investigated. Temperature dependency of water vapor

permeation in PHB and PHBHV nanocomposite films were also investigated. Moreover, effect of preparation methods on properties of PHB and PHBHV nanocomposite films was also examined.

In conclusion, this thesis report involves six chapters. The background information and related to biodegradable polymer nanocomposites was mentioned in Chapter 1 by giving the aim of this research. Chapter 2 consists of properties of biodegradable polymers and specifically polyhydroxyalkonates (PHAs). Moreover, biodegradable layered silicate nanocomposite films and literature review of PHA nanocomposites were covered in Chapter 3. In Chapter 4, experimental procedure of the polyhydroxyalkonates nanocomposites (PHANCs) preparation method and characterization of PHANCs and measurement methods of barrier, thermal, and mechanical properties were explained. Mechanical, water vapor barrier and thermal performance of OMMT loaded PHB and PHBHV were discussed by considering the effect of OMMT and valerate amount and preparation techniques in Chapter 5. Finally, conclusions of this study were given in Chapter 6.

CHAPTER 2

BIODEGRADABLE POLYMERS

Due to the environmental concerns and apparent increase in the prices of oil based polymers, the attention has been focused on the bio-based plastics for last few years. It is well known that the limited source of fossil fuels and the oblique effect of oil based polymers to climate change drive the governments and companies to find alternatives to crude oil (Shen et al. 2009; Barud et al. 2011). Due to these reasons, there is a need to produce renewable, sources based, environmentally friendly polymeric materials. These polymeric materials should overcome the demands such as not involving the use of toxic or noxious components in their manufacturing, and could allow for composting into naturally occurring degradation products (Okamoto 2005). However, it does not mean that every bio-based polymer is biodegradable, even if it composes into nature by degradation (Figure 2.1).

The definition of biodegradation was made by the scientific community and was legally incorporated into a Standard by the American Society for Testing and Materials (ASTM), under reference ASTM D6400-99, in July 1999 (Platt 2006). Biodegradable plastics are defined as a degradable plastic in which the degradation process starts by action of naturally occurring microorganisms such as bacteria, fungi, and algae (ASTM D6400-99).

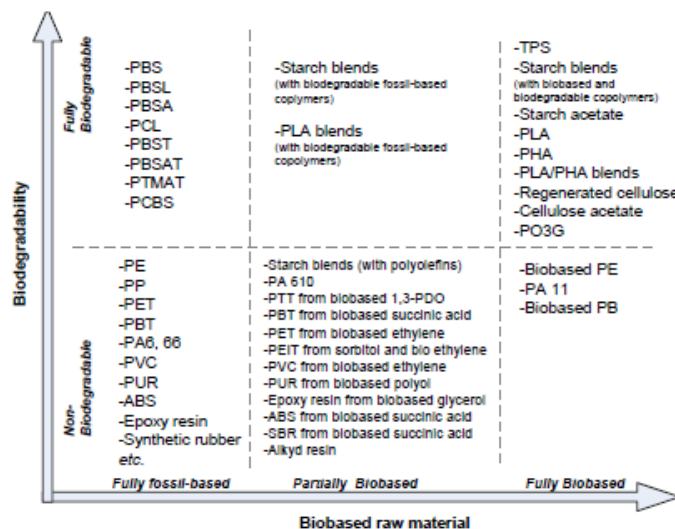


Figure 2.1. Partially bio-based plastics and their biodegradability
(Source : Shen et al. 2009)

The biodegradation process includes conversion of polymer to biomass, water, and CO₂ (Figure 2.2). The speed of biodegradation highly depends on the environmental conditions. For instance, the biodegradation occurs at home or in a supermarket very slowly comprising to composting. In industrial composting process bioplastics are converted into biomass, water and CO₂ in about 6-12 weeks (Siracusa et al. 2008) .

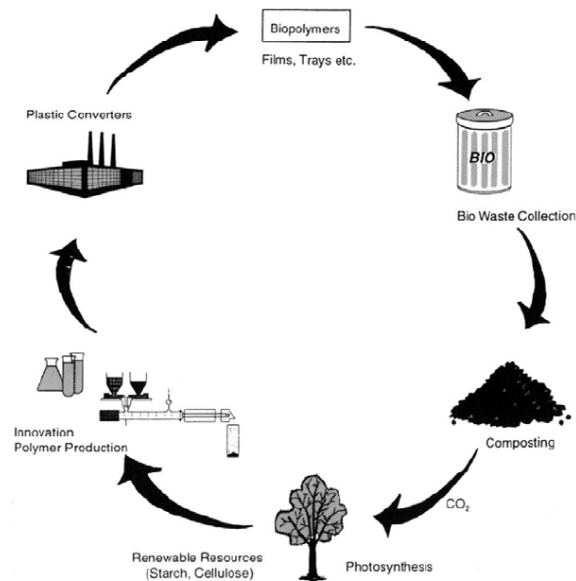


Figure 2.2. Life Cycle of biodegradable polymers
(Source: Siracusa et al. 2008)

Last decade, the market for biodegradable polymers has shown particular growth even though the price of bio-based polymers does not comparable with petrochemical based polymers. However, this situation is slowly changing with a number of major plant expansions (Platt 2006) .

Global production capacity for biodegradable polymers has grown dramatically since the 1990s. In 1990s the production was mainly on a pilot-plant basis. Table 2.1 indicates the global production of biodegradable polymers by polymer type for the years 2000, 2005 and 2010. Although the global biodegradable plastics market tonnage is about 28,000 tonnes in 2000, this number increases up to 94,800 tonnes in 2005, 214,400 tonnes in 2010. For the period of 2000-2005 the annual grow rate of total biodegradable polymer production is 19.8% compared with 55.25% in period of 2000-2010 (Platt 2006) . This trend shows that biodegradable polymers have potential to be used as an alternative to oil based polymers.

Table 2.1. Global production of biodegradable polymers by polymer type, 2000, 2005 and 2010 ('000 tonnes) (Source: Platt 2006)

	2000	2005	2010
Starch	15.5	44.8	89.2
PLA	8.7	35.8	89.5
PHA	0	0.2	2.9
Synthetic	3.9	14.0	32.8
Total	28.1	94.8	214.4

As seen in Table 2.1 starch based polymer has the largest market with 47% compared to PLA and PHAs. Even if the market tonnage of PHAs is low at the moment, PHAs promise increasing demand for the market development when the annual growth rate considered (Platt 2006). The product development and improvement play an important role in the production capacity of biodegradable polymers. Thus, different kinds of material developments covered to enhance the processing performance of biodegradable polymers. For instance, new type of renewable feedstock such as palm oil has been used for manufacture of starch-based biodegradable polymers. Moreover, improvement in fermentation processes decrease the material cost of PHA products by lowering cost feedstock (Siracusa et al. 2008). On the other hand, recent studies have focused on the biodegradable polymer blends and composites by addition of reinforcements such as montmorillonite nanoclay, carbon nanotubes, nanoaluminum oxide, nanotitanium oxide (Koo 2006)

2.1. Classification of Biodegradable Polymers

Due to the environmental concerns and being the realization that the petroleum resources are finite, polymers from renewable sources have been attracting an increasing interest. Polymers derived from renewable sources are classified into three groups as based on their sources (Figure 2.3). Natural polymers such as starch, protein and cellulose; synthetic polymers from bio-derived monomers such as poly(lactic acid) (PLA); and polymers from microbial fermentation such as polyhydroxyalkonates (Yu 2009).

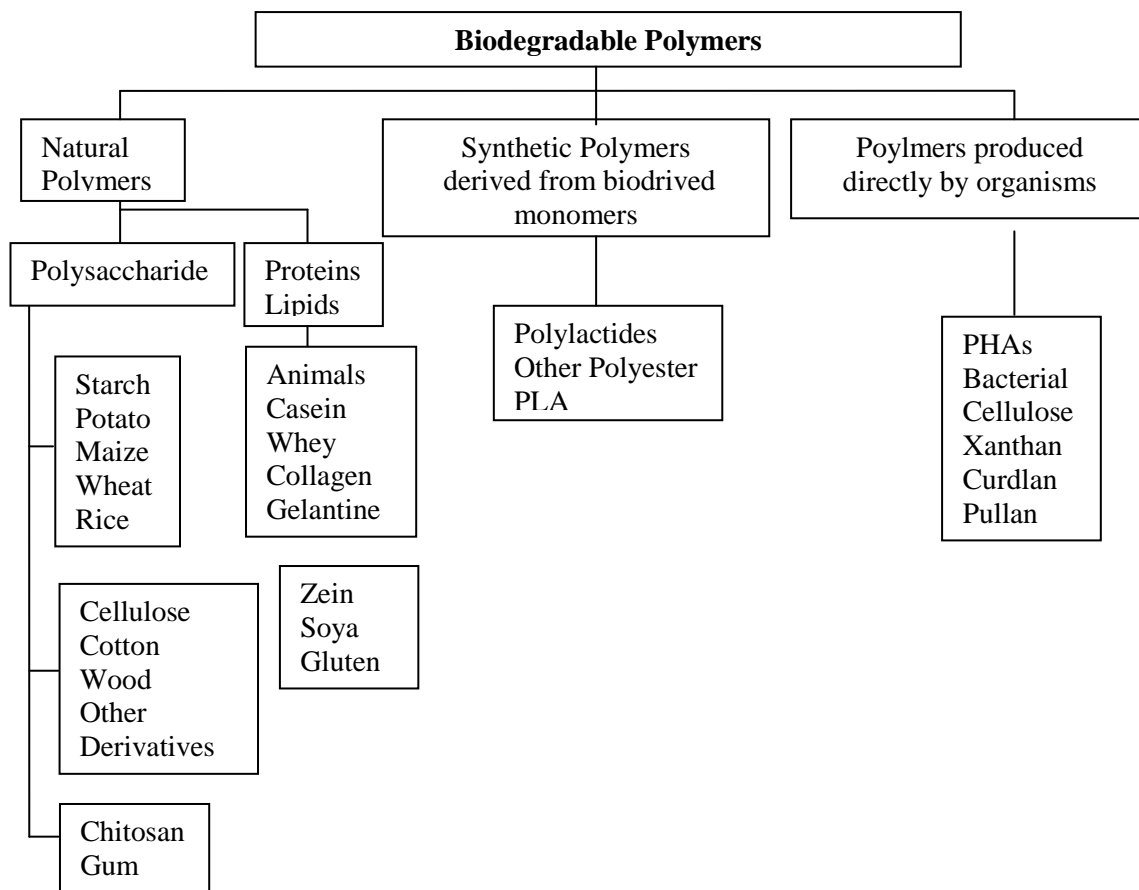


Figure 2.3. Biodegradable polymers and their origin based on method of production (Source: Weber 2000)

The first class of biodegradable polymers is natural polymers that are directly extracted from biomass such as polysaccharides such as cellulose, starch, and chitin and proteins such as casein, corn zein, whey, and collagen. All the polymers in this group are “truly green” since they all have biological origins and the completely decompose in the nature. Starch is one of the natural polymers that is the storage polysaccharide of cereals, legumes and tubes. Starch is a renewable and widely available raw material suitable for a variety of industrial uses. However, due to the inadequate mechanical properties (high percentage elongation, tensile and flexural strength), starch is treated by plasticizers, chemical modification or blending with other materials to use as packaging materials. The major drawback of this group is their low mechanical strength and hydrophilicity. Due to the hydrophilic character of these polymers, processing and performance problems mostly occur in humid conditions, especially in packaging products. However, these polymers are known to be excellent gas barrier properties. Second category is polymers produced from classical chemical synthesis from biobased monomers. Today’s packaging materials produced from polymers that synthesized by

mineral oil can be also manufactured from renewable monomers. These monomers are generally obtained by fermentation of carbohydrate feedstock. However, production of monomers is not economically feasible due to the cost of the production (Weber 2000).

Despite the natural polymers produced by living organisms, synthetic polymers are produced from bio-derived monomers. However, biodegradation process is same for both which includes enzyme-catalyzed and produced in aqueous media. The major category of this group is aliphatic polyesters with a hydrolysable linkage such as polylactic acid (PLA) (Platt 2006). The properties of the PLA are a promising alternative to oil based polymers used for food packaging applications. PLA is the first novel biobased material produced on a major scale (Platt 2006).

2.1.1. Polyhydroxyalkonates (PHAs)

Polyhydroxyalkonates (PHAs) are fully biodegradable polymers that belongs the family of aliphatic polyesters produced by different types of microorganisms as an carbon and energy storage products (Figure 2.4) .PHB was the first isolated and characterized in 1925 by French microbiologist Maurice Lemoigne. PHA have been attracting considerable attention as biodegradable plastics due to their similar properties to various thermoplastics used in many products, and completely degraded to water and carbon dioxide upon disposal under various environments. However, the use of PHAs in a wide range of applications has been complicated by their high production cost.

The plastic like properties and biodegradability of PHAs make them a potential replacement for oil based polymers such as polyethylene and polypropylene especially in packaging and agricultural applications. Moreover, biocompatibility of PHAs supplies unique properties for biomaterials applications (Cheng 2003).

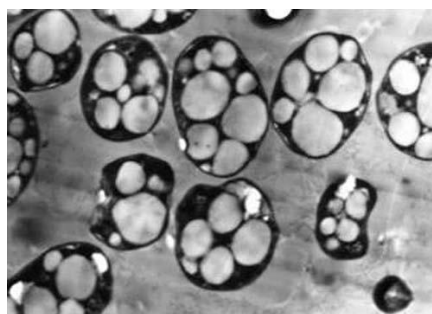


Figure 2.4. Bacterial cell containing PHA granules imaged by scanning electron microscopy (Source: Yu 2009)

2.1.2. Production of Polyhydroxyalkonates (PHAs)

Many gram-positive and gram-negative bacteria from at least 75 different genera synthesize PHAs. PHAs are accumulated intracellularly 90% of the cell dry weight under conditions of nutrient stress and act as carbon and energy reserve (Reddy et al. 2003) Non-storage PHA that is of low molecular weight, poly (3HB), have been detected in the cytoplasmic membrane and cytoplasm of *Escherichia coli*. More than 100 different monomer units have been identified as constituents of the storage PHA which supply an extensive range of properties with different kinds of biodegradable polymers (Reddy et al. 2003)

Bacterially produced polyhydroxybutyrate and other PHA have sufficiently similarity to conventional plastics such as polypropylene when compared in terms of molecular mass. Poly (3-hydroxybutyrate) (PHB) is the most common type of polyhydroxyalkonate studied and therefore it is the best characterized one among the family of PHAs. As the feeding of substrate changes copolymers of PHB can be formed and may result in the formation of polymers containing 3-hydroxyvalerate (3HV) or 4-hydroxybutyrate (4HB) monomers. Polymers that contain these monomers form a class of PHA. PHA can be produced from a different kinds of substrates such as renewable resources (sucrose, starch, cellulose, triacylglycerols), fossil resources (methane, mineral oil, lignite, hard coal), by products (molasses, whey, glycerol), chemicals (propionic acid, 4-hydroxybutyric acid) and carbon dioxide (Reddy et al. 2003). The metabolic pathway of PHA synthesis in bacteria from different carbon sources is summarized in Figure 2.5. The carbon source is first transferred from the extracellular environment into the cells by a specific transport system or diffusion. The carbon source is the converted into an α -hydroxyacyl-CoA thiesters (a substrate of the PHA syntheses) by anabolic or catabolic reactions, or both. Finally, PHA inclusions with a concomitant release of coenzyme A. (Reddy et al. 2009)

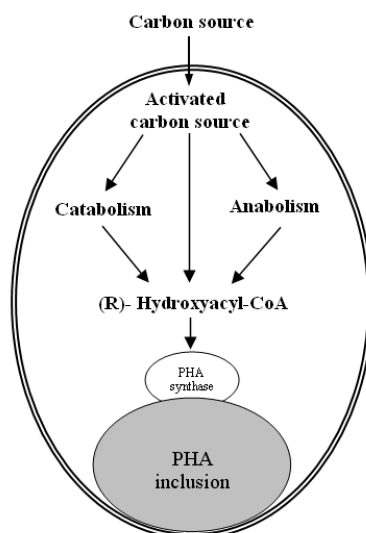


Figure 2.5. A schematic representation of the biosynthesis of PHA in bacteria (Source: Platt 2006)

The price of the PHA ultimately depends on the substrate cost, PHA yield on the substrate and the efficiency of product formulation in the downstream processing. The PHA yield is implied as a percentage of cell dry weight and high productivity. Thus Table 2.2 indicates the product cost and yield as the substrate changes.

Table 2.2. Effect of substrate cost and PHB yield on the production cost (Source: Madison and Huisman 1999)

Substrate	Substrate price (US\$ kg ⁻¹)	P(3HB) Yield g P(3HB) (g substrate) ⁻¹	Product Cost (US\$ (kg P(3HB))) ⁻¹
Glucose	0.493	0.38	1.30
Sucrose	0.290	0.40	0.72
Methanol	0.180	0.43	0.42
Acetic Acid	0.595	0.38	1.56
Ethanol	0.502	0.50	1.00
Cane Molasses	0.220	0.42	0.52
Cheese whey	0.071	0.33	0.22
Hemicellulose hydrolysate	0.069	0.20	0.34

2.1.3. Chemical Properties of Polyhydroxyalkanotes

General molecular formula of PHAs is given in Figure 2.6. *M* represents the number of CH₂ molecule in the chain, for *m*=1, 2, 3, with *m*=1 the most common; *n* can range from 100 to several thousands. *R* is variable. When *m*=1, *R*=CH₃, the monomer structure is 3-hydroxybutyrate; with *m*=1 and *R*=C₃H₇, the monomer is a 3-hydroxyhexanoate monomer.

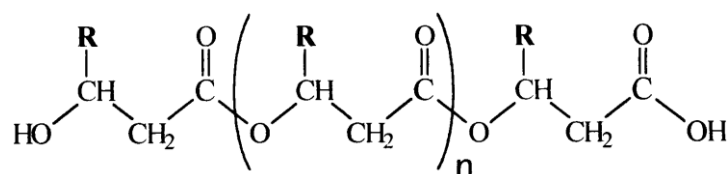


Figure 2.6. Molecular structure of polyhydroxyalkonates (PHAs).

The chemical bonds of polyhydroxybutyrate can be characterized by Fourier Transform Infrared (FT-IR) spectroscopy. Barud et al. studied FTIR analysis of bacterial poly (3-hydroxybutyrate) and summarized the characteristic peaks of PHB. The main bands observed were assigned to C-O stretching (1282 cm⁻¹) and C=O stretching (1730 cm⁻¹) peaks at 2853 cm⁻¹, 2926 cm⁻¹ and 2972 cm⁻¹ refer to C-H stretching and the peak at 3437 cm⁻¹ refers to hydroxyl en groups (Barud et al. 2011).

2.1.4. Physical Properties of Polyhydroxyalkonates

PHA is a semicrystalline polymer with a high melting temperature (~ 175 °C) and a high degree of crystallinity. The molecular weight of PHAs ranges around 1,000 to over one million depending on its production process. Thermal instability above 180 °C and brittleness has been the main disadvantages in many potential applications. Conventional techniques that enhance the processability temperature might be resulted in the reduction of molecular weight or poor mechanical properties. Thus, different techniques have been derived in order to PHA polymers to be processed with minimal loss in molecular weight. PHAs cover a broad range of physical properties and can behave both as traditional thermoplastic polymers and as elastomers. However, PHA suffers from brittleness causes poor mechanical properties. Thus, researches have been

carried on to enhance mechanical properties such as blending with conventional polymers (Verhoogt et al. 1994) or addition of nanoparticles (Ratnayake et al. 2009; Oguzlu and Tihminlioglu 2010). One of the application areas of PHAs is food packaging which makes the barrier properties more important. PHAs have lower moisture vapor transmission rate than other biodegradable polymers. The oxygen transmission rates for unoriented PHA films are 25-30 cc-mil/(100 in²-day) at 77 °C, 0% relative humidity (Platt 2006) .

PHAs offer hydrolytic stability under service conditions but when exposed to microbial organisms they break down enzymatically in soil, waste water, and marine environmentally. Unlike other biodegradable polymers, PHAs decompose to carbon dioxide and water in anaerobic environments. Next section gives the properties of PHB in detail.

2.1.5. Solubility of PHAs

Solvents for polymers materials are important for fundamental studies on solutions, to provide molecular weight and thermodynamic parameters. Viscosity can be important for defining the application area of concerning polymer. Furthermore, knowledge of a variety of solvents is important because it restricts the usage area due to given present environmental restrictions. Thus, interaction of polymer and solvent becomes important (Hansen 2000).

There are two methods that commonly used to define solubility of polymers. The one is Hildebrand approach and the other one is Hansen Solubility Parameter (HSPs). The Hildebrand approach is based on cohesive energy density. However, according to empirical or theoretical information, for polar polymers like poly(3-hydroxyalkonate) (P3HA), Hansen 's method is more reliable than Hilderbrand approach while predicting the solubility of PHAs (Terada and Marchessault 1999).

Hansen's defined the solubility using three dimensional solubility parameters based on dispersion forces between structural units, interactions between polar groups and hydrogen bonding forces. These parts compose three dimensional sphere consists of three coordinates. The coordinates includes dispersion part δ_d , polar part δ_p , and hydrogen bonding part δ_h . This sphere shows the soluble region of polymer which lies

within the sphere whose center corresponds to the coordinates of the polymer and the radius (Terada and Marchessault 1999).

Hansen developed an equation that predicts the solubility of a polymer in an organic liquid.

$$R^{ij} = [4(\delta d^i - \delta d^j)^2 + (\delta p^i - \delta p^j)^2 + (\delta h^i - \delta h^j)^2]^{\frac{1}{2}} \quad (2.1)$$

Symbols that equation involves, i and j represent the solvent and polymer respectively. Even if the three solubility parameters are different for each solvents, they might have the same value of ${}^{ij}R$ which shows that the same solvent power. The Hansen's equation has inherent value jR . The inherent value satisfies the condition that the polymer is soluble in a solvent for ${}^jR > {}^{ij}R$ and insoluble for ${}^jR < {}^{ij}R$. Furthermore as ${}^{ij}R$ value decreases the solubility increases as well. The reciprocal of ${}^{ij}R$ is used to represent a point in the three dimensional solubility region that corresponds to distance of a solvent from the center of the solubility sphere in the space (Terada and Marchessault 1999).

Terada and Marchessault studied the solubility of PHB in different kinds of solvents based on Hansen's solubility parameters. The solubility sphere of PHB was found to be as ${}^j\delta d=15.5$, ${}^j\delta p=9.0$, ${}^j\delta h=8.6$. Table 2.3 indicates the solubility parameter of various solvents for PHB (van Krevelen and Hoftyzer 1990). The jR value of PHB is found as 8.5 (Terada and Marchessault 1999). Table 2.3 shows the possible solvents for PHB. Considering the ${}^{ij}R^b$ value of PHB, chloroform and trichloroethylene are the good solvents, in contrast, ethylacetate and methylene chloride are not.

Table 2.3. Solubility parameters and distance, ${}^{ij}R$, of various solvents for PHB (Source: van Krevelen and Hoftyzer 1990)

Name	δ	δ_d	δ_p	δ_h	${}^{ij}R^b$
Methylene Chloride	19.9	17.4-18.2	6.4	6.1	5.2-6.5
Chloroform	18.9-19.0	17.7-18.1	3.1	5.7	7.9-8.4
1,2-Dichloroethane	20.0	17.4	5.3	4.1	7.0
1,1,2,2-Tetrachloro ethane	20.1	18.7	5.1	5.2	8.2
Trichloroethylene	19.0	18.0	2.9	5.3	8.5
Ethylacetate	18.6	15.2	5.3	9.2	3.8
Dimethylformamide	24.9	18.4-19.3	16.4	10.2	9.5-10.7

2.1.6. Barrier Properties of PHAs

Barrier properties of the polymeric materials play an important role for the potential use in number different applications. For instance, many foods require specific atmospheric conditions to sustain their freshness and quality during storage. Thus, foods are packed by protective polymer films which supply the specific environment. The packaging material should have certain barrier properties to ensure a constant gas composition inside the package (Weber 2000).

There are several processes are involved when a gas or vapor permeates through a polymer membrane. The driving force behind the transport process that involves sorption, diffusion and permeation is the concentration difference. Gas is sorbed at the entering face firstly, and then dissolves there. The dissolved penetrant molecules diffuse through the membrane, after diffusion step desorbing of the penetrant molecule at the exit face is observed. Then mechanism of permeation involves both solution and diffusion. Thus, the process can be explained in terms of Fick's first law of diffusion (Cornwelle 2009). The flux of penetrant molecule is represented by J in the direction of flow which is proportional to the concentration gradient ($\delta c/\delta x$).

$$J = -D \frac{\delta c}{\delta x} \quad (2.2)$$

D is the diffusion coefficient. Equation 2.1 is applicable to the diffusion in the steady state which means the concentration does not vary with time. Depending on these assumption flux of penetrant molecule can be written as;

$$J = \frac{D(c_1 - c_2)}{d} \quad (2.3)$$

Where c_1 and c_2 are the concentration of penetrant at high and low concentration faces of the film respectively and d is the membrane thickness. The penetrant distribution in the polymer phase is defined by the Nernst distribution law (Cornwelle 2009).

$$c = KC \quad (2.4)$$

C is the ambient concentration in contact with the polymer surface and c is the sorbed penetrant concentration where K depends on both temperature and c . In the case of transport of gases and vapors, pressure p is used instead of surface concentration. According to Henry's law (Cornwelle 2009).

$$c = Sp \quad (2.5)$$

where S is the solubility coefficient. Solubility of penetrant in polymer film is dependent on the temperature and characteristic properties of polymer film. Combination of equations 2.3 and 2.5 yield the well known permeation equation.

$$J = \frac{DS(p_1 - p_2)}{d} \quad (2.6)$$

where p_1 and p_2 are the ambient pressures on two sides of a film of thickness d . When rearranging equation 2.6 by writing P which is permeability coefficient instead of DS , equation 2.6 becomes in terms of permeability.

$$J = \frac{P(p_1 - p_2)}{d} \quad (2.7)$$

The permeability coefficient is measured directly as material property. In order to obtain permeability coefficient P , transmission rate r_T is determined which is a measure for the volume of gas passing through a membrane of known area per unit time with thickness of film, d and pressure, p . The unit of permeability coefficient P is generally used as [$cm^3 \mu m/m^2 \cdot day \cdot mmHg$] (Cornwelle 2009).

$$P = \frac{r_T \cdot d}{p} = \frac{(quantity\ of\ permeant) \cdot (film\ thickness)}{(area) \cdot (time) \cdot (pressure)} \quad (2.8)$$

As mentioned above, barrier properties of packaging films are important to extent the shelf life of foods. When the shelf life of the foods considered two gases which are water vapor and oxygen should be considered for, these two gases have the highest concentration among other gases in air. In order to compare the barrier

properties of different kinds of biopolymers with conventional oil based polymers, many studies have been carried on (Wang et al. 2005; Lagaron et al. 2008; Oguzlu and Tihminlioglu 2010). Weber and coworkers (2000) compared the water vapor permeabilities of oil based synthetic and biopolymer films as relative to each other. Figure 2.7 illustrates the relative water vapor transmission rates (WVTR) of oil based polymers and biopolymers. WVTR of PHA was found as between PLA and LDPE. WVTR of PHB is relatively low compared to other biopolymers which make PHAs favorable to use in food packaging applications. Despite the advantages in packaging applications, not so many studies exist in the literature related to transport properties of PHB based polymers. Miguel and coworkers studied transport properties of organic liquids, water vapor and carbondioxide in PHB and PHBHV. As the valerate content of PHBHV changes barrier properties changes as well. Thus, Miguel and coworkers studied the effect of valerate content on the WVTR. They found that the permeability is essentially independent of the 3HV content (Table 2.4.) .Changes in the WVTR can be resulted from the changes in crystallinity due to the valerate content.(Miguel 1998). In conclusion water transport properties of PHB and its copolymers can be considered to be very close in magnitude to those of common thermoplastics.

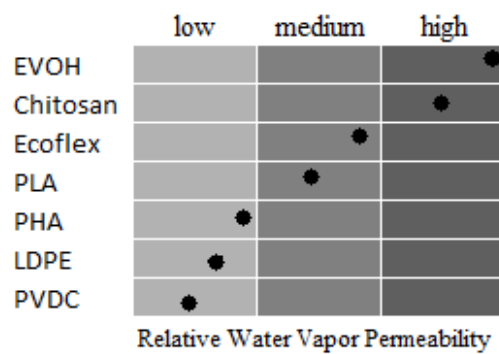


Figure 2.7. Relative water vapor transmission rates of polymers (Source: Weber 2000)

Table 2.4. Water vapor transmission rates through PHB and PHBHV at 30 °C
(Source: Miguel 1998)

Valerate Content % 3 HV	WVTR (g mm/m²day)	Standard Deviation
0	1.16	0.08
8	0.92	0.03
14	1.39	0.19
24	1.22	0.12

Sanchez-Garcia and coworkers (2007) studied the oxygen barrier properties of poly(3-hydroxybutyrate) and compared the results with different types of biopolymers. Table 2.5 indicates the oxygen permeabilities of PHB, PCL and PET. As it is seen, PHB has good barrier properties compared to PCL and PET (Sanchez-Garcia et al. 2008)

Table 2.5. Oxygen permeability of PHB, PCL and PET at 0%RH and 24°C
(Source: Sanchez-Garcia et al. 2008)

Sample	PO₂ (m³ m/m² s Pa) 24 °C, 0% RH
PHB	2.3±0.3e ⁻¹⁹
PCL	58.0e ⁻¹⁹
PET	3.3e ⁻¹⁹

Weber and coworkers (2000) compared the oxygen permeabilites of conventional oil based polymers with biodegradable films such as PLA and PHA. As it is seen from Figure 2.8 oxygen permeability of PHA is in medium level compared to other conventional polymers (Weber 2000)

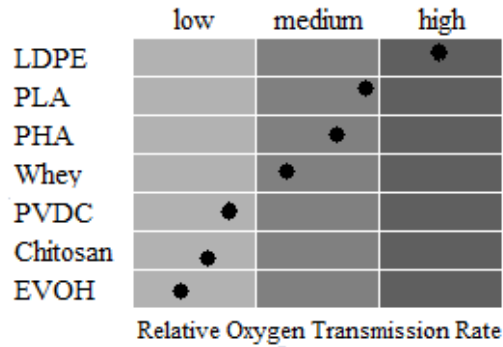


Figure 2.8. Oxygen transmission rates of polymers
(Source: Weber 2000)

2.1.7. Thermal Properties of Polyhydroxyalkonates (PHAs)

Thermal properties of materials are defined by using thermal analysis methods which consists of analytical methods by which a physical property of a substance is measured as a function of temperature. During this thermal analysis the substance is subjected to a controlled temperature regime. There are different kinds of thermal analytical methods such as differential scanning calorimetry (DSC), differential thermal analysis (DTA), thermogravimetry (TG), thermal mechanical analysis (TMA, DMTA), and thermal optical analysis (TOA) and dielectric thermal analysis (DETA) are available (Gedde 1995). Typical of these methods is that only small amounts of sample (a few milligrams) are required for the analysis. Calorimetric methods record exothermic and endothermic processes e.g melting, crystallization liquid-crystal-line phase transition, depolymerization, degradation. Some of the key features of polymers such as glass transition temperature, degradation, and melting temperatures can be evaluated by calorimetric methods (Gedde 1995).

Since one of the main drawbacks of PHB is its very low thermal stability at processing temperatures, many studies related to thermal properties of PHA's have been reported in the literature (He et al. 2001). The effect of chemical structure of PHA's on the thermal properties was reported by He and coworkers (He et al. 2001). They investigated the effect of type of repeating unit on thermal stability of PHB and its copolymers, PHBHV and PHBHHx. They reported that the copolymers had higher thermal degradation temperatures compared to PHB. Therefore, application area of

PHAs varies depending on its copolymer type due to differences in chemical and physical properties.

Madison and Huisman (1999) reported that thermal properties of PHAs changes as the valerate content varies, and PHAs exhibit similar thermal characteristics with polypropylene (PP) which makes PHAs as an alternative to PP in some applications. Table 2.6 shows thermal properties of PHAs and PP. As seen in Table 2.6, melting (T_m) and glass transition (T_g) temperatures of PHAs vary with the type of PHAs. The melting temperature of P(3HB) is about 177 °C which is very close to its degradation temperature, thus during melt compounding of PHAs, they suffer from poor thermal stability during processing. Therefore, initial biotechnological developments were focused on to enhance processability temperature of PHAs by incorporation of 3HV into the P(3HB) which resulted in poly(3-hydroxybutyrate-co-3-hydroxyvalerate) [P(3HB-3HV)] copolymer having lower T_m . Moreover, glass transition temperature of PHB is about 2 °C which is close to T_g of P(3HB-3HV) -1 °C (Madison and Huisman 1999). Crystallinity is one of the important characteristic of PHAs that affect mainly thermal and barrier properties. Additionally, the crystallinity ranges of these polymers were between 30-70% that was calculated using the equation 2.8:

Table 2.6. Thermal properties of PHAs and Polypropylene
(Source: Madison and Huisman 1999)

Parameter	P(3HB)	P(3HB-3HV)	P(3HB-4HB)	P(3HO-3HB)	PP
T_m (°C)	177	145	150	61	176
T_g (°C)	2	-1	-7	-36	-10
Crystallinity (%)	70	56	45	30	60

$$X_c = \frac{\Delta H_m}{\Delta H_{PHB}^0} \quad (2.8)$$

Where ΔH_{PHB}^0 is the enthalpy of melting of pure PHB crystals and assumed as 146 J g⁻¹ (Gunaratne and Shanks 2005) Furthermore, it was observed that thermal properties of PHB is very similar to polypropylene, so that the idea of usage of PHB instead of PP becomes more reliable.

Sato and coworkers studied the thermal behavior of PHB and P(HB-co-HV) copolymers with varying HV content by differential scanning calorimetry (DSC)

analysis. DSC analyses were performed under nitrogen atmosphere over a temperature range of -50 °C to 130 °C at heating and cooling rates of 2 and 10 °C/min. They reported the melting and crystallization temperature of PHV, PHB, and P(HB-co-HV) (Table 2.7.). It was observed that the melting temperature of PHB decreased with increasing HV content up to a point like HV content of 28.8 mol %. On contrary, above the percentage such as HV= 58.4 mol % and HV= 73.9 mol %, melting temperature increased by increasing HV content. It is well known that P(HB-co-HV) copolymers have an isomorphic crystal structure where the HV units are embedded in the HB crystalline lattice. Thus, at low percentage of HV, P(HB-co-HV) exhibits PHB type crystal structure. On contrary, the copolymer shows PHV type crystal structure at higher HV percentage (Table 2.7.) (Sato et al. 2011). One of the goals of producing copolymer of PHB with HV part is to overcome the drawbacks of PHB such hindrance as brittleness, thermal instability. However, some studies showed that beside the advantages of HV part in some characteristics of PHB, it can distinguish the barrier properties which plays crucial role in packaging applications. Therefore, HV content in PHB also confine the application areas in packaging applications. Some of the researches have been focused on enhance the PHBHV properties by diminishing the adverse effect of HV content.

Table 2.7. Melting Temperature (T_m) and crystallization temperature (T_c) of PHB, P(HB-co HV), and PHV (Source : Sato et al. 2011)

Polymer Type	HV content %	T_m (°C)	T_c (°C)
PHB	-	164-173	105
P(HB-co-HV)	HV=9 mol %	153-169	89
	HV=15 mol %	151-161	102
	HV=21 mol %	159	125
	HV=28.8 mol %	100	71
	HV=58.4 mol %	75	n.d
	HV=73.9 mol %	85	n.d
	HV=88.6 mol %	82	39
PHV		118	n.d

One of the drawbacks of PHAs is the high crystallinity which causes brittleness. Thus, crystallization kinetic of PHAs plays an important role in processing conditions of

PHAs. Moreover, the crystal percentage of polymer affects its physical properties such as barrier, mechanical, and thermal. Therefore, controlling the crystallization process is a vital point. Next section gives the crystallization kinetic model for polymers in detail.

2.1.7.1. Crystallization Kinetic Models

Crystallization kinetics of polymers have been studied using different models such as Avrami Jeziorny (Smith et al. 2005) , Ozawa (Bandyopadhyay et al. 2008), and Liu Mo models (Bandyopadhyay et al. 2008).

The kinetic parameters of Avrami equation, the exponent n (Table 2.8.) and the rate constant k_t , can be obtained using (Eq.2.9) and its double logarithmic form (Eq. 2.10).As the exponent n changes the nucleation mode and crystal growth shape differs as well.

$$1 - X_t = \exp(-k_t t^n) \quad (2.9)$$

$$\log[-\log(1 - X_t)] = \log k_t + n \log t \quad (2.10)$$

Table 2.8. The values of Avrami exponent n and K at different crystal growth shapes (Source: Stephen and Cheng 2002)

Crystal Growth Shape	Nucleation mode	Avrami Exponent (n)	Avrami rate constant (K) ^a
Rod	Heterogeneous ^b	1	$\dot{N}GA$
	Homegeneous ^c	2	$NGA/2$
Disc	Heterogeneous	2	$\pi\dot{N}G^2D$
	Homegeneous	3	$(\pi/3)\dot{N}G^3D$
Sphere	Heterogeneous	3	$(4\pi/3)\dot{N}G^3$
	Homegeneous	4	$(\pi/3)\dot{N}G^3$
Sheaf	Heterogeneous	5	-
	Homegeneous	6	-

^aA is cross-sectional area of the rod; D is thickness of the rate; G is linear growth; N is nucleation density; and \dot{N} is nucleation rate.

^bHeterogenous means that the nucleation density is constant

^cHomegeneous, also named sporadic, means that the rate of nucleation is constant

where X_t is the relative degree of crystallinity for time t . The kinetic parameters n and k_t do not have the same physical meaning as in the isothermal crystallization under nonisothermal process, the temperature changes and affects the rates of both

nuclei formation and spherulite growth (Grozdanov et al. 2007). The Avrami exponent is known to be influenced by molecular weight, nucleation type, and secondary crystallization, and in general, it is not much influenced by temperature. Thus, the final form of the kinetic parameter K_c can be given by equation 2.11 (Grozdanov et al. 2007)

$$\log K_c = \frac{\log K_t}{\phi} \quad (2.11)$$

where K_c is kinetic crystallization rate and ϕ is the cooling rate. In order to compare the evaluation of experimental result using different methods, Ozawa method can also be used.

Ozawa has extended the Avrami equation to the nonisothermal case in the following equation:

$$1 - X_t = \exp\left(-\frac{K(T)}{\phi^m}\right) \quad (2.12)$$

where $K(T)$ is the function of cooling rate and ϕ is the cooling rate, and m is the Ozawa exponent that depends on the dimension of crystal growth. Plotting the double logarithmic form $\log [-\ln (1-X_t)]$ against $\ln \phi$ and taking the slope of linear curve gives the Ozawa exponent. Ozawa assumes that there is no secondary nucleation kinetics and no volume changes during the crystallization process (Grozdanov et al. 2007) .

Besides the crystallization growth geometry and activation energy of nonisothermal crystallization can be evaluated by Kissinger's equation.

$$\frac{d[\ln (\phi/T_p^2)]}{d(1/T_p)} = -\frac{E_a}{R} \quad (2.13)$$

Where ϕ is the cooling rate, T_p is the crystallization peak temperature, E_a is activation energy and R is gas constant. The activation energy of PHB was calculated as -108 kJ/mol (Wu et al. 2007) .

Mubarak and coworkers have studied non isothermal melt crystallization kinetics of isotactic polypropylene (iPP) were investigated. Non-isothermal crystallization was carried out by cooling the melted samples down to 30 °C at constant cooling rates of 1, 5, 10, 30, 100 °C/min. In order to get rid of thermal lag between a

point in the sample and the calorimeter furnace, the recorded temperatures in non-isothermal experiments are corrected using following equation (Mubarak et al. 2001) .

$$T_{actual} = T_{disp} + 0.089\lambda \quad (2.14)$$

where T_{disp} is the display temperature and λ (°C/min) is the cooling rate) The models such as Ozawa and Avrami were applied to experimental data to explain the mechanism of crystallization. However, they found that none of the models fit the experimental data due to the induction time effect. When the induction time was considered, Ozawa model was found the most fitted model to experimental data (Mubarak et al. 2001)

Hsu and coworkers studied nonisothermal crystallization behavior of PHB at different cooling rates using Avrami model. Table 2.9 shows the crystallization onset, peak, final temperatures and Avrami parameters. The n values of PHB ranged from 3.4 to 4.3 with various cooling rates that might be due to a three-dimensional growth with an athermal nucleation during the cooling scans. The values of k increased as the cooling rate increased. It was observed that the crystallization temperature was inversely proportional to the on cooling rates.

Table 2.9. Avrami Parameters and the values of $T_o(^{\circ}\text{C})$, $T_p(^{\circ}\text{C})$, and $T_f(^{\circ}\text{C})$ at various cooling rates for PHB (Source: Wu et al. 2007)

Cooling Rate (°C/min)	$T_o(^{\circ}\text{C})$	$T_p(^{\circ}\text{C})$	$T_f(^{\circ}\text{C})$	$T_{1/2}^a(\text{min})$	n	k
2.5	122.6	114.4	108.5	6.13	4.3	0.00026
5	117.2	109.4	100.9	3.11	4.0	0.0074
10	113.1	102.7	93.6	1.87	4.1	0.0524
20	108.1	94.9	83.1	1.11	3.9	0.456
40	101.6	83.7	60.2	0.81	3.4	1.34

T_o : crystallization onset temperature

T_p : crystallization peak temperature

T_f : crystallization final temperature

2.1.8. Mechanical Properties of PHAs

Plastic market is becoming increasingly important to utilize alternative raw materials. Until now petrochemical based plastics have been increasingly used as packaging materials because their large availability at relatively low cost and because their good mechanical performance such as tensile strength. However, nowadays their use has to be restricted due to environmental concerns. Therefore, mechanical properties of biopolymers become one of the curial features that make them an alternative to conventional petrochemical plastics (Siracusa et al. 2008).

It is well known that the polymer architecture plays an important role on the mechanical properties, and consequently on the process utilized to modeling the final production such as injection moulding, sheet extrusion, blow moulding. In addition, many packing containers are commercial used at specified conditions, so it is important to assess the mechanical performance under desired conditions

Tensile test analyses are made to determine the tensile strength (MPa), the percent elongation at yield (%), the percent elongation at break (%) and the elastic modulus (GPa) of the packing material. These values are important to get mechanical information of the biopolymer materials to be compared with the commercial nonbiodegradable polymers.

Table 2.10 indicates the mechanical properties of PHAs. Conti and coworkers reported that as the valerate content increases tensile strength and modulus of elasticity decreases. This could be due to presence of ethyl group in the units of 3HV which makes the crystallization process difficult. Therefore, a polymer with less crystalline and with less perfect crystals contributes for the reduction of the tensile strength. Moreover, study of Ramsay and coworkers shows that at higher 3HV content tensile strength and modulus of elasticity became lower when compared to PHB.

Related to elongation at break, literature studies show that at higher 3HV content this property becomes higher. This could be due to superior flexibility of the copolymer structure. Similar results were reported by Ramsay and Savenkov.

Table 2.10. Mechanical Properties of PHAs

Polymer Type	HV content %	Tensile Strength (MPa)	Elongation at Break (%)	Modulus of Elasticity (GPa)	Reference
PHB	-	26.0 (± 2.6)	8.2 (± 0.4)	4.6 (± 1.1)	(Conti et al. 2006)
P(HB-co-HV)	6 mol %	21.8 (± 1.5)	12.1 (± 0.9)	2.7 (± 0.1)	(Conti et al. 2006)
	19 mol %	17.7 (± 3.9)	25 (± 8.0)	1.5 (± 1.1)	(Ramsay et al 1993)
	20 mol %	14.8	61	-	(Savenkov et al. 2000)

In order to make PHAs competitive with conventional petrochemical plastics the mechanical properties of PHAs in terms of modulus, elongation at break and tensile strength must be improved. Therefore, researches have been focused on to enhance the mechanical properties of PHAs by using different techniques.

2.1.9. Biodegradability of PHAs

Biodegradability and compostability are defined by the scientific community and were legally incorporated into a Standard by the American Society and Materials (ASTM) in July 1999. The ASTM defines a biodegradable plastic as a degradable plastic in which the degradation results from the action of naturally occurring microorganisms such as bacteria, fungi, and algae (Platt 2006).

Biodegradation is usually defined as degradation caused by biological activity, it will usually occur simultaneously with, and is sometimes initiated by, non-biological degradation such as photodegradation and hydrolysis. Biodegradation takes place through the action of enzymes or by products such as acids and peroxides secreted by microorganism. Enzymes are the biological catalysts that can induce massive increases in reaction rates in an environment. There are different kinds of enzymes that catalyzing its own unique reaction on groups of substrates or on specific chemical bonds.

There are four common approaches available for studying biodegradation processes used in literature (Platt 2006).

- Monitoring microbial growth
- Monitoring the depletion of substrates
- Monitoring reaction products
- Monitoring changes in substrate properties

The property that distinguishes PHA from petroleum based plastics is their biodegradability. PHAs are degraded upon exposure to soil, compost, or marine sediment. Biodegradation is dependent on a number of factors such as microbial activity, and the exposed surface area, moisture temperature, PH, molecular weight. The nature of the monomer units also has been found to affect degradation. Copolymers containing PHB monomer units have been found to be degraded more rapidly than either PHB or 3HB-co-3HV copolymers. Enzymes break down the polymer into its molecular building blocks, called hydroxyacids. However, biodegradation of PHAs under aerobic conditions results in carbon dioxide and water, whereas in anaerobic conditions the degradation products are carbon dioxide and methane (Reddy et al. 2003).

Shishatskaya and coworkers studied the biodegradation of PHB and its copolymer PHBV in biological media. Biodegradability was monitored by measuring the residual weight of samples in solutions. They reported that after 180 days, the mass of P(3HB) and P(3HB-co-3HV) samples was reduced to 74% and 62% of the initial mass respectively. They also concluded that, the biodegradation rate of co-polymer was 1.57- times higher than that of P(3HB) (Shishatskaya et al. 2005).

Abou-Zeid and coworkers also studied anaerobic microbial degradation of PHB and PHBV in the cultures. Degradation of the PHB and PHBV films were examined after incubation for 10 weeks at 35 °C. After 10 weeks, PHB and PHBV lost 23% and 22.5% of its weight respectively. In comparison to other biodegradable polymers for instance synthetic polyester PCL lost 7.6% of its weight in same conditions (Abou-Zeid et al. 2001).

One of the strongest competitive edges of PHAs is its biodegradability in environment when compared to conventional plastics. Therefore, researches have been studying biodegradation of PHA in different conditions so as to understand the mechanism of biodegradation.

CHAPTER 3

POLYMER NANOCOMPOSITES

Nanomaterials can be classified into two groups e.g. nanostructured materials and nanoparticle materials. Nanometer size covers a wide range from 1 nm to 200 and 300 nm. The introducing of inorganic nanoparticles as additives into polymer matrix resulted in polymer nanocomposites (PNs). Polymer nanocomposites with dimensions on the nanometer scale are currently topics of intense research in the area of polymer and material science, electronics, and biomedical science. Interaction of these additives in nanometer scale supplies unique properties for, the interaction is in atomic levels, it enhances the properties of nanocomposite materials distinctly. Thus, nanostructured materials were created with improved chemical and physical properties without changing chemical compositions of materials. The development of these new materials enables the circumvention of classic material performance tradeoffs by accessing new properties. PNs multifunctional features that consist of improved thermal and flame resistance, moisture resistance, decreased permeability, charge dissipation, and chemical resistance (Koo 2006).

Uniform dispersion of these nanoparticles supplies ultra large interfacial area per volume between the nanoparticle and the host polymer. Therefore, interaction in nanoscopic dimensions between nanoparticles and the host polymers differentiate polymer nanostructured composites from traditional fillers plastics and composites. Thus, new combinations of properties derived from the nanoscale structure of PNs (Koo 2006) The enhancement in polymer properties by addition of these nanoparticles can be found in the literature demonstrating improvement in physical and mechanical properties (Chi et al. 2012; Collier et al. 2012; Liu et al. 2012; Panaitescu et al. 2012)

All the studies that mentioned above are related to polymers that produced from fossil fuels. Due to the environmental concerns studies have been focused on biodegradable polymers. As it is known some of the biodegradable polymers suffer from poor mechanical and barrier properties. Thus, in order to improve these properties nanofillers incorporated to biodegradable polymer matrix to make these polymers competitive with oil based polymers. Biodegradable nanocomposites are the next generation of materials for future. So far, the most studied biodegradable

nanocomposites are starch, polylactic acid (PLA), polycaprolactone (PCL) and polyhydroxybutyrate (PHB). Nanocomposites of this category are expected to exhibit enhanced strength and stiffness with little sacrifice of toughness, reduced gas, water vapor permeability and increased heat deflection temperature, opening an opportunity for the use of new high performance green nanocomposite materials to replace conventional petroleum-based composites. The improvement in physical and mechanical properties of biodegradable nanocomposite films can be found in literature (Botana et al. 2010; Oguzlu and Tihminlioglu 2010; Achilias et al. 2011)

3.1. Nanoparticles

There are different kinds of nanoparticles that commercially available that can be incorporated into the polymer matrix to form polymer nanocomposites. Researchers have been studying the effect of nanoparticles on polymers. .

Table 3.1 summarizes the advantages and disadvantages of nanofillers on polymers (Koo 2006).

Table 3.1. Characteristics of Nanoparticles to Polymers
(Source: Koo 2006).

Improved Properties	Disadvantages
Mechanical Properties (tensile strength, stiffness, toughness)	Viscosity increases (limits processability)
Gas Barrier	Dispersion Difficulties
Synergistic flame retardant additive	Optical Issues
Dimensional Stability	Sedimentation
Thermal expansion	Black Color when different carbon containing nanoparticles are used
Thermal conductivity	
Ablation resistance	
Chemical Resistance	
Reinforcement	

Most commonly used nanoparticles in the literature can be listed as;

Monmorillonite organoclays (MMT)

Carbon Nanofibers (CNFs)

Polyhedral oligomeric silsesquioxane (POSS)

Carbon nanotubes

Nanosilica (N-silica)

Nanoaluminum oxide (Al_2O_3)

Nanotitanium oxide (TiO_2)

Among these nanoparticles, the most extensively researched group of nanoparticles is the layered silicate family. Next section gives the information related the most studied layered silicate; montmorillonite.

3.1.1. Montmorillonite Nanoclays

Montmorillonite (MMT) is one of the most widely used clay type in the production of nanocomposites. The origin off- MMT is the clay type of bentonite that is commonly formed in situ alternation of volcanic ash. Bentonite involves MMT but also can contain glass, mixed layer clays, illite, kaolinite, quartz, zeolite and cabonetes. Clay soil has particle size of less than 2 μm (Koo 2006; Mai and Yu 2006). The major components of MMT are silica and alumina. The structure of MMT is shown at Figure 3.1 showing its sheet structure consisting of layers containing the tetrahedral silicate layer and the octahedral alumina layer. The layered alumina silicates such as MMT are plate like particles and belong to the family of 2:1 phyllosilicates. A 2:1 layer consists of the tetrahedral silicate layer which involves SiO_4 groups linked together to form a hexagonal network of the repeating units of composition Si_4O_{10} . The alumina layer consist of two sheets of closely packed oxygens or hydroxyls, between which octahedral coordinated aluminum atoms are imbedded in such a position that they are equidistant from six oxygens or hydroxyls The two tetrahedral layers sandwich the octahedral layer, sharing their apex oxygens with the latter. These three layers form one clay sheet that has a thickness of 0.96 nm. The chemical formula of the montmorillonite clay is $\text{Na}_{1/3}(\text{Al}_{5/3}\text{Mg}_{1/3})\text{Si}_4\text{O}_{10}(\text{OH})_2$ (Mai and Yu 2006). Due to the interaction in nanometer scales, interfacial contacts of the nanoparticles with the polymer matrix become more important. Due to isomorphic substitutions in the octahedral and tetrahedral sheets the

layers have a net negative charge. The most common substitutions are Al^{3+} for Si^{4+} in tetrahedral sheet and Mg^{2+} for Al^{3+} in the octahedral sheet.

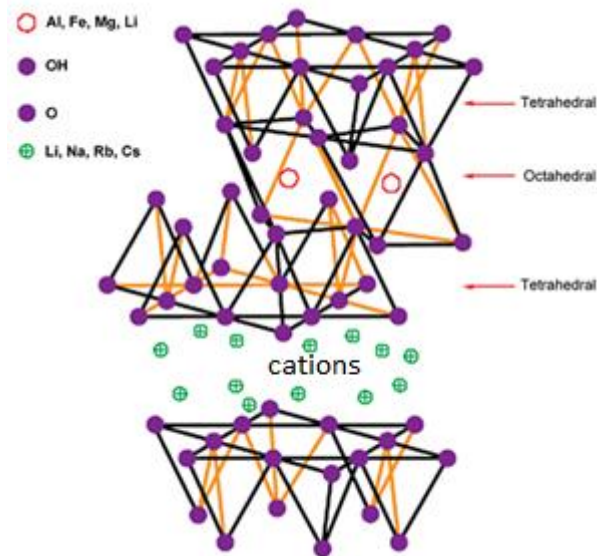


Figure 3.1. Structure of MMT
(Source : Mittal 2010)

The negative charges are counterbalanced by the interlayer alkali or alkaline earth metal cations, and as a result of these layers, they are held together in stacks by electrostatic and van der Waals forces. These inorganic materials are hydrophilic in nature, which make them incompatible with the hydrophobic polymer matrices. This inorganic cations can change with organic cations renders the clay organophilic and hydrophobic, and lowers the surface free energy of clay layers. Therefore, the interfacial interactions become stronger leads to diffuse polymer chains between the clay layers and delaminate the clay platelets to individual layers. In order to decrease surface energy of layers, long chain alkyl ammonium salts are generally used for exchanging the inorganic cations. They increase the basal spacing of the clay to a larger extent which can further be helpful in achieving exfoliation of the clay layers in polymer matrix

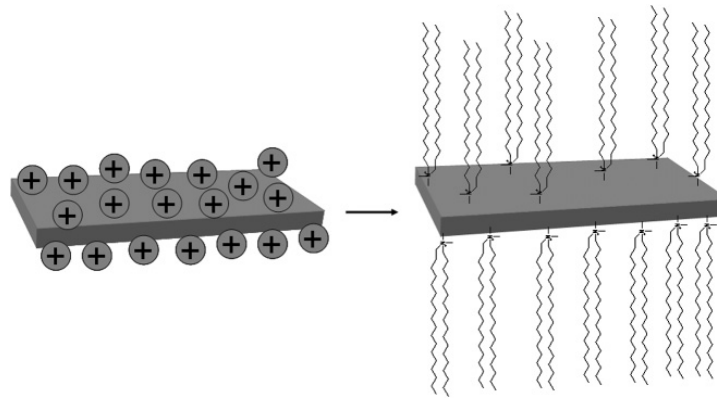


Figure 3.2. Surface modification of the aluminosilicate surface
(Source: Mittal 2010)

In order to achieve a good dispersion of MMTs in polymer matrix, organomodification plays an important role. By changing the inorganic cations by different kinds of organic modifiers, different kinds of organically modified montmorillonites (OMMTs) are formed (Figure 3.2). Some of the organically modified montmorillonites (OMMTs) and its modifiers are listed in Table 3.2.

Table 3.2. OMMTs and their organic modifiers
(Source: Mai and Yu 2006; Mittal 2010)

Trade Name of MMTs Modified and unmodified montmorillonites	Organic Modifier
Cloisite Na ⁺	None
Cloisite 15A	2M2HT (Dimethyl, dihydrogenated tallow, quaternary ammonium)
Cloisite 20A	2M2HT (Dimethyl, dihydrogenated tallow, quaternary ammonium)
Cloisite 30B	MT2EtOH (Methyl, dihydrogenated tallow ammonium)
Cloisite 93A	M2HT (Dimethyl, dihydrogenated tallow, ammonium)
Cloisite 25A	2MHTL8 (Dimethyl, dihydrogenated tallow, 2-ethylhexyl quaternary ammonium)
Cloisite 10A	2MBHT (Dimethyl, benzyl, hydrogenated tallow, quaternary ammonium)

3.2. Polymer Layered Silicate Nanocomposites

Polymer layered silicate nanocomposites (PLSNs) are produced mixing of the filler phase at nanometer level, so that at least one dimension of the filler phase is less than 100nm. Recent studies have been focused on the PLSNs owing to remarkable enhancements in the various composite properties at very low volume fractions (Maiti et al. 2003; Zhang et al. 2007; Lagaron et al. 2008).

There are different types of layered silicate nanocomposite structures are available depending on dispersion of layered silicate in polymer matrix. The major factor that affects the dispersion levels is the interaction between polymer chains and clay surfaces. As mentioned before, in order to achieve a good interaction so as dispersion of layered silicates, the organic modification of layered silicates are considered. The structure of polymer layered silicate nanocomposites can be divided into four groups:

- Phase separated
- Intercalated
- Intercalated and flocculated
- Exfoliated

Due to the poor interfacial interaction between layered silicates and polymer matrix, phase separated structure is obtained. The phase separated structure has the same property as the conventional composites. This structure is generally observed for the case of using unmodified or insufficient modified clays with hydrophobic polymers. Depending on the degree of penetration of polymer matrix into the organically modified layered silicate galleries, different nanocomposite structures ranging from intercalated to exfoliate structure (Figure 3.3) can be obtained for all other nanocomposite structures except phase separated. Polymer penetration that resulted in finite expansion of the silicate layers produces intercalated nanocomposites consisting of well ordered multilayer. On the other hand, extensive polymer penetration into galleries result in disordered and eventual delamination of the silicate layers produces nearly exfoliated nanocomposites consisting of individual silicate layers dispersed in the polymer matrix (Okamoto 2005).

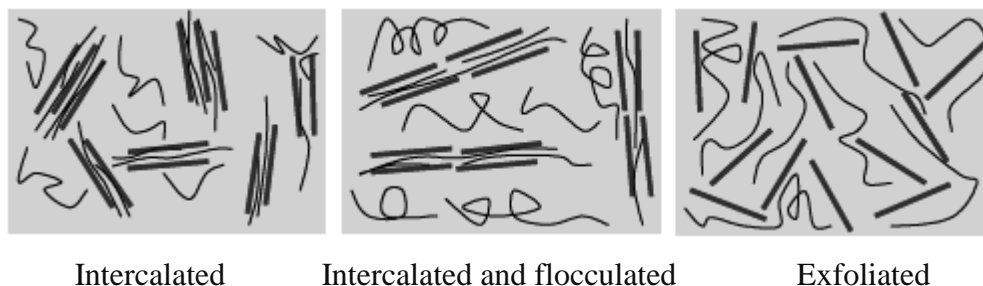


Figure 3.3. Schematic illustration of three different types of thermodynamically achievable polymer/clay nanocomposites (Source: Okamoto 2005)

3.3. Characterization of Polymer Layered Nanocomposite Films

The evaluation of structure of PLS nanocomposites plays an important role for the discussions of further analysis. Typically wide angle x-ray diffraction (WAXD) analysis and transmission electron microscope (TEM) are the most used characterization techniques for, the ease of use. The WAXD gives the position, shape, and intensity of the basal reflections of silicate layers, and by monitoring these parameters the PLS nanocomposites structure can be identified either intercalated or exfoliated. Figure 3.4 indicates three different structures based on the WAXD analysis proofed by TEM analyses. For instance, the delamination of silicate layers in polymer matrix resulted in exfoliated nanocomposites, and so extensive layer separation that results in the disappearance of any coherent x-ray diffraction from the distributed silicate layers. On the other hand, intercalated structure is obtained when the original OMLS peak broadened which is resulted from an increase in basal plane distance.

In order to understand the internal structure, spatial distribution of the various phases, and defect structure WAXD are not enough. Thus, TEM analysis allows a qualitative understanding of the structure. However, special care must be exercised to ensure that a representative cross section of the sample.

Despite of the structure analysis, Fourier transform infrared spectroscopy (FTIR) and NMR analysis can also be evaluated to understand the structure of layered silicates.

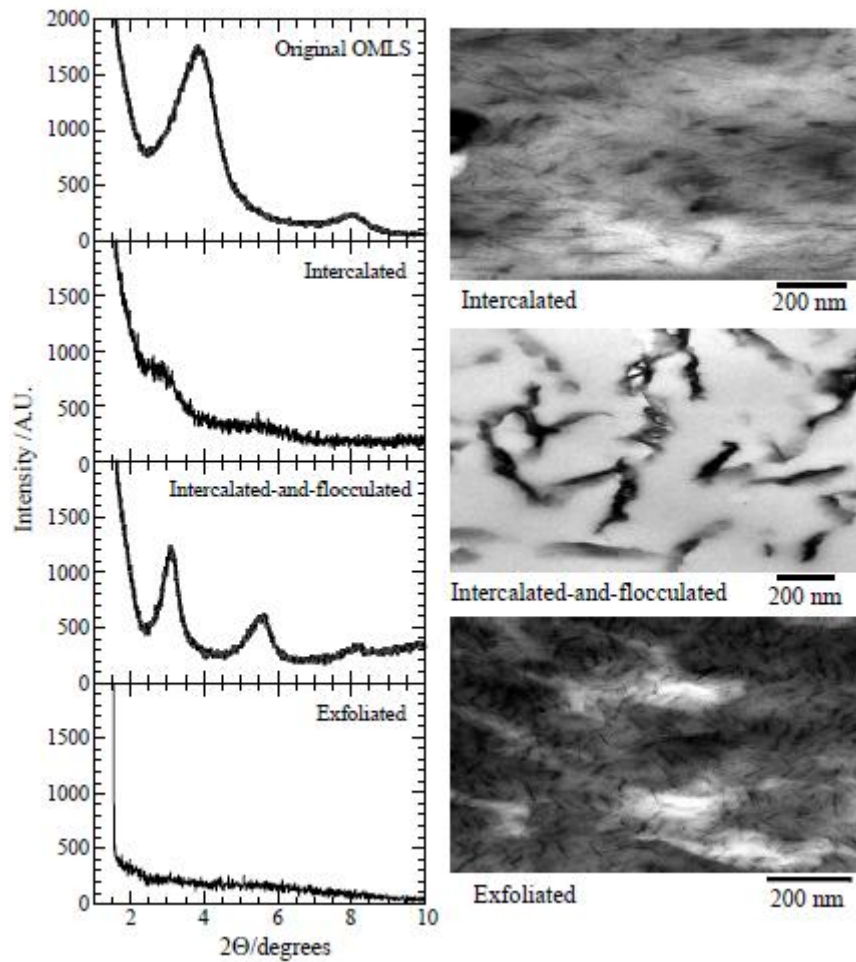


Figure 3.4. (a) EAXD patterns, and (b) TEM images of three different types of nanocomposites (Source: Okamoto 2005)

Figure 3.5 indicates the FTIR analysis of modified and unmodified montmorillonite clays. Cervantes-Uc and coworkers found that, all spectra in the band range of 3636 and 3395 cm^{-1} attributed to O-H stretching for the silicate and water respectively. The absorbance at 1639 cm^{-1} and 1040 cm^{-1} is related to O-H bending, and stretching vibration of Si-O-Si from silicate respectively. Moreover, the band at 917 cm^{-1} is due to the Al-OH-Al deformation of aluminates. The bands located at 2924 , 2842 and 1475 cm^{-1} were assigned to C-H vibrations of methylene groups from chemical structure of the surfactant (Cervantes-Uc et al. 2007).

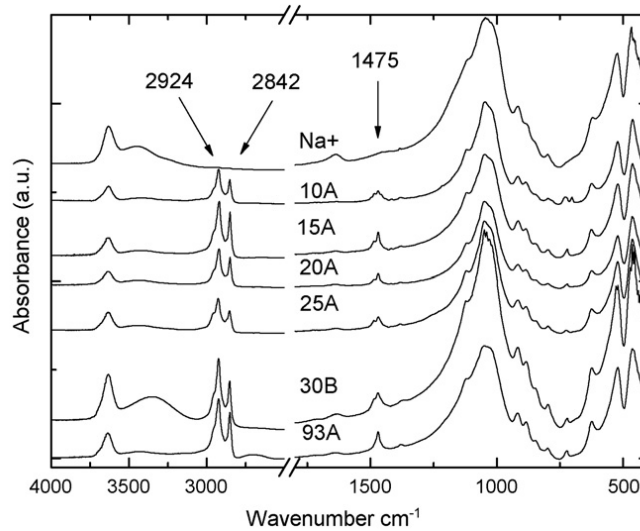


Figure 3.5. FTIR spectra of various commercial clays
(Source: Cervantes-Uc et al. 2007)

3.4. Preparation Methods of PLS Nanocomposites

There are different kinds of techniques available to prepare PLS nanocomposites. One of the major common features of these techniques is to achieve penetration of polymer matrix between silicate layers. In general, for solid thermosetting reactive prepolymers or thermoplastic polymers with solid nanoparticles, the following processing methods are recommended (Koo 2006):

In-situ intercalative polymerization

Solution intercalation

Melt intercalation

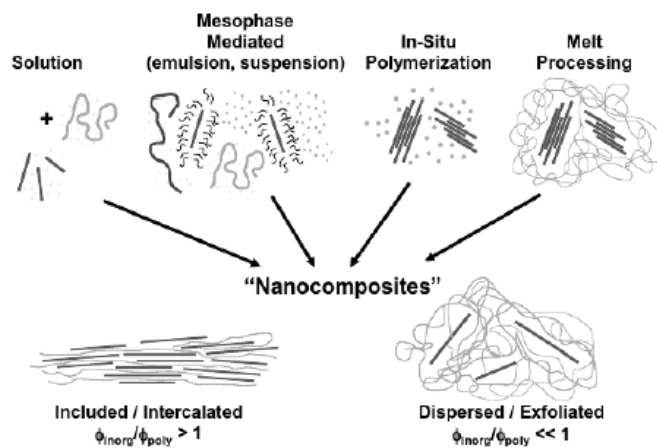


Figure 3.6. Different methods in preparation of layered silicate polymer nanocomposites (Source : Koo 2006; Mittal 2010)

3.4.1. Solution Intercalation

The layered silicate is exfoliated into single layer using solvent in which the polymer can also be soluble in this solvent. The weak forces that stack the layers together can be easily dispersed in an adequate solvent. The polymer then absorbs onto the delaminated sheets, and when evaporated, the sheet reassembles, sandwiching the polymer to form an ordered, multilayered structure. This method has been widely used in literature to prepare layered silicate polymer nanocomposites (Zulfiqar et al. 2008; Hwang et al. 2012; Jaafar et al. 2012).

Selecting the solvent plays an important role and it can restrict the application areas of polymer nanocomposites. For instance, if you are using a solvent that is not volatile enough you should consider the evaporation time of the solvent which limits the applications. On the other hand, the surface energies of solvent and silicate layers are also important since swelling degree and increase in basal spacing are directly affected from solvent clay interaction. Burgentzle and coworkers investigated the swelling ratios of clays as a function of the solvent surface energy for OMMT that is modified with 2MBHT (Figure 3.7). The aromatic solvents, such as xylene, chloroform, and ethylbenzene are the best for swelling agents due to its interaction with the benzyl group of the exchanged ion (Burgentzle et al. 2004).

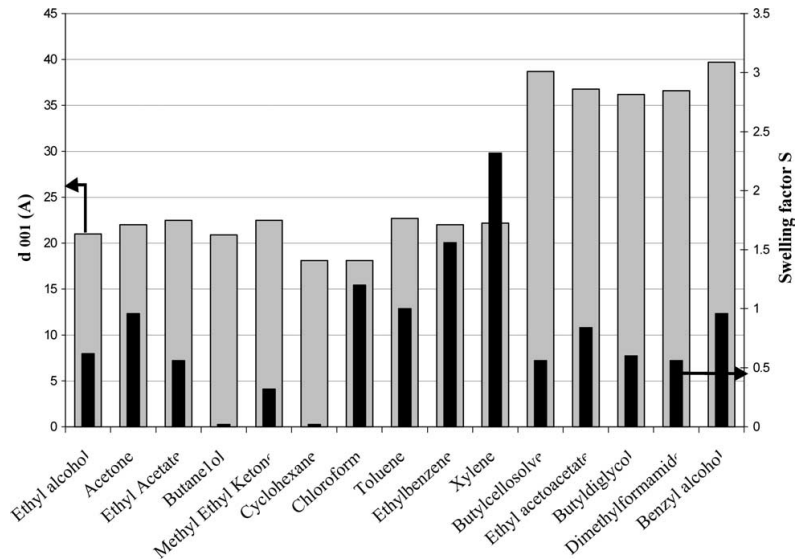


Figure 3.7. Free swelling factors, S(Black bar), and interplanar distance, d_{001} (Grey bar) determined for 2MBHT nanoclay- based suspensions in various solvents (Source : Burgentzle et al. 2004)

3.4.2. In Situ Intercalative Polymerization

This method OMMT is swollen within the liquid monomer or a monomer solution so the polymer formation can occur between the intercalated sheets. Polymerization can be initiated either by heat or radiation, by the diffusion of a suitable initiator, or by an organic initiator or catalyst fixed through cation exchange inside the interlayer before the monomer swelling step. In this method polymerization is occurred from the surface of aluminasilicate layer (Figure 3.8) (Mittal 2010).

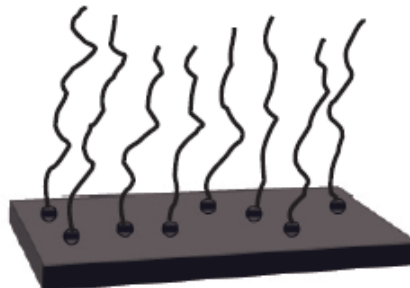


Figure 3.8. Representation of the polymerization from the surface of aluminasilicate layer (Source: Mittal 2010)

3.4.3. The Melt Intercalation Method

Melt compounding is the most commonly used approach for preparing polymer nanocomposites. High molecular weight polymers such as poly-propylene (PP), polyethylene (PE) and polystyrene (PS) can be melted at high temperature. The penetration of polymer matrix into clay galleries is achieved by heat and shear. A mixture of polymer and layered silicates are annealed above the softening point of polymer to achieve a uniform dispersion of filler. One of the advantages of this method is environmentally compared to in situ and solution intercalation method due to the absence of organic solvents. The melt intercalation method allows using polymers which were previously not suitable for in situ polymerization or the solution intercalated method (Okamoto 2005). Ammonium based surface modifications have an onset of degradation close to 200°C, which is a common temperature used for melt compounding of the polymers. Any degradation of the surface modification could have a serious impact on the composite properties (Mittal 2010).

3.5. Polyhydroxyalkonates (PHAs) Layered Silicates Nanocomposites (PHA-LSN)

As mentioned before, PHAs are the promising class of biopolymer types that can partially take place of oil based polymers. However, PHAs suffer from poor mechanical and barrier properties compared with conventional polymers. Moreover, PHAs suffers from thermal instability during aging process. Thus, researches have been focused on to enhance the properties of PHAs by different methods. Blending, copolymerization, or additives are the common methods that are used. However, the most promising method is the incorporation of layered silicates into polymer matrix (Maiti et al. 2003; Botana et al. 2010) (Erceg et al. 2010)

3.5.1. Barrier Properties of Layered Silicate Nanocomposites

It has been observed that the diffusion of small molecules through polymer matrix follows Fick's law. However, it becomes more complicated if layered silicates are incorporated to polymer matrix. The molecule diffusion from Fick's law deviates in

the presence of nanoplates, because it changes the way of penetrant molecule by blocking the diffusion path. Thus, different kinds of models were developed to explain the mechanism of the permeability of nanocomposites by considering the morphology of nanoplates including degree of dispersion, aspect ratio and orientation.

Most of the permeation property models were built upon the tortuous path theory, which is mainly based on three assumptions:

- The nanofillers are impermeable to gas or liquid molecules
- The interface between the matrix and nanofillers is perfect, thus impermeable to gas or liquid molecules
- The presence of nanofillers does not alter the permeation properties of matrix material itself.

The properties of nanocomposites need to be modeled in order to design the materials with optimum improvement in properties. However, conventional models have not been designed to explain the nanocomposite behavior and thus need to be appropriately modified. Different kinds of models are developed using different assumptions such as orientation of layered silicates in polymer matrix (Figure 3.9). Moreover, the general assumption is based on the path that penetrant molecule takes place such a way that penetrant molecule is not soluble in the filler and also filler is not permeable to penetrant molecule. Thus, while the molecule passes through the polymer matrix it passes around the filler.



Figure 3.9. a) Regular oriented b) Random oriented silicate layers in polymer matrix
(Source : Cornwelle 2009)

The permeation of gases through mineral filled polymers was first dealt in model by Nielsen. As mentioned above, the reduction in permeability in the composites is based on the increase of the pathway of a gas molecule through a composite caused by filler. The model was based on regular arrangement of two dimensional, rectangular platelets that aligned perpendicular to diffusion direction increasing the tortuosity.

Nielsen assumes that there is no structure change in layered silicate during the nanocomposite preparation. An increase in the tortuosity is resulted from the aspect ratio of layered silicates. Thus, Nielsen model takes it in account while construction the model equations. Since Nielsen Model is one of the basic models, the derivation of the mode was given below to give an idea about tortuosity based permeability models(Cornwelle 2009).

Fisk's Law explains the permeability in a basic way (equation 3.1) without considering the layered silicates. Solubility (S) and diffusion (D) are depended on the free volume fraction in polymer composites.

$$P = D * S \quad (3.1)$$

$$S = S_0(1 - \phi) \quad (3.2)$$

$$D = D_0/\tau \quad (3.3)$$

where ϕ is the volume fraction of nanoparticles located in polymer matrix. Solubility is affected from volume fraction on contrary to solubility; diffusion is depended on the tortuosity (τ). D_0 and S_0 represent the diffusion and solubility coefficients of pristine polymer. Tortuosity is depended on the aspect ratio (length of particle (L)/thickness of particle (W) and shape of nanoplates as well. Tortuosity is defined in equation 3.4.

$$\tau = l'/l \quad (3.4)$$

where l is the thickness of film, l' is the distance of a penetrant molecule that it must travel in the presence of nanoplates. Considering the definition of aspect ratio, each plates increases the diffusion path by $L/2$. Thus equation 3.4 becomes as follows;

$$l' = l + N(L/2) \quad (3.5)$$

Where N is the number of platelets on the path:

$$N = \frac{l\phi}{W} \quad (3.6)$$

Then the distance a penetrant molecule must travel (l') becomes as:

$$l' = l \frac{l\phi}{W} \quad (3.7)$$

And tortuosity (τ) defines by the combination of Equations 3.5 and 3.7.

$$\tau = l + \frac{l\phi}{2W} \quad (3.8)$$

Thus the diffusion parameter of modified Fick's Law (Equation 3.1) becomes as:

$$D = \frac{D_o}{1 + \frac{l\phi}{2W}} \quad (3.9)$$

and substitution Equation 3.2 to 3.9 resulted in the following Equation 3.10:

$$P = \frac{D_o}{1 + \frac{l\phi}{2W}} S_o (1 - \phi) \quad (3.10)$$

In order to compare the permabilities of pristine and composite polymer films Equation 3.10 is divided the permeability of neat polymer. Relative theoretical permeability of a polymer can be calculated by the Nielsen Model:

$$\frac{P}{P_o} = \frac{1 - \phi}{1 + \left(\frac{\alpha}{2}\right)\phi} \quad (3.11)$$

Volume fraction of composites can be calculated using Equation 3.12:

$$\phi = \frac{1}{1 + \left(\rho_c \frac{(1 - M_c)}{\rho_p M_c}\right)} \quad 3.12$$

where M_c is the mass fraction of filler and ρ_c , ρ_p are the densities of polymer marix and filler respectively. Dependency of relative permeability of LS composites to

aspect ratio and silicate volume fraction is predicted using Nielsen Model (Figure 3.10) As seen in the Figure 3.10, the tremendous enhancement can be obtained for higher aspect ratio since path required to be traveled by a diffusing molecule become significantly longer.)

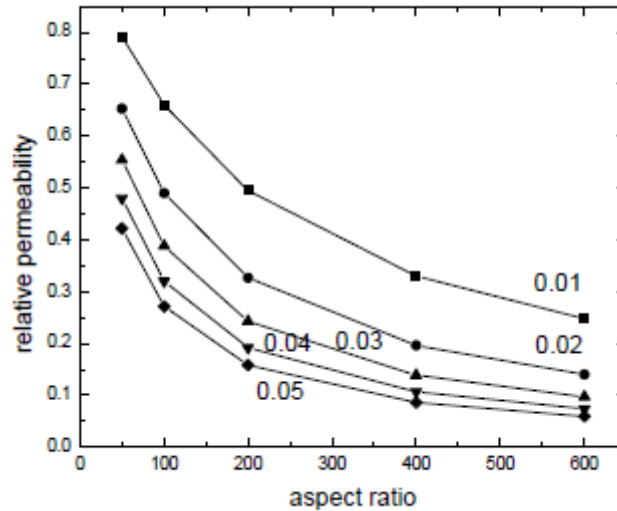


Figure 3.10. Relative permeability predictions based on Nielsen Model as a function of aspect ratio at different layered silicate volume fraction (Source: Mittal 2010)

The analytical solution provided by Nielsen was further compared with modern day simulation techniques and more refined expression was predicted. Cussler-Arris developed a mathematical model for gaseous diffusion in polymer matrix considering the geometry of layered silicates in polymer matrix. Regular and random orientations of layered silicates affect the permeability in a way that the difference in mean free paths of the molecule has to traverse in both the cases. According to their assumption in regularly and align layered silicates, the model becomes as:

$$\frac{P}{P_0} = \frac{1 - \phi}{1 + \left(\frac{\alpha\phi}{2}\right)^2} \quad (3.13)$$

However, when the alignment of LS in polymer matrix is assumed as random Cussler model becomes as:

$$\frac{P}{P_o} = \frac{1 - \phi}{\left(1 + \frac{\alpha\phi}{3}\right)^2} \quad (3.14)$$

The derived model Equation 3.14 differs from other model equations for, as mentioned before aspect ratio affect the mean free path by L/2 in regular LS dispersion, on contrary in random LS dispersion mean free path is affected by L/3 (Cornwelle 2009).

Bharadwaj extended the Cussler model by considering the direction of solute molecule to layers. Cussler and Nielsen models, it is assumed that solute molecule diffuse perpendicular to LS. However, Bharadwaj considered the effect of diffusion direction and derived a new model equation 3.15 (Bharadwaj 2001).

$$\frac{P}{P_o} = \frac{1 - \phi}{1 + \frac{\alpha\phi}{3}\left(S + \frac{1}{2}\right)} \quad (3.15)$$

where S represents the direction of diffusion to the layers which can be calculated as;

$$S = \frac{1}{2(3\cos^2\theta - 1)} \quad (3.16)$$

where θ denotes the angle between diffusion direction and the orientation of solute with respect to layers and $\cos\theta$ can vary between the value of 0 and 1.

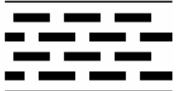
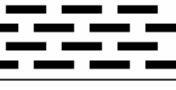

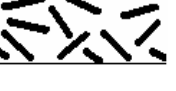
Based on different modeling approaches and assumptions in the orientation of the filler,

Table 3.3 indicates the permeability models for nanocomposite systems. These models give an idea about the aspect ratio of layered silicates in polymer matrix.

When dilute LS containing composite systems are used, the models become more applicable because, dispersion of layered silicates is achieved in exfoliated structure which supports the assumption that is made. As the degree of exfoliation increases, the aspect ratio increases as well. The aspect ratio of layered silicates was found in the range of 10 to 1000 (Sun et al. 2008). The models are more applicable when the possible interactions between the polymer matrix and nanofiller have been

ignored. In reality, it has been reported that nanofillers can nucleate or restrict crystallization of some semi crystalline thermoplastics affecting the crystallization kinetic (Cornwelle 2009).

Table 3.3 Permeability models for nanocomposites
(Source: Sun et al. 2008)

Models	Filler Type & orientation	Dimension	Aspect Ratio	Formulas
Nielsen	regular array, oriented 	2D	w/l	$\frac{P}{P_o} = \frac{1 - \phi}{1 + \left(\frac{\alpha}{2}\right)\phi}$
Cussler-regular array	regular array, oriented 	2D	w/l	$\frac{P}{P_o} = \frac{1 - \phi}{1 + \left(\frac{\alpha\phi}{2}\right)^2}$
Cussler random array	random array, oriented 	2D	w/l	$\frac{P}{P_o} = \frac{1 - \phi}{\left(1 + \frac{\alpha\phi}{3}\right)^3}$
Bharadwaj	random array, non-oriented 	2D	w/l	$\frac{P}{P_o} = \frac{1 - \phi}{1 + \frac{\alpha\phi}{3}\left(S + \frac{1}{2}\right)}$

Gatos and coworkers studied the effect of the aspect ratio of silicate platelets on the barrier properties of hydrogenated acrylonitrile butadiene rubber (HNBR)/layered silicate nanocomposites. They investigated the oxygen barrier properties of HNBR/layered silicate nanocomposites and found that the best matching model to experimental data was Bharadawaj's equation when taking the order parameter (S) as 0.90. Therefore, it is concluded that layered silicates are not fully horizontally oriented in polymer matrix (Gatos and Kargerkocsis 2007).

Sanchez-Garcia and coworkers studied the barrier properties of polyhydroxybutyrate (PHB) layered silicates nanocomposite films. The incorporation of layered silicates (4% w/w MMT) in polymer matrix resulted in decrease in oxygen permeability up to 75 % compared to pristine PHB: However, the barrier properties of

the systems did not fit the most widely applied models such as Nielsen and Fricke for oriented and random dispersion of the fillers. The enhancements in barrier properties were found to depend on the penetrant and did not clearly match morphological observations in terms of aspect ratio. This might be due to the limitations of models that does not account the factors such as polymer morphology and crsytallinity alterations, irregular morphology and orientation of filler platelet, chemical alterations in the matrix, and solubility of the penetrants in the filler (Lagaron et al. 2008) .

3.5.2. Mechanical Properties of Layered Silicate Nanocomposites

Fillers play an important role in enhancement of polymer properties and reducing cost of their composites. In order to enhance the mechanical properties of polymers, fillers such as glass bead, talc, calcium carbonate with dimensions in the micrometer are added to polymers by changing the volume fraction, shape, and size of the filler particles in polymer matrix However, Toyota research group reported that when the filler with dimension in the nanometer range is added to polymers, remarkable enhancement in physical and mechanical properties could be achieved in a larger extent (Tjong 2006) .

Improvement in mechanical properties such as Young's modulus, yield stress, ultimate stress and strain is due mainly to the nanosize dimensions of fillers. Many reports have concluded that high aspect ratio of fillers supplies a strong interaction between filler and polymer. The stiffness of polymer nanocomposites generally increases with the nanoparticles volume fraction, as long as sufficient dispersion and degree of exfoliation of these particles are ensured. Many studies exist in the literature related to the mechanical improvements by incorporation of layered silicates into polymer matrix such as chitosan (Oguzlu and Tihminlioglu 2010), polyhydroxybutyrate (Sanchez-Garcia et al. 2008), polyethyleneterephthalate (Bandyopadhyay et al. 2008) In all these studies, it was reported that addition of MMT in small amount enhanced the mechanical properties due to its high aspect ratio. In addition, the type of filler surface treatment governs the degree of dispersion thus it affects the interfacial interaction which specifies improvement in mechanical properties (Mittal 2010).Moreover, Choi and coworkers (2003) studied the effect of addition of organically modified montmorillonite (OMMT) intro to poly(hydroxybutyrate-co-hydroxyvalerate) PHBHV

matrix on mechanical properties. They concluded that even at low clay content (3 wt % organo clay Cloisite 30B), tensile strength was greatly improved about 55% compared to pristine PHBHV. This improvement is attributed to the strong hydrogen bonding between PHBHV copolymer and Cloisite 30B, indicating the importance of the organomodification of silicate layer (Choi et al. 2003). Botana and co workers studied PHB nanocomposites prepared by unmodified and modified MMT. They reported that no significant improvement in tensile strength was obtained with respect to pristine PHB. Only slight increase in Young's modulus was obtained for the modified MMT incorporated samples due to the intercalated structure of the composites. Improvements in tensile strength of layered silicate nanocomposites were attributed to degree of bonding between nanoclay and polymer matrix (Ray and Bousmina 2005; Pavlidou and Papaspyrides 2008)

In addition, Oguzlu and Tihminlioglu (2010) investigated the enhancement in properties of chitosan due to incorporation of an organically modified montmorillonite (Cloisite 10A). Besides the improvement in barrier and thermal properties, they reported enhancement in mechanical properties with addition of Cloisite 10A. Even small amount of clay loading (10 wt %) resulted in an improvement in tensile strength about 80 % compared to pristine chitosan. Moreover, the enhancement in strain at break was about 50 %. This improvement is attributed to the structure of layered silicate in polymer matrix as exfoliated/intercalated as supported by X-Ray diffraction analysis (Oguzlu and Tihminlioglu 2010). Generally, literature studies concerning layered silicate nanocomposite systems concluded that improvement in properties is related to dispersion level of layered silicates in polymer matrix (Mubarak et al. 2001; Mai and Yu 2006; Sun et al. 2008).

3.5.3. Thermal Properties of Layered Silicate Nanocomposite Films

Thermal stability of polymers is of fundamental importance in processing and in many applications point of view. An appropriate understanding of thermal stability lies under mechanism of thermal decomposition. The polymer decomposition process is a complex procedure which consists of numerous chemical reactions in the solid material. Also, physical processes that occur simultaneously upon heating and lead to formation of gaseous and solid products. At higher temperatures, degradation of polymer begins

by processes such as main chain random scission, hydrogen transfer and chain stripping (Mittal 2010). Therefore, thermal stability of polymers is highly important to application areas such as, synthesise of fire-safe polymeric materials, development of new technologies for efficient energy management; and the thermal recycling of waste plastics.

Therefore, enhancement in polymer properties by incorporation of filler into polymer matrix will also result in improvement of thermal properties (Achilias et al. 2011) .The improvement in glass transition, degradation, melting temperatures of polymer nanocomposites has been investigated. Researches in literature focused on the thermal behavior of composite polymers investigating the thermal decomposition kinetics. Besides of thermal decomposition, crystallization temperature of polymers is a key factor affecting process conditions. Current research investigations have indicated that introduction of layered silicates into polymer matrix results in improvement of thermal stability (Wu et al. 2007; Erceg et al. 2008) .

The thermal stability of polymeric materials is usually studied by thermogravimetric analysis (TGA). The weight loss due to the formation of volatile products after degradation at high temperature is evaluated as a function of temperature. Incorporation of layered silicates into polymer matrix enhance the thermal stability in a way that acting as insulator and being barrier to volatile compounds generated during decomposition. When layered silicates are incorporated in polymer matrix, volatile compounds produced during degradation follows more tortuous path than pristine polymers Therefore, the barrier affect may slow down a rate of mass loss by retarding the escape of volatile products of thermal degradation outside the degrading material. Moreover, layer silicates hinder the diffusion of oxygen into polymer matrix in thermo-oxidative degradation Thus, the barrier effect of nanolayers towards oxygen permeation results in quantitative changes of volatile compounds that evolved during oxidative degradation (Okamoto 2005; Mittal 2010) .

Besides of the barrier affect, the lewis acid sides in silicate layers act as catalysis that speed up the degradation of polymer chains. Therefore, formation of char has been indicated as a mechanism of thermal stability. The typical clay used in polymer based nanocomposites has a twofold catalytic effect on the thermal degradation of organic molecules in close contact with the clay layers. When the temperature is increased in an inert atmosphere, carbon-carbon bond scission is accelerated and this competes with the acceleration of carbon hydrogen bond scission in the presence of oxygen (Mittal 2010) .

Choi and coworkers investigated the effect of OMMT on thermal properties of poly(hydroxybutyrate-co-hydroxyvalerate) (PHBHV) nanocomposite films. As a result of TGA analysis, they found that the weight loss of pristine PHBHV copolymer started at 252 C° and that of nanocomposites with 1 and 2 wt % loaded samples increases to 259 C°. Moreover, 3 wt % loaded sample has higher weight loss temperature of 263 C°. The increase in thermal stability observed for nanocomposites may be altered to the nanodispersion of silicate layers. The well dispersed and layered structure of clay in the polymer matrix is thought to be an effective barrier to the permeation of oxygen and combustion gas, which improves thermal stability (Choi et al. 2003).

The other mechanism for thermal stability improvement is the restriction of molecular motions and related changes in the kinetic and mechanisms of reactions and physical processes. Recent studies have confirmed a change in the molecular dynamics of polymer chains is due to the filler polymer interactions that results in an increase in the glass transition temperature (Tg). Wang and coworkers concluded that by incorporation of OMMT into PHBHV resulted in to a higher glass transition temperature with increasing amount of OMMT. Moreover, OMMT acted as a nucleating agent in the PHBHV matrix, which increases the nucleation and the over-all crystallization rate of nanocomposites (Wang et al. 2005).

In order to understand thermal degradation of polymer nanocomposites, some of studies have focused on isothermal degradation kinetics. Erceg and coworkers investigated the effect of clay loading on isothermal degradation of PHB nanocomposite films. The kinetic triplet; kinetic model, activation energy, and preexponential factor were determined for PHB nanocomposite films at different amount of filler content. Kinetic analysis was performed by using reduced time plots and free isoconversional methods. Experimental data fitted very well to Avrami-Erofev kinetic model. By applying this model, the activation energy of nanocomposite samples was evaluated. They found that even at small addition of OMMT resulted in increase in activation energy. The pristine polymer PHB has the activation energy 111.1 kJ mol⁻¹ and 1 wt % OMMT loaded PHB has 136 kJ mol⁻¹. However, after 1 wt % OMMT loading the activation energy decreases with an increase of OMMT loading. Activation energy of PHB composites containing 7 wt % OMMT decreased down to 96 kJ mol⁻¹. It could be concluded that dispersion of layered silicates affect the activation energy for, layered silicates can acts as insulator thus heat transfer to polymer chains getting harder causes increase in activation energy. When the dispersion is in exfoliation level, insulation and

barrier affects increases, and therefore better thermal stability is achieved in nanocomposite films.

CHAPTER 4

EXPERIMENTAL STUDY

4.1. Materials

In this study, (PHB) and poly (hydroxybutyrate-co-valerate) (PHBHV) polymers from two different suppliers ((Aldrich and Good Fellow Company) were used throughout this thesis, PHB and PHBHV supplied from Aldrich and Good Fellow are called as PHB-S, PHBHV-S, PHB-P and PHBHV-P respectively (Table 4.1.). To prepare PHB-S composites by solvent casting method, chloroform (Merck) was used as solvent. Nanocomposites were prepared by using the commercial organomodified layered silicates montmorillonite, Cloisite 10A (125 meq/100g clay) obtained from Southern Clay Products. Inc. (Gonzales, Texas) (Table 4.2.).

Table 4.1. Properties of PHB and PHBHV polymers

Polymer Type	Density (g/m ³)	Valereta Content %
PHB-S	1.25	none
PHBHV-S	1.25	5
PHB-P	1.24	none
PHBHV-P	1.24	12

Table 4.2. Properties of Cloisite 10A

Clay Type	Density (g/m ³)	Organic Modifier	Cation Exchange Capacity (meq/100g clay)
Cloisite 10A	1.90	2MBHT	125

4.2. Preparation of PHB and PHBHV Nanocomposite Films

PHB-AL and PHBHV-AL nanocomposite films were prepared by solution intercalation method. Firstly, Cloisite 10A at different amount (1-3-5-7% w/w) was

dispersed in 20 ml chloroform solvent by stirring for 1 day. After the swelling process of layered silicates, in order to increase the interlayer distance of clay stacks, stirred solution was sonicated for 60 minutes using ultrasonic probe sonicator (Sonix Vibracell 505) working at 35% capacity of its 20 kHz output. 1 g of PHB or PHBHV was dissolved within the clay dispersion (5% w/v chloroform) at 60°C in a reflux system. In order to achieve further penetration of PHB-PHBHV into galleries of clay particles, PHB-PHBHV clay solution was sonicated for 60 minutes.

In order to prevent overheating and polymer decomposition within the polymer suspension during sonication process, cooling water bath was used at 15°C. The prepared solution was then immediately cast onto glass plates with a custom blade of 500µm in height using automatic constant speed film applicator (Sheen 1133N).

PHB-P and PHBHV-P nanocomposite films were prepared by melt intercalation method. Polymer and clay were compounded by means of Haake Rheomixer 600 (Thermofisher). The mixing was carried out in a close chamber with two rotor blades rotating in opposite directions. The rotor speed could be adjusted to achieve good dispersion of filler in polymer matrix. The mixing chamber is about 63 cm³ surrounded by three walls. Temperature of the three walls can be adjusted individually to get optimum mixing temperature. Torque of two rotors damped via “Convert Data” software can be observed during mixing. Therefore, filler can be introduced to mixing chamber at stabilization conditions via monitoring the torque data. The nanocomposites were prepared by addition of Cloisite 10A at different concentrations when the torque of pristine polymer melt became stabilize condition. The wall temperatures were set to 155 °C and 145 °C for PHB and PHBHV polymers, respectively. The optimum wall temperature was determined previously by considering mechanical properties (Figure A.1 and A.2) of the composites prepared at 145 °C, 155 °C, and 160 °C mixing temperatures for fixed Cloisite 10A loading (2 wt%). Samples at different clay content were mixed for 10 minutes and at constant rotor speed of 50 rpm. The compounded samples taken from rheomixer were compression molded via Carver hot press to form sheet like films. Samples were molded to form rectangular sheet with dimensions 150x150x0.1 mm³. PHB and PHBHV composites were heated without pressure for 5 minutes to 170 °C and 160 °C, respectively. Then molten composites were pressed at 2000 psi pressure at constant temperature for 5 minutes. The specimens were cooled down to 40 °C via city water supply flowing at same flow rate. Resulting composites were named according to polymer type, processing method and clay content in the

composite and listed in Table 4.3. For instance, PHB-S-1 was prepared by solution casting method and involves 1% w/w of Cloisite 10A.

Table 4.3. Sample codes of prepared films depending on preparation method and Cloisite 10A

Sample Code	Polymer Type	Cloisite 10A Concentration (w/w)	Preparation Method
PHB-S-N	Aldrich	0	Solution
PHB-S-1	Aldrich	1	Solution
PHB-S-3	Aldrich	3	Solution
PHB-S-5	Aldrich	5	Solution
PHB-HV-S-N	Aldrich	0	Solution
PHB-HV-S-1	Aldrich	1	Solution
PHB-HV-S-3	Aldrich	3	Solution
PHB-HV-S-5	Aldrich	5	Solution
PHB-P-N	Good Fellow	0	Melt
PHB-P-1	Good Fellow	1	Melt
PHB-P-3	Good Fellow	3	Melt
PHB-P-5	Good Fellow	5	Melt
PHB-P-7	Good Fellow	7	Melt
PHB-HV-P-N	Good Fellow	0	Melt
PHB-HV-P-1	Good Fellow	1	Melt
PHB-HV-P-3	Good Fellow	3	Melt
PHB-HV-P-5	Good Fellow	5	Melt
PHB-HV-P-7	Good Fellow	7	Melt

4.3. Determination of Film Thickness

Thickness of prepared PHB-S, PHBHV-S, PHB-P and PHBHV-P nanocomposite films with various clay contents were measured with an electronic digital micrometer (293-821, Mitutoyo) with 1 μ m sensitivity. At least ten measurements from random sections of films were measured. Thickness of polymers was used to evaluate permeability and mechanical properties of nanocomposite films.

4.4. Fourier Transform Infrared (FTIR) Analysis of PHB and PHBHV Nanocomposite Films

Chemical structure of PHB and PHBHV nanocomposite films were evaluated based on FTIR analysis. IR spectra were taken at a resolution of 4 cm⁻¹ in the range of

400 to 4000 cm^{-1} wave number range using ZnSE crystal and DTSG detector with a FTIR spectrometer (Perkin Elmer Spectrum 100) equipped with ATR accessory.

4.5. X-Ray Diffraction (XRD) Analysis of PHB-PHBHV Nanocomposite Films

The structure of Cloisite 10A and its dispersion in polymer matrix were characterized using Philips X'Pert Pro MRD (Cu $K\alpha$ radiation $\lambda=1.54\text{nm}$, 40 kV, 40 mA) between scanning range of 2° and 10° . Based on Braggs' Law interlayer distance between silicate layers were evaluated:

$$\lambda = 2d\sin\theta \quad (4.1)$$

Where, λ is the wavelength of X-Ray θ is diffraction angle and d is interlayer distance.

4.6. Water Vapor Permeability Measurements of PHB and PHBV Nanocomposite Films

Water vapor permeability measurements of PHB and PHBV nanocomposite films were carried out using Mocon Permatran 3/33. The effect of Cloisite 10A in both on PHB-S and PHBV-S polymers on water vapor permeability (WVP) of the nanocomposites was determined according to ASTM F1249 standard at 37.8 C and 90% RH. Test film was placed between two test cells. Nitrogen as a carrier gas was passed through ultra pure water to adjust the RH and flowed to the test film with 100 cm^3 per minute. The edges of the test cell are tightly sealed to prevent air entering into cell. Sample area was fixed to 5 cm^2 (Figure 4.1). Data were recorded as water vapor transmission rate (WVTR). All the results related to water vapor permeability shown in the present work represent the average of two or three independent experimental measurements. The data was recorded as water vapor transmission rate (WVTR). Permeability of the samples (g (water vapor) thickness (mm) per area (m^2) time (day) pressure (mmHg)) was calculated using Equation 4.2:

$$Permeability = \frac{WVTR}{S(R_1 - R_2)} * L_{film} \quad (4.2)$$

where:

WVTR: Water Vapor Transmission Rate

R₁: Relative humidity at the source expressed as fraction

(R₁=1.00 for a 100% RH Chamber, and for 90% RH chamber R₁=0.90)

R₂: Relative humidity of the vapor sink expressed as fraction

S: Vapor pressure of water at the test temperature

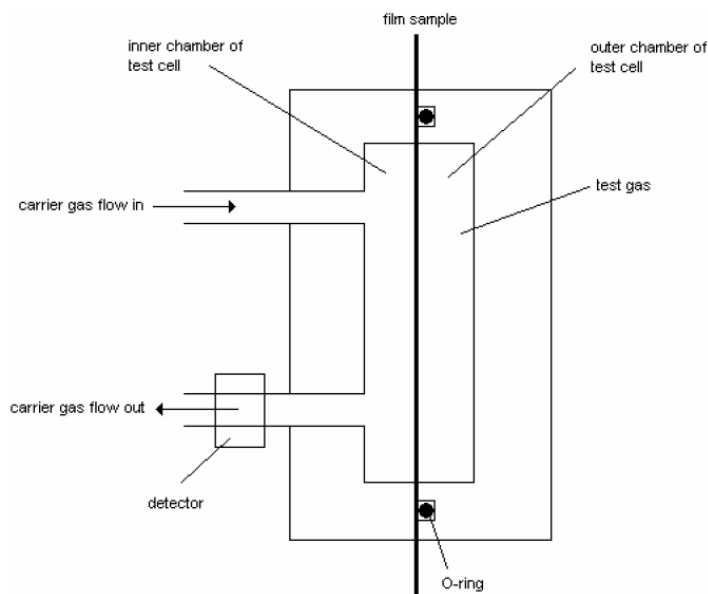


Figure 4.1. Representation of water vapor transmission measurement

4.7. Mechanical Property Determination of PHB-PHBHV Nanocomposite Films

Mechanical properties such as modulus of elasticity, tensile strength percent elongation at break, yield strength and percent elongation at yield were determined with texture analyzer (TA XT Plus) equipped with a 5 Kgf load cell in tensile mode. Mechanical properties were tested according to ASTM D-882 standart. The films were cut in 10mm width and 120mm in length and kept into environmental chamber at 50% RH and 23 °C before testing. The initial gauge length and testing speed were fixed at 100mm and 10 mm/min. Percent elongation at break which indicates the ratio of length of the sample at rupture of film to initial length of the sample were read from stress-

strain curve. Young's moduli of tested films were calculated from slope of the linear part of stress-strain curve. At least seven films samples were tested and the average of five results was reported.

4.8. Thermal Stability of PHB-PHBHV Nanocomposite Films

In order to investigate thermal stability of nanocomposite films, differential scanning calorimetry (DSC), and thermal gravimetric analysis (TGA) analyses were performed. Analyses were carried out by means of TA instruments Q10

In order to investigate thermal stability of PHB and PHBV nanocomposite films isothermal degradation and nonisothermal crystallization kinetics were carried out by TGA and DSC analyses.

Besides of kinetic studies, glass transition, crystallization, melting and degradation temperatures were evaluated.

4.9. Isothermal Degradation Study of PHB and PHBV Nanocomposite Films

Isothermal degradation study was carried out at different temperatures to evaluate the isothermal degradation kinetic parameters. Samples were heated under nitrogen flow (50ml/min) from room temperature to 230, 240 and 250 °C at rate of 10°C/min.

4.10. Non-Isothermal Crystallization Study of PHB and PHBV Nanocomposite Films

In order to evaluate temperature dependency of crystallization process, DSC analyses were carried out under nitrogen flow of 50L/min with different heating and cooling rates of 5, 10, and 20 °C/min. First of all, samples were heated from 25 °C to 190 °C, and then in order to erase the crystal history, samples were kept at 190 °C for 5 minutes. After that, samples were cooled down to -20 °C and also kept at that temperature for 5 minutes. Then, samples were heated up to 250 °C.

4.11. Contact Angle Measurements of PHB-PHBHV Nanocomposite Films

Contact angle measurements of PHB-PHBHV nanocomposite films were carried out by means of Attention Theta Optical Tensiometer, KSV. The surface wettability property of films was performed by dropping 6 μ l of water on the film surface. Images of water droplet were recorded in trigger mode. Each measurement was evaluated by taking ten images of water droplet at one second interval. At least ten measurements at random places of surface of the films were reported. Left and right side of contact angle of water droplet on nanocomposite films were analyzed via the software of device.

4.12. Color Measurements of PHB-PHBHV Nanocomposite Films

The color change due to addition of clay particles to PHB and PHBV polymers were investigated using a colorimeter (Avantes). Pristine PHB and PHBV films were used as reference background. Based on Hunter method; L, a, and b values were averaged from three readings for each film. Readings from horizontal and vertical axis represented as L, a, and b values respectively. L indicates the lightness ranging from black to white as vertical axis. The a and b values are the chromatic coordinates (ranging from a: greenness to redness and b: blueness to yellowness). The results are reported as the total color difference (ΔE) that can be calculated with the following equation;

$$\Delta E = \sqrt{\Delta L^2 + \Delta a^2 + \Delta b^2} \quad (4.3)$$

4.13. Biodegradation of PHB-P Nanocomposite Films

Biodegradability of prepared PHB-P nanocomposites was evaluated via enzymatic degradation via *Pseudomonas* Lipase. Each piece of PHB-P films with 1x10 cm² size was placed in a 15 ml centrifuge tube filled with 10 ml of pH 7.0 phosphate buffer with 600 μ g (lipase)/ml concentration. Degradation process was performed in an environmental chamber at 37 °C. Samples were taken from the degradation medium

after 1, 2, 3, 4, 5, 8 weeks. Degradation process was monitored based on gravimetric measurements of each samples.

CHAPTER 5

RESULTS AND DISCUSSION

PHB and PHBHV nanocomposites were prepared via solution intercalation and melt mixing methods. Nanocomposites were prepared by introducing at different amount of Cloisite 10A (1, 3, 5, 7% w/w) into polymer matrix.

The goal of the study was to investigate the effects of Cloisite 10A content and preparation techniques of nanocomposites on the water vapor permeability (WVP), mechanical, thermal, and optical properties of prepared nanocomposites were investigated. Moreover, structural characterizations of nanocomposites were also carried by XRD and FTIR analysis.

5.1. Structural Analysis

In order to characterize interaction between silicate layers and polymer chains structural analyses of prepared PHB and PHBHV nanocomposites films were carried out via XRD, FTIR, and SEM analyses.

5.1.1. X-Ray Diffraction (XRD) Analysis

XRD analysis is commonly used for the interpretation of nanocomposite structure. This technique helps to quantify changes in basal plane spacing in the layered silicates due to penetration of polymer chains. The changes in basal plane spacing lead to information regarding the possible structure of layered silicates in polymer matrix. The intensity of X-ray diffractograms is generally taken as a measure of classifying the microstructure as either intercalated or exfoliated. Moreover, the distance between layers can be determined via Bragg's Law. Additionally, if the basal reflections of layered silicate polymer nanocomposites do not change with respect to characteristic peak of nanoclay, phase separated structure is obtained (Mittal 2010) .

Figure 5.1 indicates the XRD pattern of Cloisite 10A. The characteristic peak of Cloisite 10 A was obtained at 4.65° scanning angle. The inter planer distance (basal d-

spacing) was calculated as 1.92 nm via Bragg's Law. Position of characteristic Cloisite 10A peak was in agreement with the value reported by the producer.

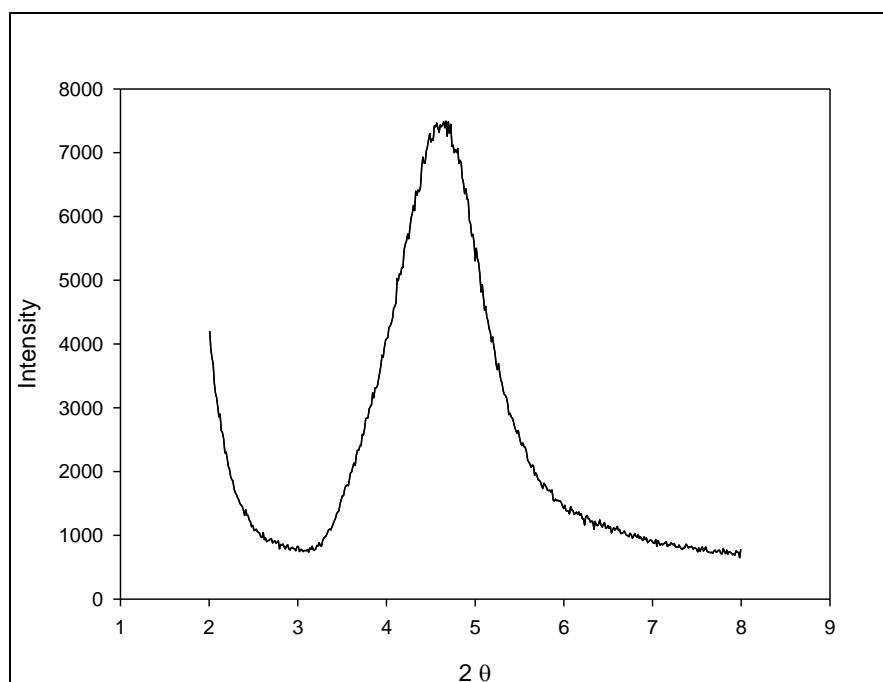


Figure 5.1. XRD Pattern of Cloisite 10A

Figure 5.2 indicates the XRD patterns of PHB-S nanocomposites prepared via solution intercalation method. X-Ray diffractograms of PHB-S-N did not exhibit any peak around 2-9° scan angle interval. It is an evident that there is not any characteristic peak of pristine PHB which can be overlap with characteristic peak of Cloisite 10A. Even if PHB-S-1 coded sample containing 1% w/w of Cloisite 10A, the characteristic peak of Cloisite 10A was not observed due to the, disappearance of characteristic peak as a consequence of exfoliated structure obtained for PHB-S-1 nanocomposite. However, in the case of sample PHB-S-3, the characteristic peak at 3.65° was observed. The movement of the basal reflection of clay to lower angle indicates that the formation of an intercalated nanostructure (Okamoto 2005). The basal plane space of PHB-S-3 nanocomposite was calculated as 2.30 nm. Increase in basal space was due to penetration of polymer chains into silicate layer galleries. In literature, many studies showed that exfoliated structure was obtained at lower content of clay loading (Gatos and Kargerkocsis 2007; Sanchez-Garcia et al. 2008; Oguzlu and Tihminlioglu 2010) .

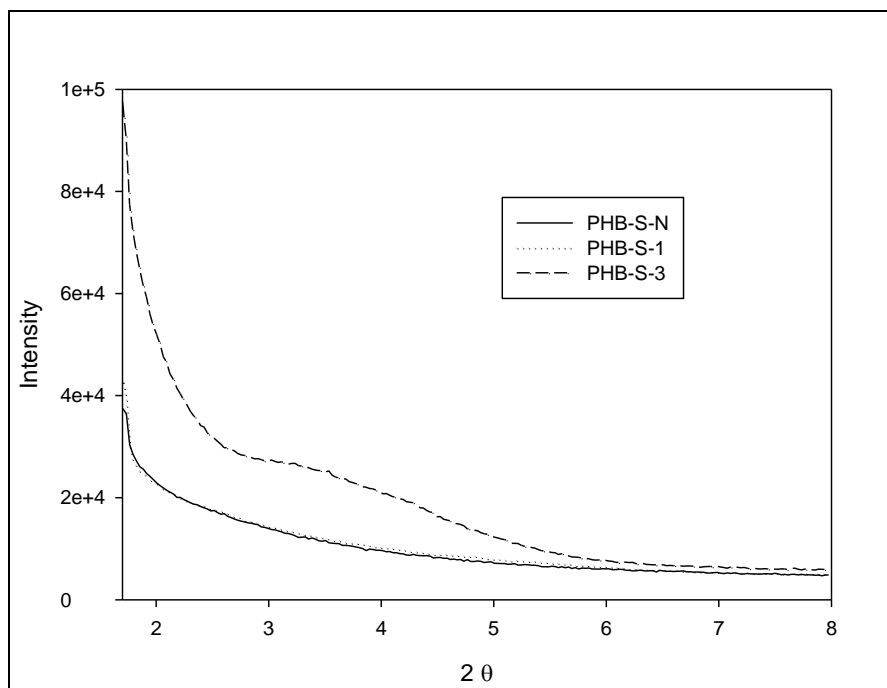


Figure 5.2. XRD Patterns of PHB-S nanocomposites at different Cloisite 10A content

X-Ray diffraction patterns of PHBHV-S and its nanocomposites at different Cloisite 10A content are shown at Figure 5.3. XRD result of PHBHV-S-N indicated no characteristic peak in the scanning range of 1-9°. Moreover, characteristic peak of Cloisite 10A was also disappeared for 1%w/w clay loaded sample (PHBHV-S-1). The vanishing X-ray diffraction pattern of Cloisite 10A is due to exfoliation of silicate layers into polymer matrix. Many literature studies showed that exfoliation of silicate layers are achieved at lower clay content loading (Cervantes-Uc et al. 2007; Gatos and Kargerkocsis 2007). Broadened characteristic peak was observed in the x-ray diffraction patterns of PHB-HV-S-3 sample. Shifting and broadening of characteristic peak is attributed to increase in d-spacing of layer silicates. As the d-spacing increases, the dispersion level of layered silicate increases as well. Therefore, the sample of PHBHV-S-3 can be interpreted as in intercalated structure as being in the case of PHB-S-3.

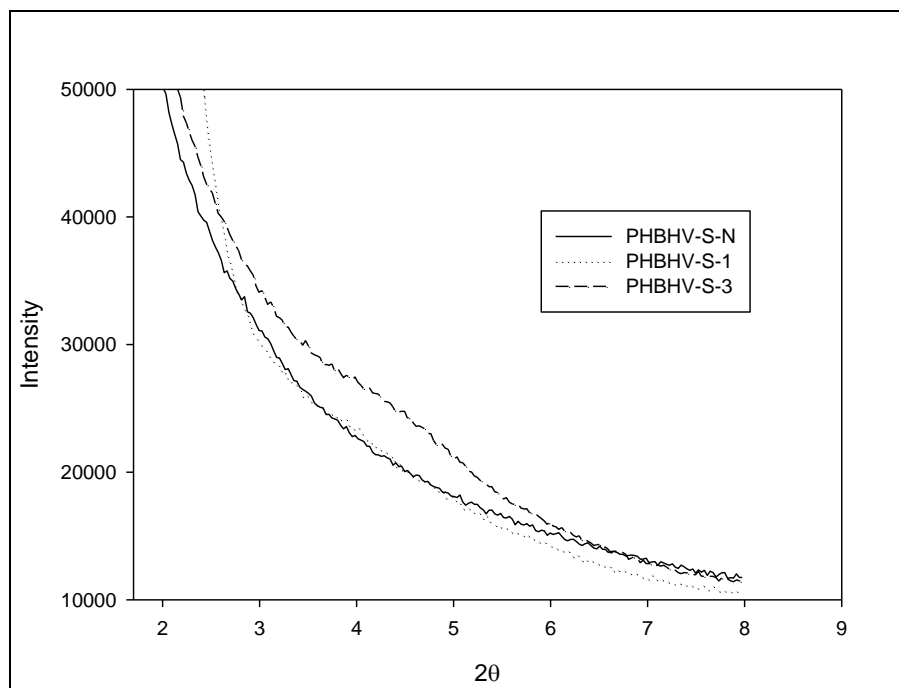


Figure 5.3. XRD Patterns of PHBHV-S nanocomposites at different Cloisite 10A content

XRD results of PHB-S and PHBHV-S nanocomposites showed that at lower Cloisite 10A concentration (1% w/w), exfoliated structure of silicate layers was obtained. However, at higher clay loading (3% w/w) the characteristic peak of Cloisite 10A shifted to lower angles and broadened to larger scan range which was attributed to intercalated structure of silicate layers in polymer matrix. Exfoliation and intercalation showed that penetration of the polymer chains into silicate galleries was achieved due to high interaction between silicate layers and polymer matrix (Mittal 2010).

5.1.2. Fourier Transform Infrared (FTIR) Analysis of PHB and PHBHV nanocomposites

Intercalated or exfoliated structure of silicate layers is dependent on degree of penetration of polymer chains into silicate layer galleries. Penetration of polymer chains into silicate galleries can be resulted in new bond creation due to strong interaction in nanometer scale.(Cervantes-Uc et al. 2007) In this manner, FTIR analyses of the prepared composites were carried out to get information related to bond creations and interactions.

Cloisite 10A was prepared in pellet form using KBr. The FTIR spectrum of Cloisite 10A was carried out in 4000-400 cm^{-1} region (Figure 5.4). FT-IR spectra bands at 3636 and 3395 cm^{-1} are attributed to O-H stretching for the silicate and water, respectively. In addition, a spectrum shown at 1639 cm^{-1} was related to O-H bending. The broad band at 1045 cm^{-1} was assigned to stretching vibration of Si-O-Si from silicate and 916 cm^{-1} from Al-OH-Al deformation of aluminates (Cervantes-Uc et al. 2007). Due to organic modification, bands located at 2924, 2842 and 1475 cm^{-1} were assigned to C-H asymmetric, symmetric stretching and bending vibrations of methylene respectively. In addition, FTIR spectra located at 460 cm^{-1} and 520 cm^{-1} wave numbers assigned to Al-O stretching and Si-O bending, respectively (Cervantes-Uc et al. 2007).

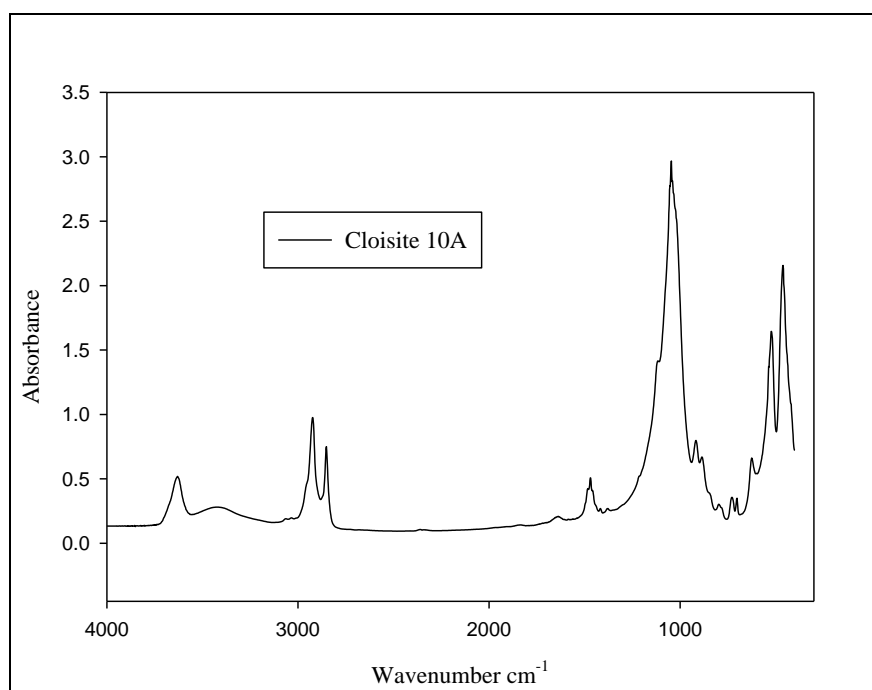


Figure 5.4 FTIR spectra of Cloisite 10A

PHB-S nanocomposite films were analyzed qualitatively via FTIR-ATR. The IR transmittance spectrum of pristine PHB-S-N was shown in Figure A.3. The C=O carbonyl stretching bond of the ester group at 1722 cm^{-1} and symmetric wagging of CH_3 groups were observed at 1380 cm^{-1} . The band at 1230 cm^{-1} was assigned to conformational bond of the helical chains, however no amorphous bands of the same group was not seen. The bond 1184 cm and 1133 cm^{-1} are the asymmetric and symmetric stretching vibration of the C-O-C group respectively (Karbasi et al. 2010).

FTIR spectra of pristine PHB-S-N and its nanocomposites were shown at band range of 1300 to 400 cm^{-1} in Figure 5.5. Due to the alkyl chains from both polymer and Cloisite 10A, nanocomposites at different clay content exhibited the presence of characteristic absorption. Moreover, the most obvious characteristic peak of Cloisite 10A in which indicates the stretching vibration of Si-O-Si at 1040 cm^{-1} did not clearly seen from the spectra of PHB-S nanocomposites. However, the shoulder like behavior of spectrum at 1040 cm^{-1} became sharper compared to pristine PHB-S-N film (see arrows Figure 5.5). Moreover, as the clay content increased, the sharpness of spectrum line increased as well. This behavior at that spectrum could be attributed to vibration of Si-O-Si bond (Lagaron et al. 2008). In addition, the increase in transmittance intensity of spectrum at 460 cm^{-1} could be assigned to Si-O bending. . Moreover, the characteristic peak at 3626 cm^{-1} from Cloisite 10A represents the stretching vibration from O-H bonds (Figure 5.4) was also observed in PHB-S nanocomposite samples (see arrows Figure 5.6)

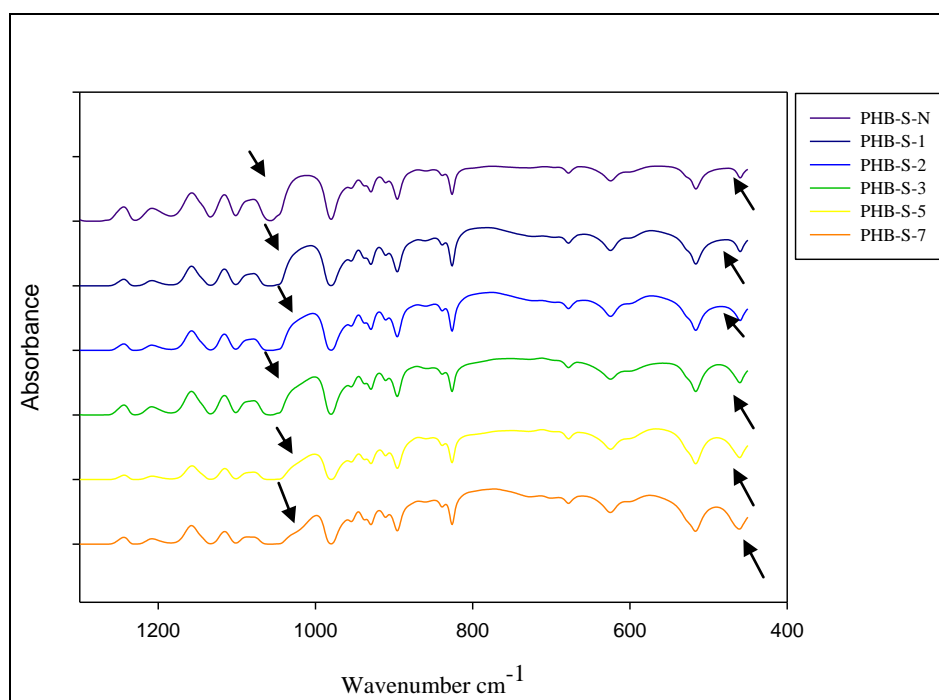


Figure 5.5. FTIR spectra of PHB-S and its nanocomposites at different amount of Cloisite 10A in 1300-400 cm^{-1} region

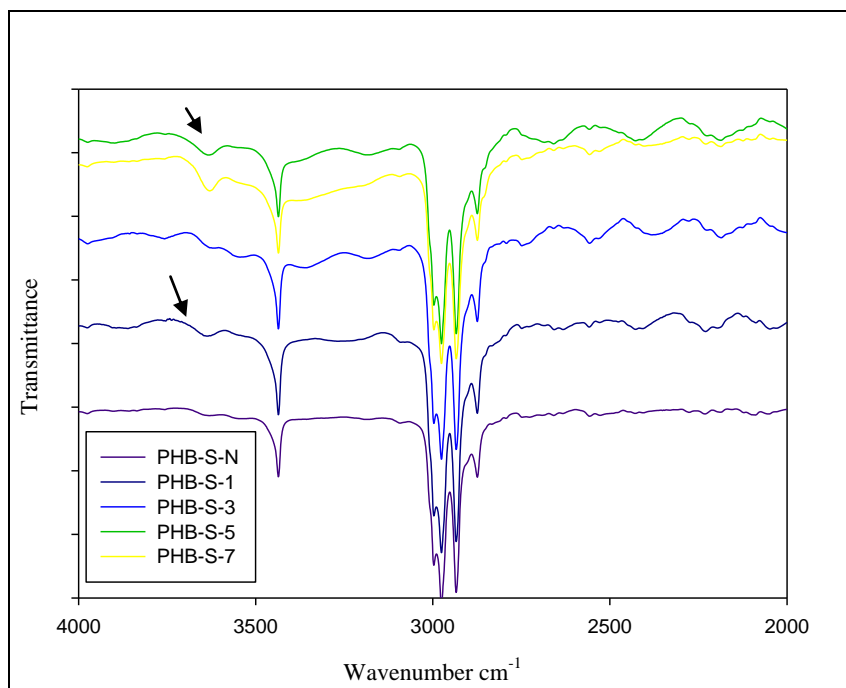


Figure 5.6. FTIR spectra of PHB-S and its nanocomposites at different amount of Cloisite 10A in 4000-2000 cm^{-1} region

The spectra of PHBHV-S nanocomposites showed the same behavior observed for PHB-S nanocomposites (Figure 5.7). The change in spectra at 1040 cm^{-1} and 460 cm^{-1} was attributed as stretching vibration of Si-O-Si and Si-O bending, respectively due to the changes in the interaction between polymer and clay.

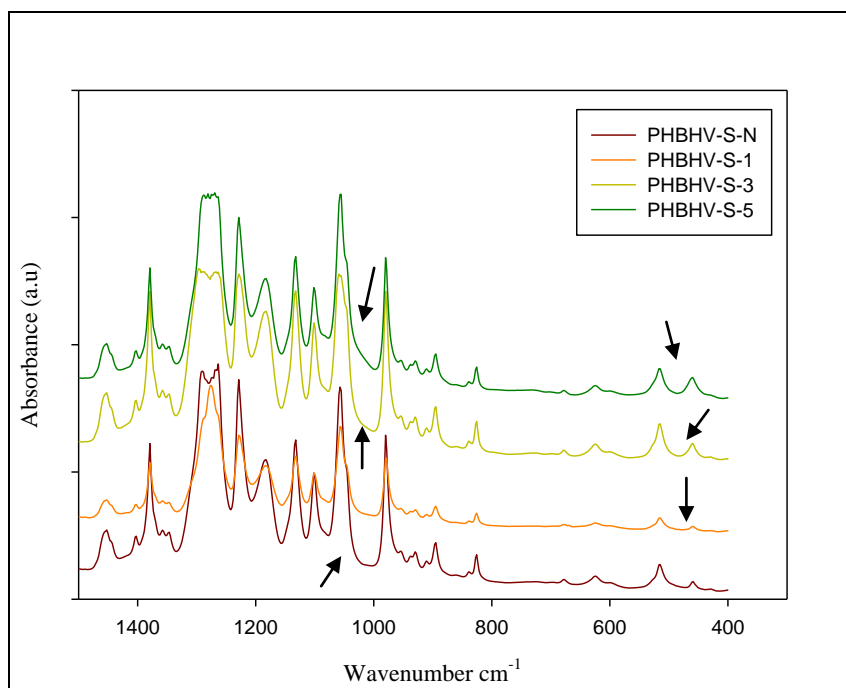


Figure 5.7. FTIR spectra of PHBHV-S and its nanocomposites at different amount of Cloisite 10A in 1500-400 cm^{-1} region

The most obvious changes in nanocomposites due to interaction of Cloisite 10A and polymer chains were observed at PHB-S nanocomposites. This could be resulted from the level of transmittance of IR through the PHB-S and PHBHV-S nanocomposites compared to PHB-P (Figure A.5), and PHB-HV-P (Figure A.4) nanocomposites. Due to the lack of transmittance, the characteristic spectra of Cloisite 10A at 1050 cm^{-1} could not observed as it was in the case of PHB-S and PHBHV-S nanocomposites.

5.2. Water Vapor Permeability of PHB and PHBHV Nanocomposite Films

In food packaging applications, the specific barrier requirement of the package system is related to the product. Generally plastics are relatively permeable to small molecules such as gases, water vapor, and organic vapor. Water vapor permeability (WVP) is one of the most important features of packaging materials, for the packaged product whose physical or chemical deterioration is related to its equilibrium moisture content, that are of great importance for maintain or extending its shelf life. In this manner, this study is aimed to enhance the water vapor barrier properties of pristine PHB and PHBHV films by introducing Cloisite 10A into polymer matrix. This section deals the effect of clay content in both PHB and PHBHV nanocomposite films on water vapor permeability properties. WVPs of all PHB and PHBHV nanocomposite films were tabulated in Table A.1.

Figure 5.8 shows the effect of clay loading on the WVP of PHB-S nanocomposites films. As seen in Figure 5.8, even small amount (1%w/w) of Cloisite 10A addition caused 32.9% reduction in WVP value. Moreover, 2%w/w Cloisite 10A loading resulted in 41.1% reduction in WVP of pristine PHB-S. However, at higher Cloisite 10A loadings (3%, 5%, and 7%w/w), WVP of PHB-S nanocomposites increased significantly. Although the same trend was also observed in PHBHV-S nanocomposite films (Figure 5.9), the improvement was less significant than PHB-S nanocomposites. Moreover, WVPs of nanocomposites prepared via melt intercalation method (PHB-P and PHBHV-P) exhibited same trend however the improvement is only obtained for 1%w/w Cloisite 10A loaded sample, PHB-P-1 and in overall, the enhancement in water vapor barrier properties of both PHB-P and PHBHV-P was not as

significant as improvement in PHB-S and PHBHV-S. In all composites, a critical limit of Cloisite 10A content was observed due to the changes in nanostructure after certain nanoclay loadings. This behavior was also reported by many researchers in the literature for many polymer-layered silicate systems (Oguzlu and Tihminlioglu 2010; Botana et al 2010). Consequently, the nanocomposites prepared via solution intercalation method exhibited better enhancement in water vapor barrier properties than those prepared by melt intercalation method. This could be resulted from dispersion level of silicate layers into polymer matrix since the enhancement in barrier properties was attributed to presence of ordered dispersed particle layers with large aspect ratios in polymer matrix. Moreover, due to the dispersion of layered silicates within the polymer matrix, the more tortuous pathway was obtained. Therefore, as the tortuosity increases, water vapor permeability decreases (Bharadwaj 2001; Mittal 2010). Enhancement in water vapor barrier properties by incorporation of small amount of layered silicates into polymer matrix was reported by many studies (Botana et al. 2010) (Lagaron et al. 2008).

Moreover, the improvement in barrier properties is associated with X-Ray diffraction analysis result which indicated dispersion level of layered silicates in polymer matrix as mentioned in section 5.1.1. XRD results showed that at low concentration of Cloisite 10A (1%w/w) loading, exfoliated structure was obtained for PHB-S (Figure 5.2) and PHB-HV (Figure 5.3) nanocomposite films. Exfoliated structure resulted in higher tortuosity due to large aspect ratio of layered silicates. In addition, many literature studies reported that enhancement in barrier performance was associated with XRD analysis and they concluded that improvement in barrier properties was due to exfoliated structure of layered silicates in polymer matrix (Oguzlu and Tihminlioglu 2010) (Botana et al. 2010)

Since polypropylene (PP) is excellent barrier to water vapor, therefore preferred to be used in many food packaging applications, our results were compared with the PP. It was found that nanocomposites had almost 2 times smaller than WVTR of PP which is 2.62 g/m²/day (Manikantan and Varadharaju 2011). Therefore, it can be concluded that PHB and PHBHV are promising polymers for food packaging applications

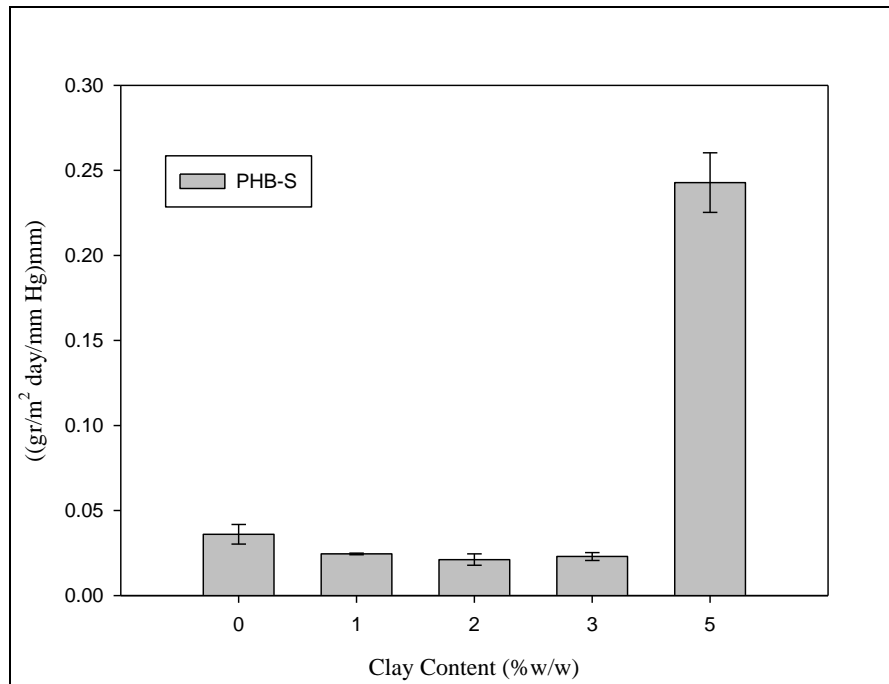


Figure 5.8. Water vapor permeabilities of PHB-S nanocomposites films at different clay contents

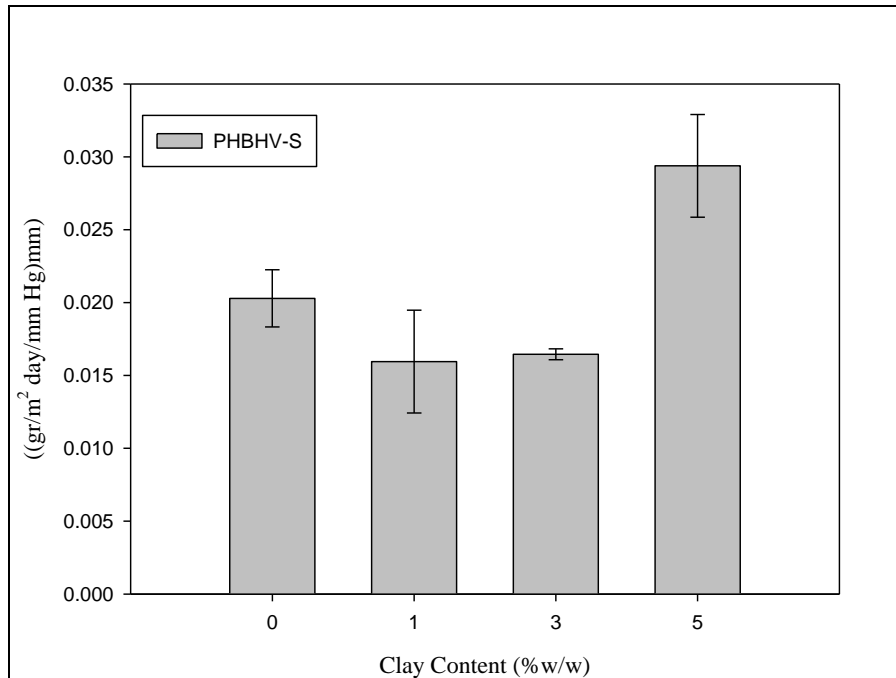


Figure 5.9. Water vapor permeabilities of PHBHV-S nanocomposites films at different clay contents

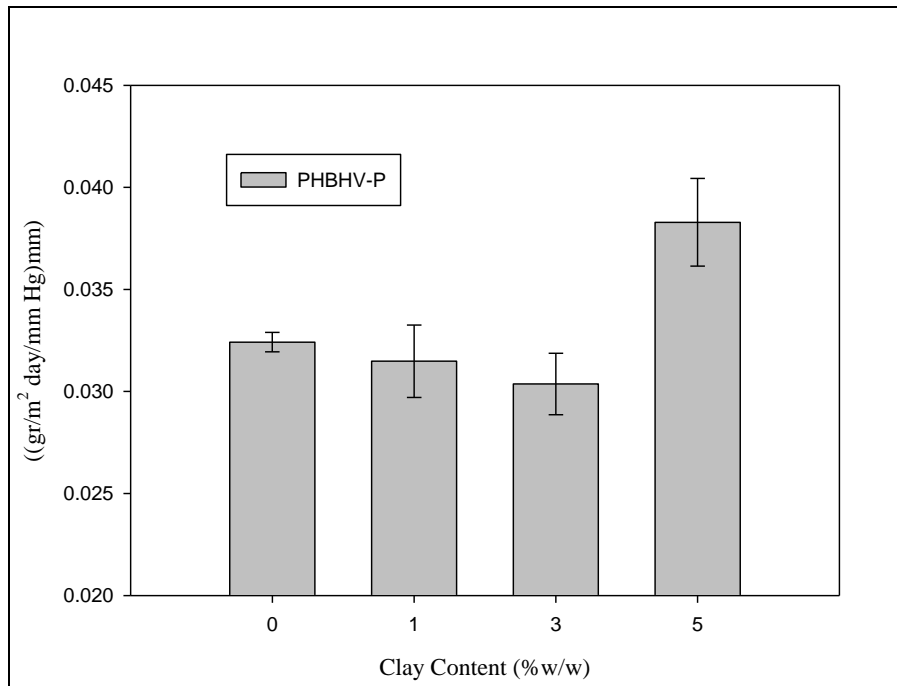


Figure 5.10. Water vapor permeabilities of PHBHV-P nanocomposites films at different clay contents

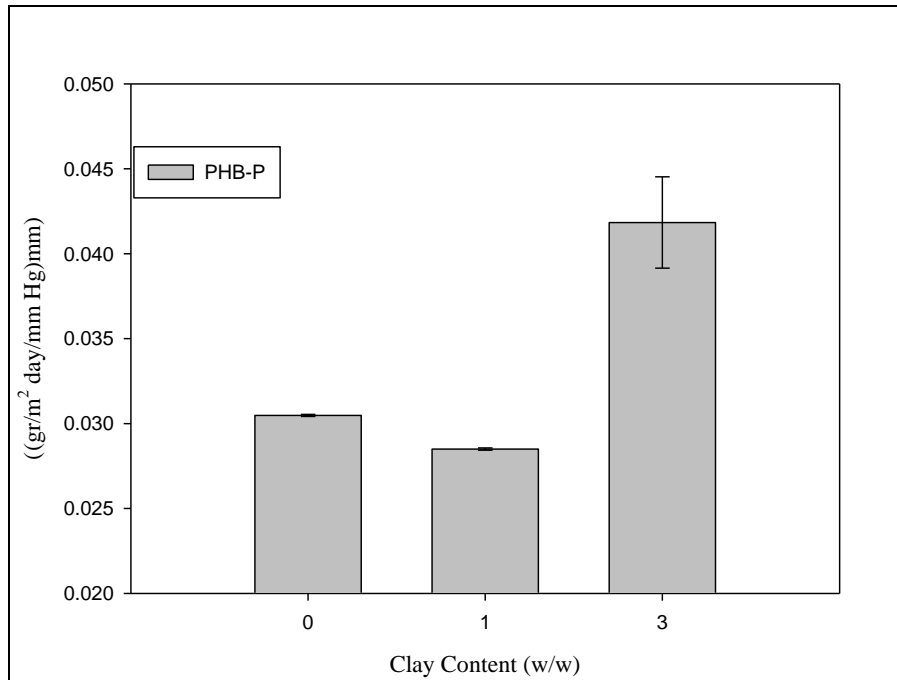


Figure 5.11. Water vapor permeabilities of PHB-P nanocomposites films at different clay contents

Based on different assumptions such as filler geometry and orientation in polymer matrix, several models were developed to describe the permeability of diffusing molecule in filled polymers (Table 2.1). As mentioned above, significant improvement in barrier properties was achieved via dispersion of layered silicates in polymer matrix which formed a tortuous path due to high aspect ratio of filler. In order to evaluate aspect ratio, models were fitted to experimental data with a general assumption that nanoparticles are impermeable to penetrant molecule and permeating molecules are forced to wiggle around filler and hence diffuse through a tortuous pathway. Increment in aspect ratio resulted in the decrease in area available for diffusion, a result of impermeable filler replacing with permeable polymer hence permeability decreases (Cornwelle 2009).

Permeability models were applied to experimental data for PHB and PHBHV nanocomposites. The average aspect ratio layered silicates can be evaluated via permeability models by using experimental permeability data. In this manner, models were fitted to experimental water vapor permeability data of PHB-S nanocomposites (Figure 5.12). As seen in, Figure 5.12 the Cussler Regular and Random models gave the best fitting curve to experimental WVP data of PHB-S nanocomposite films. Moreover, when the error values, which indicate deviation of theoretical permeability from experimental data, of models were taken into account Cussler Regular and Random models gave the minimum error among other models (Table A.2). Both Cussler Regular and Random models gave aspect ratios around 160 and 240, respectively for WVP data, which is in good agreement with the reported aspect ratio range (10-1000) for layered silicates (Herrera-Alonso et al. 2009; Oguzlu and Tihminlioglu 2010). Moreover, Sanchez-Garcia and coworkers evaluated aspect ratio of layered silicates in PHB matrix via TEM analysis, and they found that average aspect ratio was greater than 100 which is consistent with the results found by Cussler Regular and Random models.

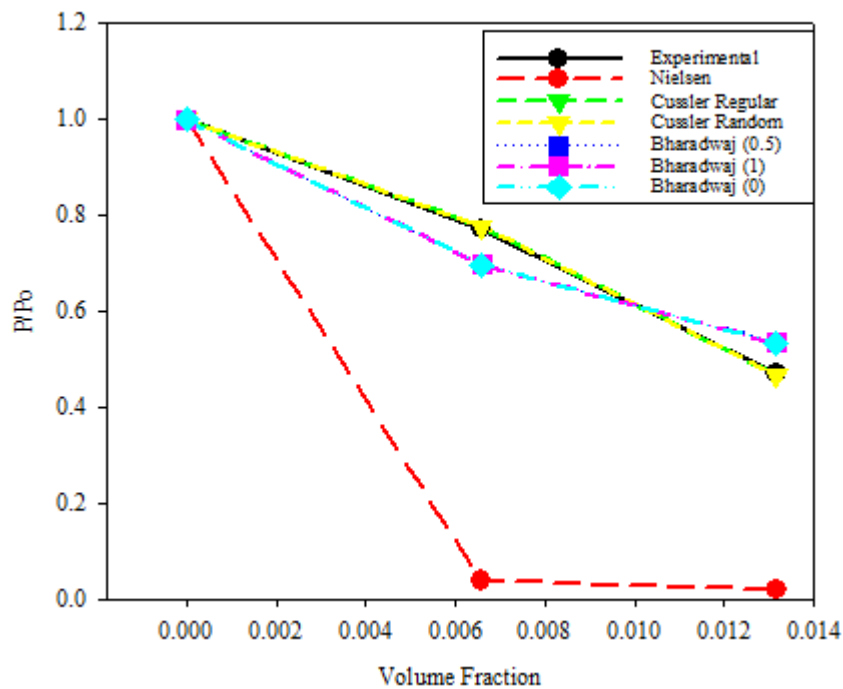


Figure 5.12. Permeability models fitted to experimental water vapor permeability of PHB-S nanocomposite films

However, it should be taken into account that there are a number of morphological factors that these simple models eliminate. For instance, layered silicates in polymer matrix are not perfectly aligned or completely random. Moreover, the morphological changes mainly crystallinity, crystalline morphology, relative humidity effect, molecular degradation and molar mass reduction, amorphous and interfacial changes and heterogeneity in the aspect ratio of the filler are not taken into account (Lagaron et al. 2008).

5.2.1. Temperature Effect in WVPs of PHB-S and PHBV-S Nanocomposites

Foods are preserved in different conditions such as in refrigerator or in a basic shelf. Therefore, the conditions that affect the shelf life of foods vary depending on its storage conditions. In addition, packaging material plays a key role in preserving foods from external stimulants that act on spoiling. For instance, storage conditions such as temperature and relative humidity are most affective and variable parameters that determine the shelf life of a food. Moreover, as the temperature changes,

thermomechanical and barrier properties of packaging materials change hence, the spoiling of foods indirectly affected. Some of literature studies focused on the thermomechanical properties of nanocomposites (Wang et al. 2005; Maiti et al. 2007; Fujimori et al. 2008; Oguzlu and Tihminlioglu 2010). In this manner, temperature dependence of water vapor permeabilities of PHB-S and PHBHV-S nanocomposite films were evaluated at 10 °C, 20 °C, 30°C and 40°C. The activation energy in other words acceleration of permeation by temperature was found by using Arrhenius relation (Eqn. 5.1). By plotting Arrhenius plots activation energies of nanocomposites were evaluated.

$$P = P_0 e^{-E_a/RT} \quad (5.1)$$

where P and P₀ water vapor permeabilities at the test temperature of T and T₀, respectively. E_a is the activation energy that is the energy that penetrant molecule owing. R is the universal gas content which is 8.314 j mol⁻¹ K⁻¹. WVPs of PHB-S nanocomposites at different temperatures were shown in Figure 5.13 and Table A.6. An exponential increase in P with increasing temperature was observed. This behavior can be resulted from dependence of WVP to both temperature and partial pressure of water vapor across the sample. Therefore, pressure difference across the sample at higher temperature increases hence, as seen in Figure 5.13, it is an evident that the deviations among WVPs of PHB-S nanocomposites were higher at test temperature of 40 °C when compared to lower test temperatures. These findings are also in good agreement with Hulsmann and coworkers study. They studied the temperature-dependency of water vapor permeation and they concluded that as the temperature increased WVTR increases exponentially (Hulsmann et al. 2009). The lowest permeability was found at 10 °C as expected, for partial pressure of water vapor was lowest among test temperatures. Arrhenius plots of PHB-S nanocomposites were indicated in Figure A.6. The slope and r-squared value of each regression lines that approximates experimental Arrhenius plots and activation energies were tabulated at Table 5.1. The activation energy describes the acceleration of permeation by temperature. Cloisite 10A addition at low content (1% and 2% w/w) resulted in decrease at activation energy. In other words, pristine PHB-S-N is more temperature dependent in permeation of water vapor than clay containing PHB-S-1 and PHB-S-2 samples. This behavior can be explained by barrier performance of layered silicates. In addition, relaxation of polymer chains is

restricted by layered silicates which are well dispersed in polymer matrix. Therefore, free volume of polymer created by holes was prevented via layered silicates. In addition, this free volumes can cause cluster affect which increases permeability of water vapor in polymers (Mittal 2010) The sample PHB-S-3 showed the highest activation energy with a value of 58 kJ mol⁻¹. It is an evident that dispersion of layered silicates affect activation energy of water vapor permeability. It was proofed that exfoliated structure was formed at low content (1%w/w) of Cloisite 10A and exfoliation resulted in better interaction with polymer chains. This behavior is also in good agreement with findings of activation energy values.

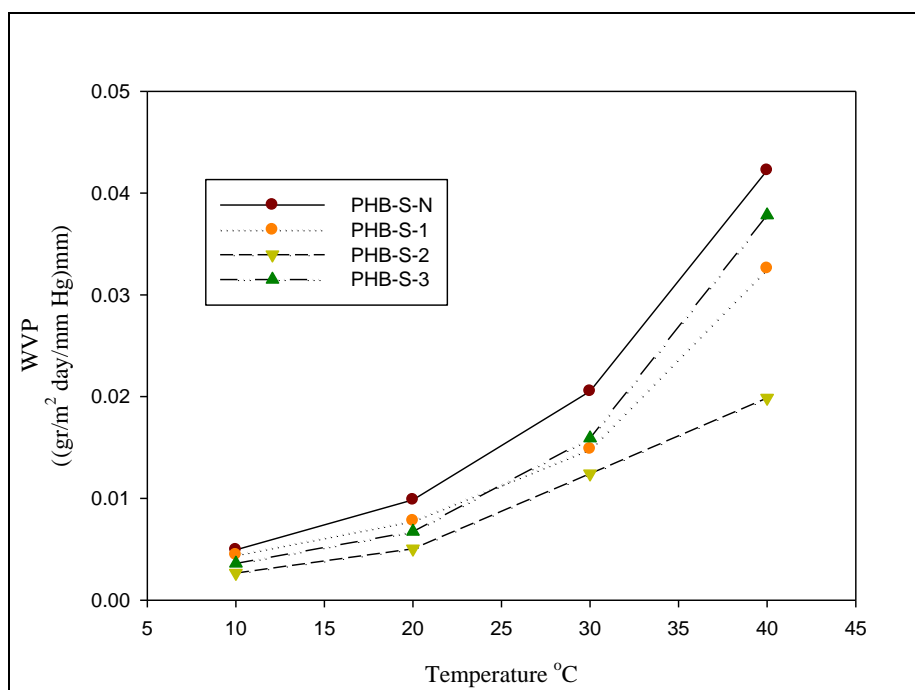


Figure 5.13. Temperature dependence of WVP of PHB-S nanocomposite films

Table 5.1. Slope and R² values of Arrhenius plot and WVP Activation energies of PHB-S nanocomposites films

Sample	R-Squared	Slope	Ea(kj/mol)
PHB-S-N	0.99830	-6350.1	52.79
PHB-S-1	0.98880	-5849.9	48.64
PHB-S-2	0.98940	-6147.1	51.11
PHB-S-3	0.98950	-6992.5	58.14

The temperature dependent water vapor permeabilities of PHBHV-S nanocomposites were also evaluated via permeation tests at different temperatures.

WVPs of PHBHV-S nanocomposites at 10 °C, 20 °C, 30 °C, and 40 °C were shown in Figure 5.14. and Table A.6. The slope and r-squared value of each regression lines that approximates experimental Arrhenius plots and activation energies of PHBHV-S samples were tabulated at Table 5.2. As it was in PHB-S measurements, PHBHV-S samples exhibited same trend in activation energy; exfoliated structure was obtained at 1%w/w Cloisite 10A loading and Cloisite 10A addition at low content (1% w/w) resulted in decrease in activation energy. In other words, water vapor permeation in PHBHV-S-N sample was more temperature dependent then PHBHV-S-1. This could be resulted due to restriction of mobility of polymer chains via strong interaction between layered silicates and polymer chains (Hulsmann et al. 2009). However, PHBHV-S-5 exhibited higher activation energy then pristine PHBHV-S. This could be resulted due to intercalated structure, which allows chain mobility, of Cloisite 10A in polymer matrix.

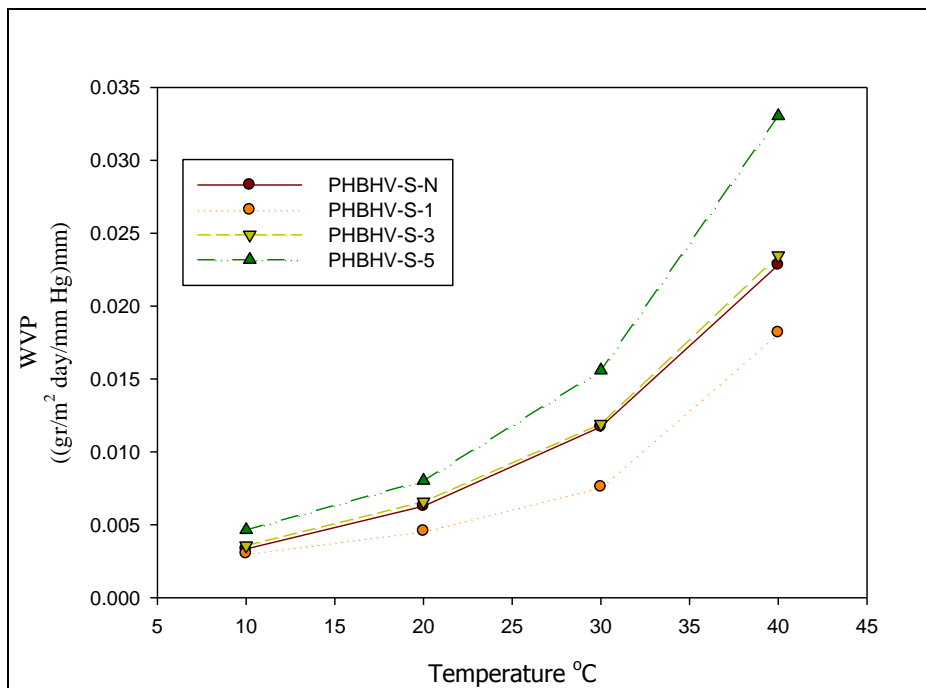


Figure 5.14. Temperature dependence of WVPs of PHBHV-S nanocomposite films

Table 5.2. Slope and R² values of Arrhenius plot and WVP Activation energies of PHB-S nanocomposites films

Sample	R-Squared	Slope	Ea(kj/mol)
PHBHV-S-N	0.9981	-5655.1	47.01
PHBHV-S-1	0.9575	-5190.8	43.16
PHBHV-S-3	0.9900	-5790.4	48.14
PHBHV-S-5	0.9968	-5925.9	49.94

The permeation process is the mass transport dependent on time through a solid piece of material with at least two surfaces acting as interfaces to the surrounding gas. Therefore, when the activation energy of water vapor permeation is considered, the mechanism of permeation should be taken into account. There are four steps occurred while a gas molecule penetrates through a membrane;

- The adsorption on top of one surface
- The absorption inside the material
- The diffusion
- Desorption out of the material.

Layered silicate affect on these four steps in water vapor permeation that should be considered. For instance, the adsorption on top of one surface can be related to surface characteristics such as hydrophobic nature which was evaluated via contact angle measurements. The absorption of water vapor inside the material is related to dissolution obeying Henry's law plus "hole filling" obeying Langmuir expression. However, the gas molecules are only soluble in amorphous phase which can be related to see the effect of layered silicate on crystallization kinetic of nanocomposites films (Mittal 2010).

5.3. Mechanical Properties of PHB and PHBHV Nanocomposites

Mechanical properties of biodegradable polymers are a crucial feature that restricts its application areas. To make biodegradable polymers competitive with conventional plastics, different kinds of methods have been carried out in literature (Chen et al. 2004; Chen et al. 2007). The improvement in mechanical performances of nanocomposites is attributed mainly to the nanosize dimensions of fillers in extremely large aspect ratios (Choi et al. 2003; Sinha Ray and Okamoto 2003) . In this study, the

effect of clay addition on the mechanical properties of the PHB and PHBHV nanocomposite films was investigated via tensile testing. The sample stress-strain diagrams of PHBHV-S nanocomposites were shown at Figure 5.15. As it is clearly seen, the mechanical properties improved much better at low clay loading (1%w/w) than those of at higher clay loading.

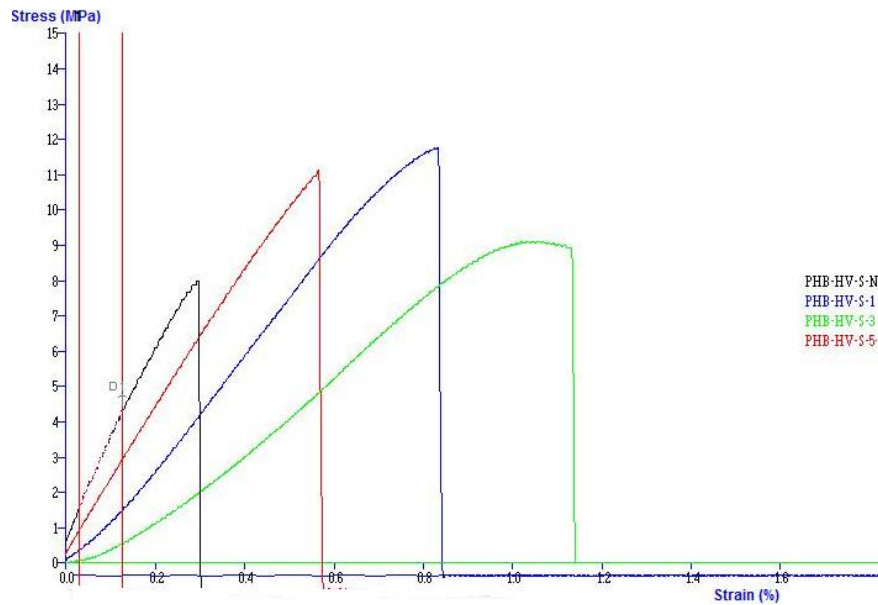


Figure 5.15. Sample stress-strain curves of PHBHV-S nanocomposites

The mechanical properties; tensile strength, Young's modulus (stiffness) and strain at break values, were evaluated and tabulated at Table A.8 for each nanocomposite samples. The pristine PHB-S-N had a tensile strength of 11.6 MPa and strain at break of 0.43 %. Small amount of clay addition (1%w/w) increased tensile strength of PHB-S nanocomposites at about 156.1% (Figure 5.18). Moreover, Young's modulus in other word stiffness of pristine PHB-S-N was enhanced at about 54% by addition of 1%w/w Cloisite 10A. An increase of about 214.8 % in tensile strength and of strain at break 69 % was achieved for PHB-S-2 (2 wt % clay loaded) nanocomposite films (Figure 5.17). In addition, the copolymer PHBHV-S nanocomposite films exhibited same trend in which Young's modulus increased by addition of Cloisite 10A, with PHB-S nanocomposites samples. Moreover, small amount of Cloisite 10A addition (PHBHV-S-1) to pristine PHBHV-S-N improved Young's modulus at about 100% which is close to improvement in PHB-S nanocomposites (Figure 5.16). Additionally, enhancement in tensile strength was 85%, when 1%w/w clay was introduced to PHBHV-S nanocomposites (Figure 5.18). However, PHBHV-S nanocomposites

exhibited lower tensile strength and Young modulus than PHB-S nanocomposites except elongation at break (Figure 5.17). The mechanical properties of PHB-P and PHBHV-P nanocomposites which were prepared via melt compounding were tabulated in Table A.8. The improvement in Young's modulus of PHB-P and PHBHV-P nanocomposites was shown in Figure 5.16. However, enhancement in Young's modulus was not as significant in melt compounded samples as solution intercalated samples. In addition, Cloisite 10A addition to PHBHV-P samples had diverse affect on elongation at break. As the clay content increased, strain of PHBHV-P nanocomposites decreased opposite to the other systems. In fact, the significance of the negative affect was much more at higher clay loadings (3%, 5% w/w) than low clay loaded sample (PHBHV-P-1). This trend could be resulted due to dispersion of clay particles. Intercalated or flocculated structure of layered silicates can diminish mechanical properties so as the weak interaction between polymer and clay achieved (Mittal 2010). However, exfoliated structure of layered silicates was not exhibited diverse affect as much as intercalated structure. On the other hand, clay addition to PHB-P samples resulted in increase in strain property up to a point. In most studies, improvement in mechanical properties was attributed to dispersion level of layered silicates in polymer matrix (Maiti et al. 2007; Oguzlu and Tihminlioglu 2010).

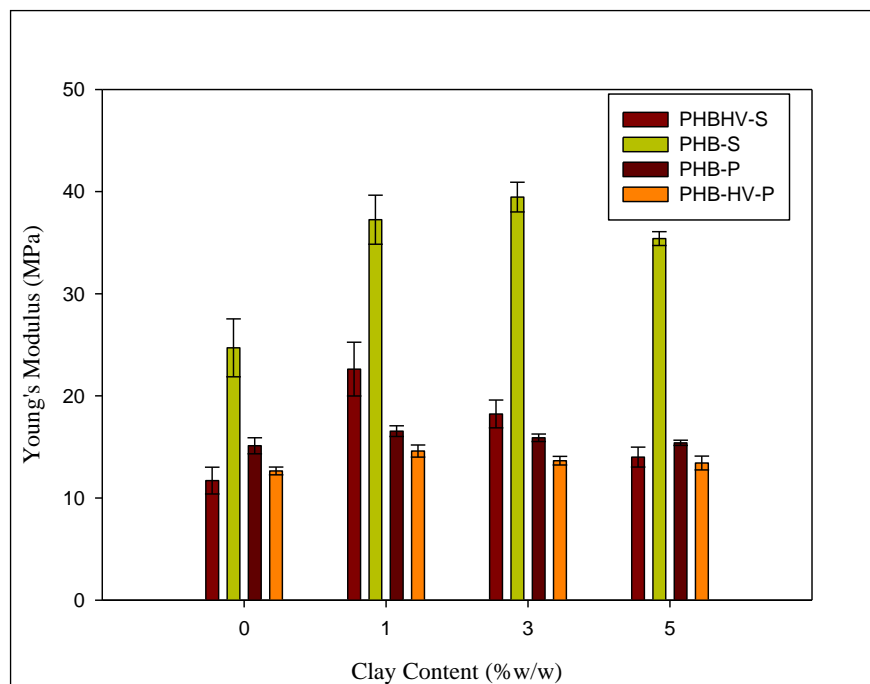


Figure 5.16. Young's Modulus of PHB and PHBHV nanocomposites

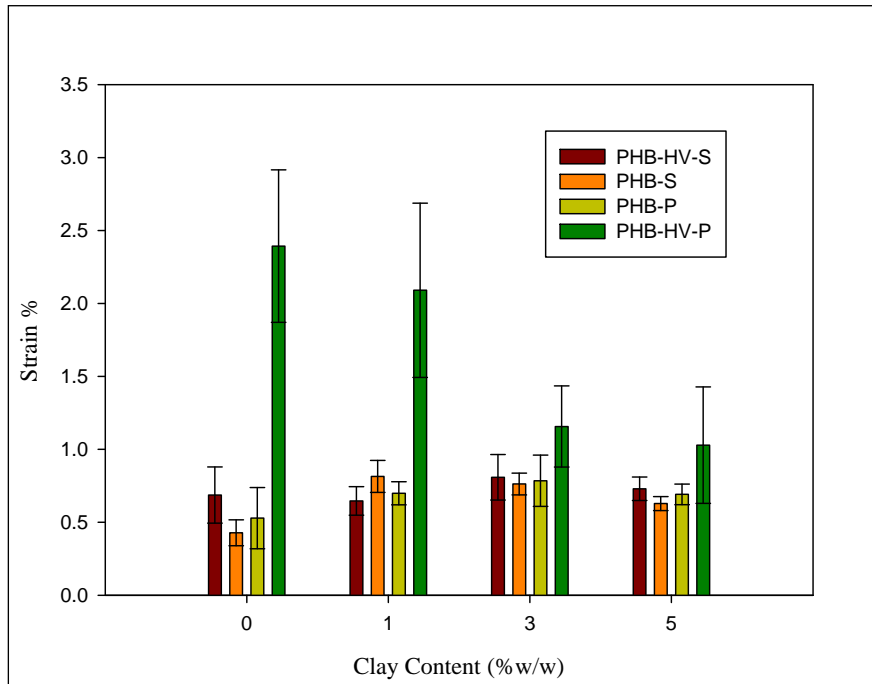


Figure 5.17. Strain of PHB and PHBHV nanocomposites

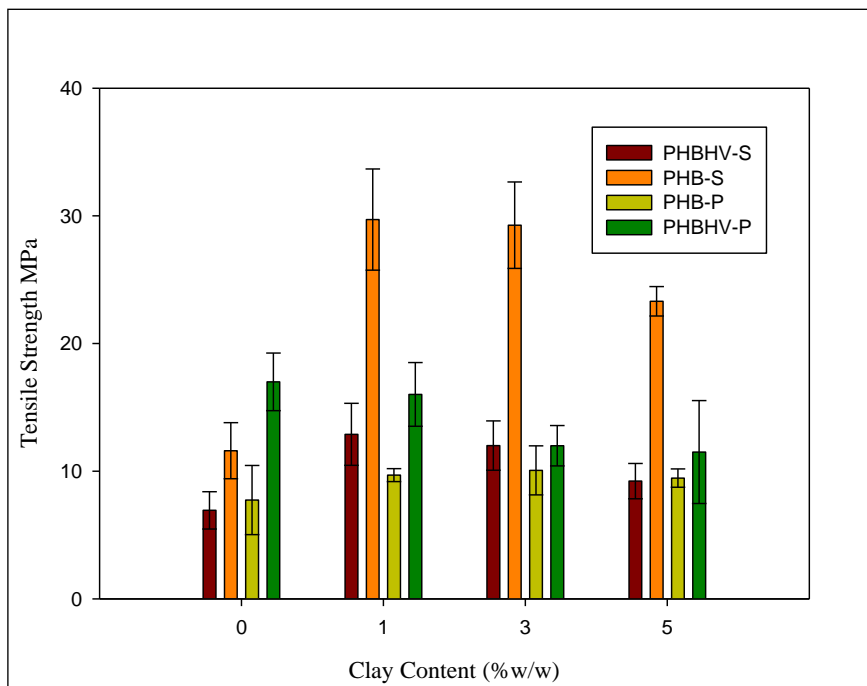


Figure 5.18. Tensile strength (MPa) of PHB and PHBHV nanocomposites

Dispersion plays key role in the improvement of mechanical properties. In fact, a good dispersion of nanofillers in the polymer tends to improve the tensile strength and strain at break (Mittal 2010). The stiffness of polymer nanocomposites generally increases with the nanoparticles volume fraction, as long as a sufficient dispersion and

degree of exfoliation of these particles are ensured. Therefore, the increase in Young's Modulus was greater at a low Cloisite 10A content; this indicates that the fillers were better dispersed and exfoliated. Moreover, mechanical analysis results were consistent with XRD results (Figure 5.2). In addition, results are in good agreement with the study of Chen and coworkers in which, nanocomposites exhibited poor mechanical properties at higher clay loadings (Chen et al. 2004) .

5.4. Thermal Characterization of PHB and PHBHV Nanocomposites

Thermal properties of PHB and PHBHV nanocomposites were investigated via differential scanning calorimetry (DSC) and thermogravimetric analysis (TGA). Thermal decomposition of nanocomposites was evaluated isothermally and kinetic models were applied so as to understand the effect of Cloisite 10A in thermal decomposition process of nanocomposites. Additionally, in order to understand crystallization mechanism, non isothermal crystallization kinetic of nanocomposites was evaluated via DSC analysis that performed at different cooling rates. Several studies have been reported in the literature to understand thermal decomposition and crystallization of nanocomposites (Yeo et al. 2010)

5.4.1. Thermogravimetric Analysis (TGA)

An appropriate understanding of the thermal decomposition of a particular polymer is an important stage in thermal stabilization of that polymer. One of the important drawbacks of bacterial PHB and PHBHV is thermal instability during melt processing because thermal degradation temperature is close to melting temperature of PHB and PHBHV. Current research investigations have indicated that the introduction of a nanoparticulate filler into polymer matrix will result in the versatile improvement of a variety of properties, including an increase of thermal stability (Thellen et al. 2005; Chen et al. 2007; Maiti et al. 2007) . In this manner, effect of Cloisite 10A addition on thermal decomposition of PHB and PHBHV nanocomposites were investigated via thermogravimetric analysis (TGA). Thermal stability of PHB and PHBHV nanocomposites was discussed by considering thermal degradation properties:

- Onset temperature of thermal degradation (T_{onset})

- End temperature of thermal degradation (T_{end})
- The yield of charred residue (char%)
- 20 wt% loss temperature ($T_{0.2}$)
- 50wt% loss temperature ($T_{0.5}$)

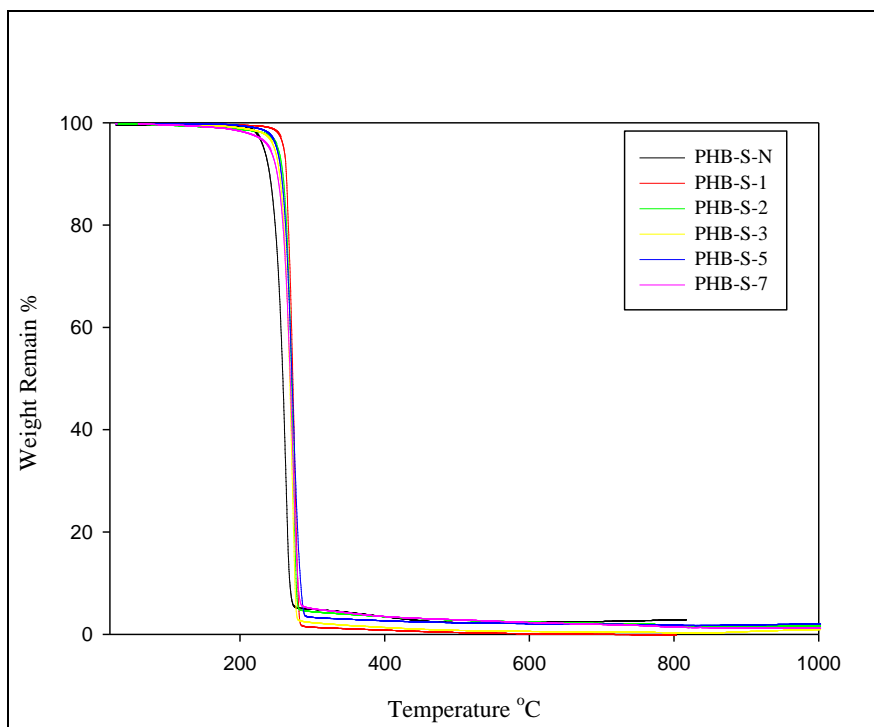


Figure 5.19. TGA curves of PHB-S nanocomposite films

The thermogravimetric weight loss curves of PHB-S nanocomposites were shown in Figure 5.19. As it is seen, the addition of 1% w/w of Cloisite 10A in polymer matrix resulted in significant improvement in thermal stability by increasing the thermal degradation onset temperature (T_{onset}). However, the improvement was not as significant as in the case of higher clay loaded samples, but even at higher clay loadings, T_{onset} temperature was higher when compared to pristine PHB-S-N. This could be due to restriction of thermomechanical motion of polymer chain by layered silicates.

The thermogravimetric weight loss curves of the prepared nanocomposites were shown in Appendix A. Thermal degradation properties (T_{onset} , T_{end} , char%, $T_{0.2}$, and $T_{0.5}$) of Cloisite 10A, PHB and PHBHV nanocomposites were tabulated at Table 5.3. Onset decomposition temperature of Cloisite 10A was observed at 240.63 °C (Figure 5.20) which is important, for decomposition temperature should be higher than processing temperature of PHB and PHBHV so that the thermal stability can be achieved. The 20%

and 55% weight loss of Cloisite 10A was observed at 263.7 °C and 807 °C, respectively. This showed that almost 50% of Cloisite 10A is organic modifier. In accordance with literature, onset decomposition temperature of Cloisite 10A were also observed at around 200-250 °C (Koo 2006; Mittal 2010).

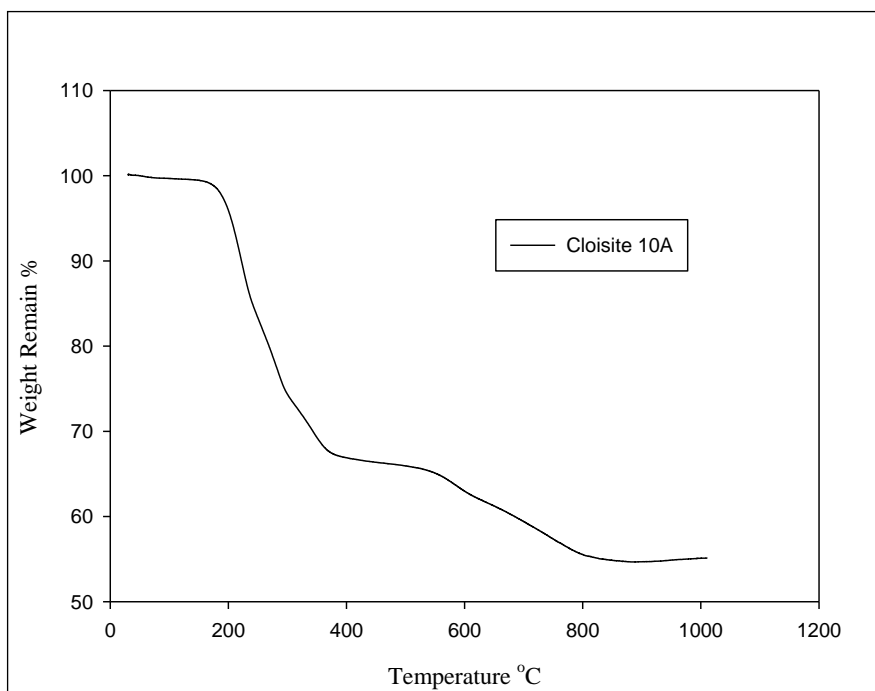


Figure 5.20. TGA curve of Cloisite 10A

The onset decomposition temperature of pristine PHB-S film increased about 11 °C by addition 2%w/w Cloisite 10A. In addition, 50% weight loss temperature increased to 268.15 °C. In contrast, at higher Cloisite 10A loading, the onset and end decomposition temperature decreased to the value of pristine PHB-S. The improvement in thermal stability parameters of PHB-S films achieved at low content of Cloisite 10A can be attributed to dispersion level of layered silicates in polymer matrix. Moreover, the same trend was also observed for PHBHV-S samples; in addition, 1%w/w Cloisite 10A resulted in increment in onset decomposition temperature about 32 °C compared to pristine PHBHV-S. Moreover, at higher Cloisite 10A loaded samples thermal decomposition parameters were found to be even higher than pristine PHBHV-S samples. The significant enhancement in thermal decomposition properties of PHB-P and PHBHV-P was also obtained by addition of Cloisite 10A to polymer matrix. Therefore, it can be concluded that exfoliated structure of layered silicates enhanced thermal decomposition properties of PHB and PHBHV nanocomposites. Enhancement

in thermal stability by incorporation layered silicates to polymer matrix was also reported in several studies (Sinha Ray and Okamoto 2003; Maiti et al. 2007). When percent of char formation of nanocomposites is taken into account, Cloisite 10A was lost its 50% by weight at the end of 1000 °C. However, char formation was higher in PHB-S-N nanocomposite compared to PHB-S-1 sample. This could be explained by catalytic effect of clay particles in polymer decomposition process. The products formed during the decomposition of the polymer can be changed due to catalytic effect of clay particles. Metals present in the clay and in acidic sites (Lewis acid sites) inherently present on the clay surface, or formed as a result of the decomposition of alkylammonium salts, showed catalytic activity towards degradation reaction. Therefore, more volatile compounds can be created during decomposition process (Mittal 2010).

Table 5.3. Thermal degradation properties of PHB and PHBHV nanocomposites

Sample	T _{onset} (°C)	T _{end} (°C)	Char %	T _{0.2} (°C) 20% mass loss	T _{0.5} (°C) 50% mass loss
Cloisite 10A	240.64	807.89	55.36	263.27	-
PHB-S-N	234.76	274.56	2.74	251.02	260.42
PHB-S-1	240.08	283.69	0.81	263.55	267.14
PHB-S-2	245.31	278.70	1.83	271.67	268.15
PHB-S-3	237.30	278.84	1.13	259.06	266.79
PHB-S-5	238.5	285.76	2.21	259.96	267.81
PHB-S-7	236.78	284.59	1.39	258.01	268.05
PHBHV-S-N	218.95	267.05	6.63	240.99	249.99
PHBHV-S-1	250.68	284.46	5.51	270.73	275.83
PHBHV-S-3	248.61	283.76	4.03	265.20	271.43
PHBHV-S-5	244.77	291.27	2.32	263.00	270.30
PHB-P-N	258.95	297.87	2.67	276.60	281.43
PHB-P-1	261.26	297.32	3.17	273.61	277.93
PHB-P-3	263.64	298.74	4.12	273.66	277.77
PHB-P-5	260.91	294.70	3.64	272.42	277.39
PHB-P-7	246.33	294.78	8.71	266.33	274.31
PHBHV-P-N	243.60	286.98	1.34	264.33	270.35
PHBHV-P-1	256.38	285.8	2.27	265.40	271.15
PHBHV-P-3	250.84	284.13	2.90	261.96	268.82
PHBHV-P-5	247.48	288.13	3.97	259.18	266.22
PHBHV-P-7	235.68	287.37	5.33	253.82	262.51

5.4.1.1. Isothermal Degradation of PHB-P and PHBHV-P Nanocomposites

The thermal degradation of PHB and PHBHV has been suggested to occur almost exclusively by a nonradical random chain scission reaction involving six membered ring transitions state (Erceg et al. 2009). Thermal instability of PHB and PHBHV in the melt prevents it from substituting the nonbiodegradable polymeric materials in commercial products. Therefore, understanding thermal degradation behavior of PHB and its copolymer PHBHV is very important. In this manner, effect of Cloisite 10A on thermal degradation of PHB-P and PHBHV-P nanocomposites were investigated via isothermal degradation processes at 230 °C, 240 °C, and 250 °C. The aim of the kinetic analysis is to determine the of kinetic triplets for the investigated process, kinetic model, $g(\alpha)$, activation energy, E, and preexponential factor A.

The isothermal TG curves for PHB-P and PHBHV nanocomposites at 230 °C, 240 °C and 250 °C were shown in Figures A11-A16, respectively. It is well known that recommended temperature range for processing of PHB and PHBHV is 180-200 °C (Erceg et al. 2010). Based on the results of non isothermal decomposition (Table 5.3), the thermal stability of PHB and PHBHV nanocomposites could be improved under isothermal degradation. Therefore, isothermal degradation of nanocomposites were performed considering nonisothermal TG analysis and three different temperatures, 230°C, 240 °C and 250 °C were chosen. At these temperatures, the degradation rate of PHB and PHBH increased and constant mass was established within 120 min (Figure A.11-A.16).

The theoretical kinetic models cannot exactly fit the experimental data, therefore, Avrami-Eroffev kinetic model was used and the parameter “m” (eqn. 5.1) calculated from experimental results.

$$[-\ln(1 - \alpha)]^{1/m} = kt \quad (5.1)$$

$$\ln t = \frac{1}{m} \ln[-\ln(1 - \alpha)] - \ln k \quad (5.2)$$

In order to calculate “m” and degradation rate constant “k” were determined by using of equation 5.2 which is logarithm of equation 5.1. Then from the slope of plots $\ln t$ vs $\ln[-\ln(1-\alpha)]$ (Figures A.17-24), “m” can be obtained for each temperature of

isothermal degradation. The plots for PHB-P and PHBHV nanocomposites were shown in Figures A.17-A.24. The “m” values for PHB-P-N at 230, 240, and 250 °C were 3.91, 5.08 and 7.32 respectively, which gave an average value of 5.44. In the same way, parameter “m” for all nanocomposites was determined, and the empirical kinetic model $g(\alpha)$ constants were tabulated in Table 5.4.

Table 5.4. Values of empirical kinetic triplets obtained by Avrami-Eroffev model

Sample Code	Conversion, a	$g(a)$	E / kJmol^{-1}	$\ln A / \text{min}^{-1}$	r^2
PHB-P-N	0,1-0,9	$[-\ln(1-a)]^{1/5,89}$	60.38	10.88	0.9973
PHB-P-1	0,1-0,9	$[-\ln(1-a)]^{1/5,76}$	77.15	14.46	0.9979
PHB-P-3	0,1-0,9	$[-\ln(1-a)]^{1/4,08}$	110.25	22.02	0.9943
PHB-P-5	0,1-0,9	$[-\ln(1-a)]^{1/3,84}$	64.59	11.49	0.9980
PHBHV-P-N	0,1-0,9	$[-\ln(1-a)]^{1/5,44}$	55.54	9.76	0.9971
PHBHV-P-1	0,1-0,9	$[-\ln(1-a)]^{1/4,57}$	105.01	20.00	0.9798
PHBHV-P-3	0,1-0,9	$[-\ln(1-a)]^{1/4,16}$	175.68	37.00	0.9972
PHBHV-P-5	0,1-0,9	$[-\ln(1-a)]^{1/4,78}$	69.14	12.00	0.9973

The intercept of the plots $\ln t$ vs $\ln[-\ln(1-\alpha)]$ is “ $-\ln k$ ” and consequently rate constant “ k ” values of PHB-P, PHBHV-P nanocomposites and their dependence on Cloisite 10A content and temperature of isothermal degradation were illustrated in Figure 5.21 and 5.22 respectively. The results showed that addition of Cloisite 10A into polymer matrix decreased the “ k ” values of the isothermal degradation of PHB-P and PHBHV nanocomposites. The most pronounced effect was observed in 3% w/w Cloisite 10A loaded PHB and PHBHV samples. The change in “ k ” values is consistent with the study of Erceg et al. They also found that, addition of OMMT into polymer matrix resulted in decrease in “ k ” values (Erceg et al. 2010). When the activation energies E , of PHB-P and PHBHV-P nanocomposites considered, 3% w/w Cloisite 10A addition increased E value of pristine PHB-P from $60.38 \text{ kJ mol}^{-1}$ to 110 kJ mol^{-1} . Moreover, this increment in PHBHV-P nanocomposite was about three times compared to pristine PHBHV-P sample. Therefore, it can be concluded that small addition of Cloisite 10A to pristine PHB and PHBHV polymer matrix improved thermal properties significantly.

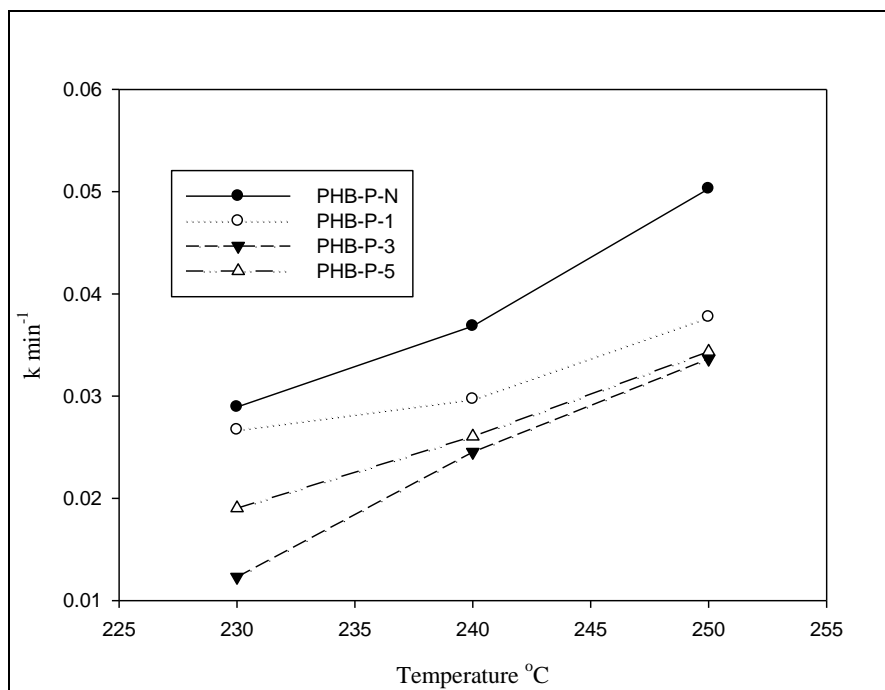


Figure 5.21. Dependence of “k” on Cloisite 10A content and temperature of isothermal degradation of PHB-P nanocomposites

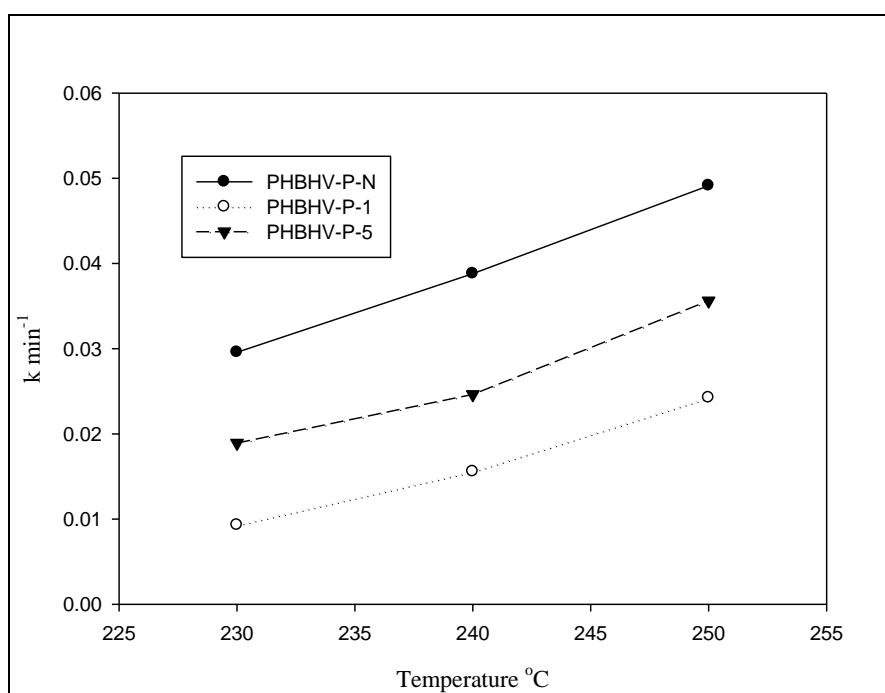


Figure 5.22 Dependence of “k” on Cloisite 10A content and temperature of isothermal degradation of PHBHV-P nanocomposites

5.4.2. Differential Scanning Calorimetry (DSC) Analysis of PHB and PHBHV Nanocomposites

Recent studies have showed that thermal properties of biodegradable polymers can be improved by addition of clay particles to polymer matrix (Lagaron et al. 2008; Sanchez-Garcia et al. 2008). In this manner, DSC measurements aimed at obtaining further information regarding the influence of Cloisite 10A on thermal characterization of PHB and PHBHV nanocomposites. DSC measurements were performed in three main steps; in order to observe the melting peaks (first melting: T_{m1} , second melting: T_{m2}), heating process took place from room temperature to 180 °C, then cold crystallization temperature (T_c) were obtained by cooling the melted samples to -40 °C, after that second heating took place so as to obtain second melting temperatures (first melting of second heating: T_{m21} , second melting of second heating: T_{m22}) were obtained. Moreover, endothermic and exothermic endotherms of melting and crystallization peaks were also evaluated to clarify the effect of amount of Cloisite 10A on thermal properties of nanocomposites.

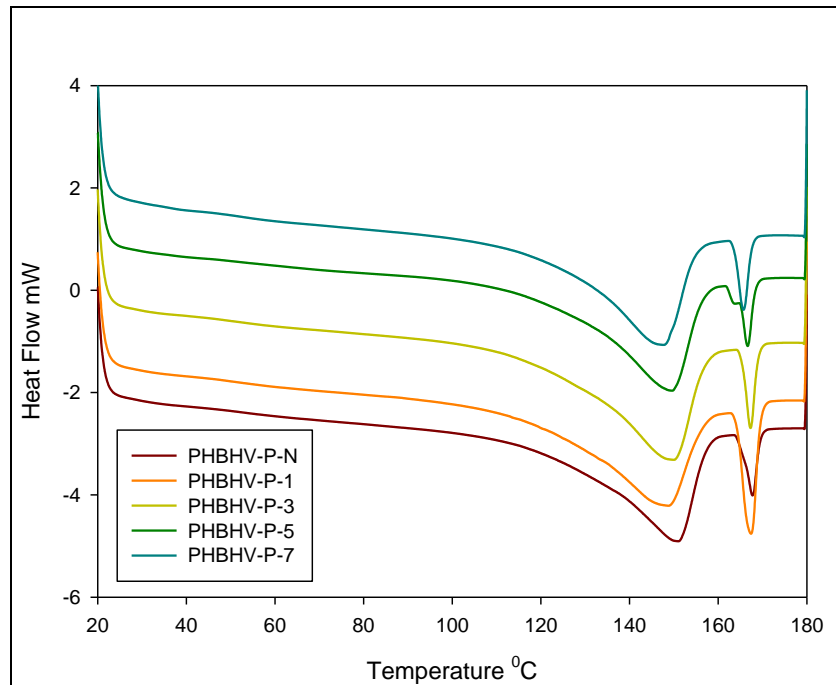


Figure 5.23. First heating run of DSC analysis of PHBHV-P nanocomposites

The melt behavior of PHBHV-P nanocomposites at first heating runs of DSC analysis were shown in Figure 5.23. As it is seen, there are two melting peaks of

samples PHBHV-P were observed. The same trend was also observed in samples, PHB-P (Figure B.1), PHBHV-S (Figure B.3). The first and second melting peaks could be due to differences in lamellar thickness of crystals (Mittal 2010). The second melting curves of samples differ as the amount of clay addition increases which shows that clay addition resulted in changes in crystal thickness (Figure 5.23). However, PHB-S nanocomposites did not show the same trend (Figure B.1). Although PHB-S-N sample exhibited one melting peak curve, addition of clay to pristine PHB-S-N resulted in two melting peaks. This could be due to nucleation effect of layered silicate in crystallization process of polymer chains. Since, two melting peaks indicate fusion of crystals that formed homogeneously and heterogeneously. Homogeneous nucleation takes place via polymer chains aggregation themselves, on the other hand heterogeneous nucleation occurs when a particular or nucleating agent is introduced to polymer matrix (Mittal 2010). Therefore, it is the reason why there are not any two different melting peaks in first heating run of pristine PHB-S-N (Figure B.1).

The addition of Cloisite 10A to PHB-S and PHBHV-S matrix did not alter the T_{m1} temperatures (Table 5.5). However, samples prepared via melt compounding (PHB-P, PHBHV-P) exhibited lower T_{m1} at lower content of Cloisite 10A (PHB-P-1, PHBHV-P-1). However, changes in T_{m1} were not so significant. Mook and coworkers also found that addition of clay into polymer matrix lowered first melting temperature (Won Mook Choi 2003). When the enthalpy changes of first melting peaks (ΔH_{m1}) were considered, there were not significant changes in PHB-S and PHB-P nanocomposites. On the other hand, melting enthalpies of samples prepared via melt compounding (PHB-P-N, PHBHV-P-N) decreased when small amount (1%w/w) of Cloisite 10A introduced to pristine samples. In contrast, enthalpies of second melting of PHB-P-1 and PHB-P-3 increased by addition of Cloisite 10A. This could be due to nucleation effect of Cloisite 10A at lower content. Therefore, heterogeneous nucleation increased in the presence of low amount of Cloisite 10A. Wang and coworkers also concluded that addition of clay into polymer matrix resulted in increase in heterogeneous nucleation (Wang et al. 2005). In addition, when the percent crystallization taken into account (Homogeneous: X_{c1} , Heterogeneous: X_{c2}), the addition of Cloisite 10A at small content lowered the X_{c1} values compared to pristine samples PHB-P, PHBHV-P, and PHBHV-S. In contrast, the X_{c2} values increased via nucleation effect of layered silicates. Moreover, the total crystallinity ($X_{c\text{total}}$) of PHB-S and PHBHV-S

nanocomposites increased. In contrast, slight decrease was observed in the total crystallinity of PHB-P and PHBHV-P nanocomposites.

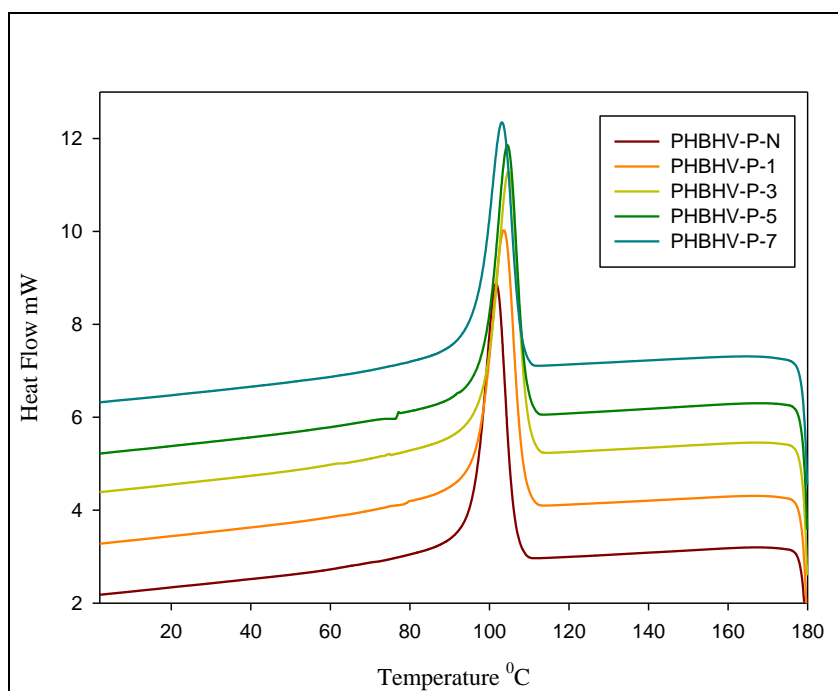


Figure 5.24. Cooling run of DSC analysis of PHBHV-P nanocomposites

Cold crystallization temperature of (T_c) was evaluated during the cooling of melted samples (Figure 5.24). As it is seen from the Figure, 1% w/w addition of clay to polymer resulted in a slight increase in the cold crystallization temperature of pristine polymer. The cold crystallization curves of PHB-P, PHBHV-S, and PHB-S nanocomposites were given in Figures B4, B5 and B6 respectively.

For better understanding the effect of clay and valerate content, cold crystallization temperature values were tabulated in Table 5.5. It can be observed in Table 5.5 that the value of T_c , for PHBHV-S-N was less than that of PHB-S-N. It could be resulted due to presence of HV content offering a larger free volume of molecular movement. However, addition of Cloisite 10A did not alter the T_c of nanocomposites. In order to understand effect of layered silicate in crystallization of nanocomposites non-isothermal crystallization studies at different cooling rates reported in literature (Xu et al. 2001; Wu et al. 2007).

The most obvious effect of Cloisite 10A was observed in crystallization of nanocomposites. Moreover, the presence of layered silicate in polymer matrix altered the crystallization process from homogenous to heterogeneous process. In addition, it

was found that exfoliated structure of layered silicates had more obvious effect in heterogenous crystallization than that of intercalated structured samples. This was attributed to stronger interaction between layered silicate and polymer chains. Therefore, the following section reported the effect of addition of Cloisite 10 A to PHB on crystallization kinetic which was investigated via differential scanning calorimetry measurements at different cooling rates.

Table 5.5. DSC result of PHB and PHBHV nanocomposites

Sample Code	1 st Heating Run				1 st Cooling Run			2 nd Heating Run			2 nd Heating Run			
	T _{m1} °C	ΔH _{m1} J/g	T _{m2} °C	ΔH _{m2} J/g	T _c °C	ΔH _c J/g	T _{m12} °C	ΔH _{m12} J/g	T _{m21} °C	ΔH _{m21} J/g	ΔH _{m_{total}} J/g	X _{c1} %	X _{c2} %	X _{c_{total}} %
PHB-S-N	172.13	91.92	-	-	114.12	83.71	168.70	90.09	-	-	90.09	61.70	-	61.70
PHB-S-1	172.30	94.98	-	-	114.01	86.68	169.63	95.98	-	-	95.98	65.73	-	65.73
PHB-S-2	172.90	89.13	-	-	111.46	79.65	169.31	91.51	-	-	91.51	62.67	-	62.67
PHB-S-3	172.18	87.14	-	-	112.91	80.57	169.21	89.55	-	-	89.55	61.33	-	61.33
PHB-S-5	171.74	83.83	-	-	111.99	76.13	168.84	85.83	-	-	85.83	58.78	-	58.78
PHB-S-7	171.86	79.15	-	-	111.87	74.33	168.40	81.31	-	-	81.31	55.69	-	55.69
PHB-HV-S-N	153.39	16.4	163.34	47.19	102.96	68.32	153.05	33.12	163.83	33.29	66.41	12.74	36.676	49.42
PHB-HV-S-1	152	17.78	167.99	52.97	97.7	62.11	159.4	24.23	170.06	21.14	45.37	13.81	41.168	54.98
PHB-HV-S-3	152.05	10.82	168.01	51.54	104.71	66.13	160.62	32.07	170.14	12.14	44.21	8.409	40.057	48.46
PHB-HV-S-5	152.1	12.3	167.91	46.41	105.28	65.44	160.34	26.29	169.91	10.72	37.01	9.559	36.069	45.62
PHB-P-N	160.69	47.84	174.19	11.06	112.57	62.89	156.66	42.59	165.48	5.24	47.83	32.76	7.575	40.34
PHB-P-1	158.35	36.9	174.16	18.16	111.85	60.62	156.77	26.31	165.07	4.709	31.02	25.27	12.43	37.71
PHB-P-3	157.5	29.43	173.39	23.72	113.2	58.73	157.63	35.06	165.99	2.677	37.74	20.15	16.24	36.40
PHB-P-5	159.47	63.77	-	-	114.1	59.3	157.74	62.36	-	-	62.36	43.67	0	43.67
PHB-P-7	159.28	31.75	173.91	13.74	112.91	54.18	158.1	59.08	-	-	59.08	21.74	9.410	31.15
PHB-HV-P-N	151.06	47.19	167.76	4.095	101.68	52.81	147.42	39.36	157.22	7.592	46.95	38.05	3.302	41.35
PHB-HV-P-1	148.79	41.22	167.47	8.994	103.61	51.13	147.31	29.74	156.55	6.604	36.34	33.24	7.253	40.49
PHB-HV-P-3	150.02	45.73	167.35	3.941	104.75	50	145	26.44	154.31	6.801	33.24	36.87	3.178	40.05
PHB-HV-P-5	149.67	43.56	166.67	4.124	104.54	49.82	142.28	24.38	151.98	7.838	32.22	35.12	3.325	38.45
PHB-HV-P-7	147.68	46.26	165.73	3.761	103.16	45.84	137.56	22.02	147.92	8.388	30.41	37.30	3.033	40.33

5.4.3. Non-isothermal Crystallization Study of PHB-S Nanocomposites

Crystallization is widely observed for a large number of polymers with structural regularity. The crystallization process of polymers consists of two steps, nucleation and growth. Nucleation occurs due to spontaneous cooling and no second phase of their nuclei exists, this type of nucleation is known as homogeneous nucleation (Mittal 2010). When the nucleation is induced in the presence of any other second phase, such as a foreign particle of surface, then the nucleation is referred as heterogeneous nucleation. Different kind of experimental techniques have been used under both isothermal and nonisothermal conditions. The most common techniques have been used to investigate mechanism of crystallization are differential scanning calorimetry DSC (Bandyopadhyay et al. 2008) and optical microscopy (OM) (Zhou et al. 2009).

Avrami model is used to analyze isothermal crystallization kinetics of polymer taking into account of developing relative crystallinity with respect to time. However, in most non isothermal crystallization studies Avrami models was used, therefore it should be considered that Avrami kinetic parameters does not indicate the same meaning as in isothermal crystallization (McFerran et al. 2008). In addition, kinetic constants evaluated via Avrami model was modified by Jeziorny since, the Avrami assumed that nucleation is a function of crystallization time, however in the case of non-isothermal crystallization nucleation is both dependent on crystallization time and temperature (Stephen and Cheng 2002). Moreover, primary nucleation kinetics was evaluated via Ozawa Model. Ozawa model is extended of Avrami model assuming that the non-isothermal crystallization process could be composed of small isothermal steps (Stephen and Cheng 2002). Many studies reported that, large banded spherulites, which belong to second nucleation growth, were formed during crystallization of PHB and PHBHV samples (Zhang et al. 2007) . Therefore, spherulite growth kinetics in other words secondary nucleation kinetics was evaluated via Lauritzen Hoffman Model.

5.4.3.1. Primary Nucleation Kinetics by Avrami Jeziorny, Ozawa and Lui Mo Models for Nonisothermal Crystallization

The crystallization exotherms of pristine and PHB-P naocomposites at various cooling rates are presented in Appendix C. In order to describe non isothermal

crystallization behavior of nanocomposites, parameters such as crystallization temperature (T_c), relative degree of crystallinity (X_c), half crystallization time ($t_{1/2}$) were obtained via DSC analysis at different cooling rates. Crystallization exotherms of PHB-P-N, PHB-P-1 and PHB-P-3 were shown in Figures C1, C2 and C3, respectively. T_c values also tabulated at Table C.1 for better understanding the effect of cooling rate on crystallization temperature. T_c of pristine PHB-P-N and its nanocomposites decreased with increasing cooling rate. This could be attributed the lower time scale that allow the polymer to crystallize as the cooling rate increases, therefore requiring a higher undercooling to initiate crystallization. Moreover, when the specimens are cooled fast, the motion of PHB molecules are not able to follow crystallization temperature. Xu and co workers reported that as the cooling rate increased the crystallization temperature decreased, they attributed this finding due to time dependency of crystallization process (Xu et al. 2001).

Relative degree of crystallinity (X_T) as a function of crystallization temperature T , is defined as:

$$X_T = \int_{T_0}^T \left(\frac{dH_c}{dT} \right) dT / \int_{T_0}^{T_\infty} \left(\frac{dH_c}{dT} \right) dT / \quad (5.3)$$

Where T_0 and T_∞ are the onset and end of crystallization temperatures, respectively. Appendix C includes the relative degree of crystallinity as a function of temperature for PHB-P nanocomposites at different cooling rates. It can be seen that all these curves have the same sigmoidal shape. The half time ($t_{1/2}$) can be obtained from relative crystallinity data. Table 5.6 shows the half time ($t_{1/2}$) required to reach 50% of its relative crystallinity of nanocomposites at different cooling rates. It can be seen that the higher the cooling rate, the shorter the time for crystallization. However, the $t_{1/2}$ value of the PHB-P-1 nanocomposite was lower than that of pristine PHB-P-N, signifying that exfoliated layered silicates act as nucleation agent, therefore time needed to crystallization decrease. On the other hand, $t_{1/2}$ value of the PHB-P-3 nanocomposite was higher than that of PHB-P-1. This could be also attributed to steric hindrance to limit the transportation of PHB polymer chains. Wu and coworkers also reported that, addition of OMMT to polymer matrix resulted in decrease half time ($t_{1/2}$) (Wu et al. 2007).

Avrami approach adopted to understand crystallization mechanism using equation 2.9 (Stephen and Cheng 2002). Where the exponent n is as mechanism constant

dependent on the type of nucleation and growth process parameters, and the parameter k_t is a composite rate constant that involves both nucleation and growth rate parameters. Using equation 2.10 which is in logarithmic form of Avrami equation and plotting $\ln[-\ln(1-X_t)]$ against $\ln t$ for each cooling rate, a straight line was obtained (Appendix C). Avrami plots of pristine PHB-P-N and its nanocomposites PHB-P-1 and PHB-P-3 was shown in Figure C.5, Figure C.6 and Figure C.7, respectively. The k_t and n values determined from the intercept and the slope of Avrami plots (Table 5.6). In order to obtain a straight line the data at low degree of crystallinity were only used since at higher relative crystallinity secondary nucleation in other words, spherulite formation took place. It must be taken into account that in nonisothermal crystallization, k_t and n parameters do not have the same physical meaning as in the isothermal crystallization since the temperature changes constantly in nonisothermal process. This affects the rates of both nuclei formation and spherulite growth ascribed to their temperature dependence. In this case, Jeziorny expanded Avrami equation to use in nonisothermal crystallization process (Stephen and Cheng 2002). The k_t values were used to find K_c by using equation 2.11. The results, obtained from Avrami plots and the Jeziorny method, are also listed in Table 5.6. The exponent n varied from 4.7 to 5.1 for pristine PHB-P-N, from 3.0 to 4.1 for PHB-P-1 and from 3.6 to 6.34 for PHB-P-3 nanocomposites. The n values of PHB-P-N might be corresponding to a three dimensional growth with an athermal nucleation during the cooling scans. The values of n for nanocomposites vary compared to pristine PHB-P-N. This could be due to complexity of crystallization mechanics of nanocomposite systems (Wu et al. 2007). The values of K_c were increased as the cooling increased. In addition, addition of Cloisite 10A to polymer matrix increased the K_c which shows that layered silicates increased the rate of heterogeneous nucleation of polymer. The results are in good agreement with the DSC result of nanocomposites in where heterogeneous nucleation took place of homogenous nucleation. As indicated in Table 5.5, addition of Cloisite 10A at low content increased the ΔH_{12} value compared to pristine PHB.

Many studies reported that addition of layered silicates at low amount resulted in the decrease in half time crystallization values due to nucleating effect of layered silicates in polymer matrix (Xu et al. 2001; 2003)

Ozawa extended the Avrami equation to the nonisothermal condition. Assuming that the nonisothermal crystallization process may be composed of small isothermal crystallization steps, equation 2.12 was derived by Ozawa (Stephen and Cheng 2002).

Table 5.6. Avrami Jeziorny parameter for PHB-P nanocomposite at different cooling rates

Sample Code	ϕ (K/min)	k_t	K_c	n	$t_{1/2}$
PHB-P-N	20	3.251	1.052	5.1	0.74
	10	0.178	0.697	7.8	1.12
	5	0.050	0.537	4.7	1.75
PHB-P-1	20	9.877	1.118	3.0	0.415
	10	1.426	1.018	3.2	0.8
	5	0.059	0.571	4.1	1.69
PHB-P-3	20	3.219	1.061	6.3	0.56
	10	1.013	1.001	3.8	0.85
	5	0.123	0.658	3.7	1.75

Taking the logarithm of equation 2.12 and plotting $\ln[-\ln(1-X_t)]$ against $\ln \phi$ at a given temperature, a straight line should be obtained if the Ozawa model is valid (Xu et al. 2003). Ozawa plots of PHB-P nanocomposites were shown in Appendix C. The curvature in Figure C.10 prevents an accurate analysis of the nonisothermal crystallization data. This can be explained that, at a given temperature, the crystallization processes at different cooling rates are at different stages, that is, the lower cooling rate process is toward the end of the crystallization process, whereas at the higher cooling rate, the crystallization process is at an early stage. However, as it is seen from Ozawa plots, curvatures are far away from being linear. Non linear behavior means that the parameter m is not a constant during crystallization, indicating that Ozawa's approach is not a good method to describe the nonisothermal crystallization process of PHB-P nanocomposites.

A method developed by Lui Mo (Stephen and Cheng 2002) was also employed to describe the nonisothermal crystallization for comparison. Ozawa and Avrami equation was arranged and following equation was formed by Mo:

$$\ln \phi = \ln F(T) - \alpha \ln t \quad (5.4)$$

Where $F(T) = \left[\frac{K(T)}{K_t}\right]^{1/m}$ refers to the cooling value and α is the ratio of the Avrami exponent n to the Ozawa exponent m ($\alpha=n/m$). According to the equation 5.4, $F(T)$ and α were found by plotting $\ln \phi$ versus $\ln t$ at a given degree of crystallinity

(Appendix C). The data of kinetic triplet parameter $F(T)$ and α were found from the intercept and slope for PHB-P nanocomposites and tabulated in Table 5.7. It can be seen that $F(T)$ increases with the increase in the relative degree of crystallinity for the PHB-P nanocomposites. The α values vary from 1.43 to 1.7 for pristine PHB-P-N, from 0.59 to 0.61 for PHB-P-1 nanocomposite and from 1.71 to 1.80 for PHB-P-3 nanocomposites. The results are in good agreement with the result of Avrami approach. As $F(T)$ decreases crystallization rate decreases. In addition, at higher relative crystallinity values $F(T)$ reached its maximum values due to secondary nucleation process. In addition, activation energies at different cooling rates were evaluated by using Kissinger equation 5.5. The Kissinger plots, $\ln(\phi/T_p^2)$ versus $1/T_p$ were plotted and the slope was used to evaluate activation energy of nanocomposites. The activation energies of PHB-P nanocomposites were tabulated in Table 5.7. Addition Cloisite 10A lowered activation energy, however decrease in activation energy was not so significant. In contrast, according to Avrami approach, small amount of addition of Cloisite 10A showed in nucleation effect by increasing the nucleation rate. This behavior could be resulted due to secondary nucleation effect.

$$\frac{d[\ln(\frac{\phi}{T_c^2})]}{d(\frac{1}{T_c})} = \frac{-\Delta E}{R} \quad (5.5)$$

Table 5.7. Nonisothermal Crystallization Kinetic Parameters at Different Degree of Crystallinity

Sample Code	X_t	$F(T)$	α	E_a (kJ/mol)
PHB-P-N	20	9.48	1.7	223.031
	40	11.47	1.65	
	60	13.06	1.59	
	80	14.87	1.43	
PHB-P-1	20	5.64	0.6	220.521
	40	6.29	0.61	
	60	6.89	0.61	
	80	7.46	0.59	
PHB-P-3	20	6.55	1.8	226.008
	40	8.67	1.78	
	60	11.02	1.75	
	80	14.29	1.71	

5.5. Contact Angle Measurements of PHB and PHBHV Nanocomposite Films

The measure of surface wettability or spreadability of PHB and PHBHV nanocomposites was determined via contact angle measurements. In order to observe the effect of clay (Cloisite 10A) loading on PHB and PHBHV nanocomposite surface wettability, static contact angle measurements were evaluated at room temperature. Measured water contact angles of PHB and PHBHV nanocomposites were tabulated in Table 5.8. The water contact angle of pristine PHB-S-N sample was 75.99°. However, when the small amount of Cloisite 10A (1% and 2% w/w) was incorporated, the water contact angles of PHB-S nanocomposites significantly increased, and it reached its highest value of 81.62°, in comparison to pure PHB-S sample. This implies decrease in degree of wetting for PHB-S-1 and PHB-S-2 samples due to the exfoliation of layered silicates so as the surface became more hydrophobic. In addition, at higher amount of Cloisite 10A loading (7%w/w), the water contact angle decreased to 69.62° and became even lower than pristine PHB-S samples.

Table 5.8. Static contact angles measured for PHB and PHBHV nanocomposites

Sample Code	Left Angle(θ)	Right Angle(θ)	Mean Value(θ)
PHB-S-N	76.21±1.10	75.77±1.97	75.99±0.31
PHB-S-1	82.11±1.37	81.12±1.15	81.62±0.70
PHB-S-2	79.70±1.90	80.90±2.97	80.30±2.26
PHB-S-3	73.21±0.84	75.16±.38	74.19±1.38
PHB-S-5	74.14±2.21	73.21±2.31	73.68±0.66
PHB-S-7	69.12±3.32	70.12±3.53	69.62±0.71
PHBHV-S-N	83.34±0.99	82.93±1.85	83.13±0.28
PHBHV-S-1	87.43±1.25	85.46±1.03	86.44±1.40
PHBHV-S-3	82.91±1.79	82.00±2.85	82.45±0.64
PHBHV-S-5	75.20±0.73	74.65±0.26	74.93±0.39
PHB-P-N	68.43±2.10	67.91±2.19	68.17±0.37
PHB-P-1	70.83±3.21	69.86±3.41	70.34±0.69
PHB-P-3	71.07±1.69	69.70±1.67	70.38±0.96
PHB-P-5	66.22±3.42	65.30±3.52	65.76±0.65
PHB-P-7	67.09±3.17	65.12±4.36	66.11±1.40
PHBHV-P-N	69.92±4.13	68.93±4.45	69.43±0.71
PHBHV-P-1	76.57±2.60	74.95±3.11	75.76±1.15
PHBHV-P-3	75.73±4.65	74.81±4.89	75.27±0.65
PHBHV-P-5	75.24±2.35	74.48±2.08	74.86±0.54
PHBHV-P-7	71.34±2.22	71.37±2.32	71.36±0.02

Similarly, the same trend was also observed for the PHBHV-S, PHB-P, and PHBHV-P nanocomposites. This effect of hydrophilic and hydrophobic nature of clay was also investigated in literature (Thellen et al. 2005; Ratnayake et al. 2009; Anadao et al. 2010). They found that addition of unmodified clay since it has hydrophilic nature into polymer matrix, resulted in increase in hydrophilic nature of polymer surface.

When the effect of addition of Cloisite 10A contact angle values of the samples prepared via melt compounding and solvent casting was compared, it was observed that nanocomposites prepared via solvent casting (PHB-S and PHBHV-S) had higher values than melt compounded nanocomposites (PHB-P and PHBHV-P). In addition, results showed that the copolymers PHBHV-S and PHBHV-P were more hydrophobic than PHB-S and PHB-P polymers. The trend in contact angle measurements was in good accordance with the water vapor permeability results.

As the degree of surface hydrophobicity increased with an increase Cloisite 10A content, WVP of nanocomposites decreased indicating relationship between contact angle changes and water vapor permeability due to changes in the structure of nanocomposite. Hydrophobic nature of polymer surface can limit the adsorption of water vapor molecules, so the first necessary step needed for permeation process is affected by surface characteristic.

5.6. Biodegradation of PHB-P Nanocomposite Films

In order to reduce the environmental pollution caused by conventional oil based plastics waste, hydrolytic degradation of biopolymers such as PLA, PCL, PHB, and PHBHV have been investigated in literature (Wang et al. 2005; Parulekar et al. 2007; Someya et al. 2007; Ozkoc and Kemalolu 2009). Although many studies have been reported on biodegradable polymer/clay nanocomposites, few studies are available for the biodegradation of PHB and PHBHV clay nanocomposites. Therefore, this study is aimed to investigate effect of Cloisite 10A addition to PHB-P and PHBHV polymers on biodegradation properties of prepared nanocomposites films. Biodegradation of the samples was investigated in enzymatic solution medium by measuring the residual weight of samples.

Figure 5.25 shows the residual weight of PHB-P nanocomposites in enzyme phosphate buffer solution. After degradation for one week, the weight loss of pristine

PHB-P was about 8%., weight losses of nanocomposites for PHB-P-1, PHB-P-3, PHB-P-5, and PHB-P-7 were 10.6%, 6.83%, 3.6%, and 4.3% respectively. Additionally, the rate of erosion of nanocomposites for PHB-N, PHB-P-1, PHB-P-3, PHB-P-5, and PHB-P-7 were 1.56, 1.75, 1.21, 0.91, and 1.11 $\text{mg w}^{-1} \text{cm}^{-2}$ respectively (Figure 5.25). Small addition of Cloisite 10A (1% w/w) resulted in higher erosion rate compared to pristine PHB-P. In contrast, rate of erosion decreased significantly at higher content of Cloisite 10A loaded samples (Figure 5.26). This could be attributed to dispersion level of clay particles in polymer matrix. As it is known, degradation process occurs in amorphous phase of polymers (Mittal 2010). Therefore, degree of crystallinity of polymer is important in degradation process. Moreover, the melt crystallized films exhibit large banded spherulites and the spherulitic morphology so as degree of crystallinity are dependent on crystallization conditions (Abe and Doi 1999). DSC analysis showed that exfoliated structure of layered silicates resulted in lower crystallinity when compared with pristine samples. Thus, it can be concluded that exfoliated structure of layered silicates increased erosion rate due to decrease in total crystallinity. The results consistent with the study of Wang et al in which the weight loss degradation at small amount of clay loaded PHB sample is greater than higher clay loaded samples (Wang et al. 2005).

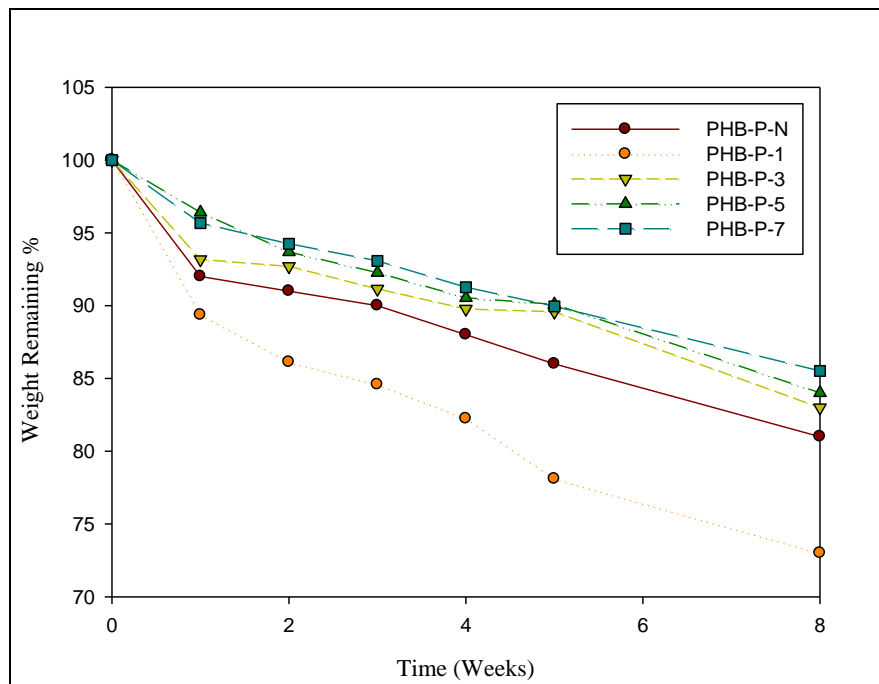


Figure 5.25. Weight remaining of PHB-P nanocomposites in enzymatic degradation

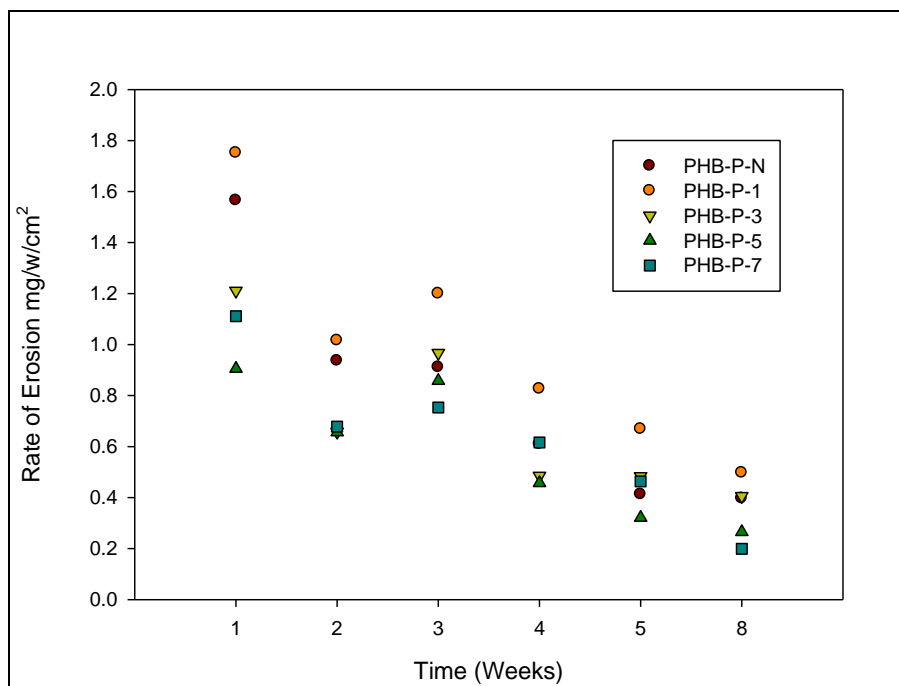
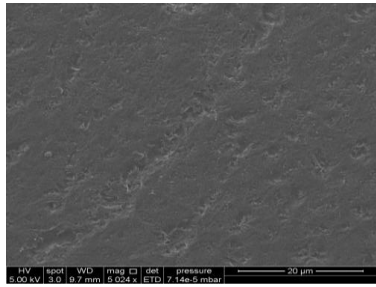
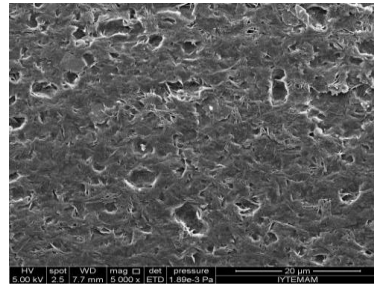


Figure 5.26. Rate of erosion of PHB-P nanocomposite films

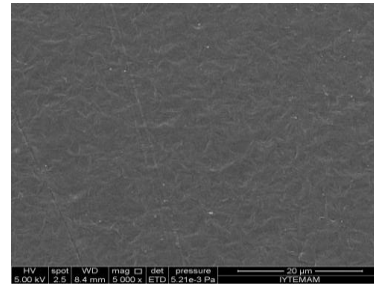
Enzymatic degradation occurred on the surface of PHB-P nanocomposite films, and the weight loss is dependent on surface area of samples. In order to investigate the effect of degradation on surface morphology of PHB-P nanocomposites, SEM images of the surfaces before and after biodegradation were taken (Figure 5.27).



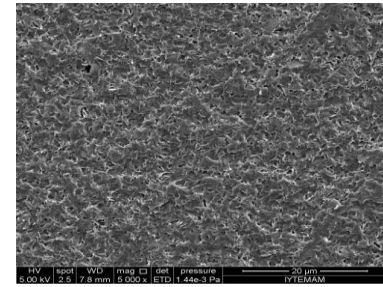
a)



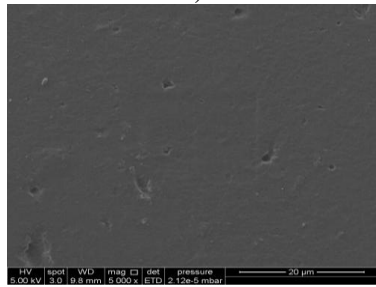
b)



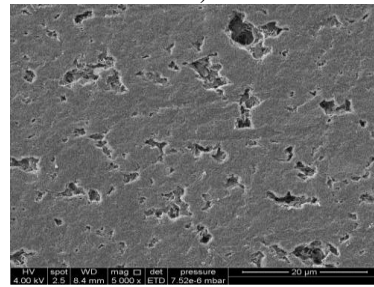
c)



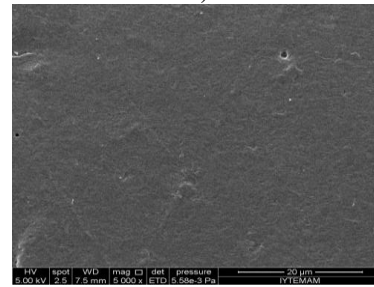
d)



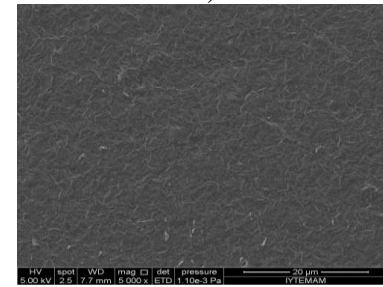
e)



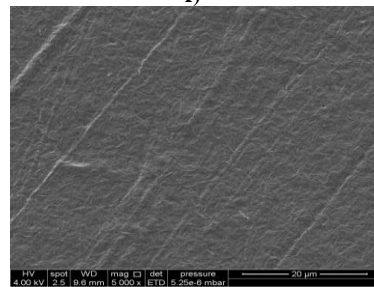
f)



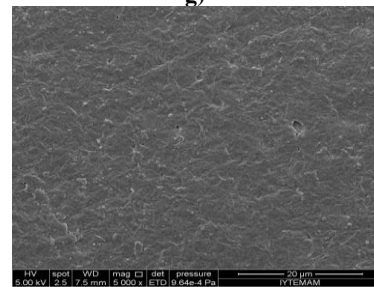
g)



h)



i)



j)

Figure 5.27 Scanning electron microscope of PHB-P nanocomposites before and after biodegradation a) PHB-P-N before degradation b) PHB-P-N after degradation, c) PHB-P-1 before degradation d) PHB-P-1 after degradation, e) PHB-P-3 before degradation f) PHB-P-3 after degradation g) PHB-P-5 before degradation h) PHB-P-5 after degradation i) PHB-P-7 before degradation j) PHB-P-7 after degradation for 8 weeks

As it is seen in Figure 5.27 the surface of the films was relatively smooth before degradation, however after degradation the surfaces were apparently blemished by the action of depolymerase secreted by enzyme. The pore density was the highest for PHB-P-1. The uniformity in degradation could be resulted due to the exfoliation of layered silicates. However, for higher clay loaded sample (PHB-P-3) bigger and random holes were observed. This could be due to intercalated structure of layered silicates in polymer matrix. Moreover, there were no holes observed at PHB-P-5 and PHB-P-7 since agglomerated layered silicates did not give access to enzyme for degradation. SEM results are in good accordance with the residual weight results of nanocomposites at the end of degradation (Figure 5.25).

5.7. Color Changes in PHB-S and PHBHV-S Nanocomposite Films

Color changes in PHB-S and PHBHV nanocomposites due to addition of fillers are also very important for their possible use as packaging film since the commercial plastics (e.g. PP) used in packaging applications are generally transparent.. In this manner, the effect of Cloisite 10A loading on color properties of pristine PHB-S and PHBHV-S composite films were evaluated by using Hunter Method. The total color differences (ΔE) of the coated films were calculated using the parameters L, a and b of nanocomposites. The evaluated color differences in nanocomposites (PHB-S and PHBHV-S) were tabulated in Table 5.9. The lightness parameter L did not change significantly by addition of clay into PHB and PHBHV matrix. The parameters “a and b”, which are the measure of redness-greenness, yellowness, respectively, also did not change significantly compared to pristine PHB-S-N and PHBHV-S-N samples. When total color difference is greater than 3 ($\Delta E > 3$), the changes in the color can be recognized by human naked eye (Oguzlu and Tihminlioglu 2010). Since total color differences ΔE were lower than 3 for all nanocomposites samples, it can be said that, incorporation of Cloisite 10A to pristine PHB-S and PHBHV-S matrix did not alter color properties significantly.

Table 5.9. The total color difference (ΔE) and color parameters of prepared PHB-S and PHBHV-S nanocomposites

Sample Code	L	a	b	ΔE
PHB-S-N	87.38	-0.72	2.92	0.00
PHB-S-1	86.25	-0.59	3.54	1.29
PHB-S-2	86.94	-0.63	3.44	0.70
PHB-S-3	86.61	-0.58	3.41	0.94
PHB-S-5	87.06	-0.60	3.57	0.76
PHB-S-7	87.06	-0.69	3.31	0.51
PHB-HV-S-N	86.34	-0.75	1.88	0
PHB-HV-S-1	85.22	-0.62	2.50	1.29
PHB-HV-S-3	85.57	-0.61	2.37	0.92
PHB-HV-S-5	86.01	-0.63	2.53	0.74

CHAPTER 6

CONCLUSION

In this study, bionanocomposites, based on biodegradable thermoplastic polyester polymers, PHB and PHBHV were prepared by incorporation of organomodified monmorillonte (OMMT) via solution intercalation and melt mixing techniques. As an alternative to conventional food packaging plastics, prepared nanocomposites were characterized by investigating the effect of addition of OMMT into polymer matrix on barrier, thermal, mechanical and optical properties.

Structural characterization of prepared nanocomposites was carried out by FTIR and XRD analyses. The possible chemical alteration due to interaction between layered silicate and polymer matrix were evaluated via FTIR analysis. It was observed that the characteristic bands of Si-O bending (460 cm^{-1}) and Si-O-Si stretching vibration (1040 cm^{-1}) of layered silicates slightly changed the FTIR spectra of nanocomposites in comparison to pristine polymer. Moreover, XRD results of nanocomposites showed that the exfoliated structure of layered silicates was obtained at low content of Cloisite 10A (1%w/w). However, at higher Cloisite 10A loaded samples, intercalated structure was observed due to poor dispersion of layered silicates in polymer matrix. The effect of dispersion level on characteristic properties of nanocomposites was also examined in this study.

Addition of 2%w/w OMMT into PHB matrix resulted in 41% reduction in WVP of pristine PHB-S films. Improvement in water vapor barrier performance of all nanocomposites was observed up to a critical limit of Cloisite 10A content due to the changes in nanostructure after a certain nanoclay loadings. However, nanocomposites prepared via solution intercalation exhibited better enhancement in water vapor barrier performance than those prepared by melt intercalation method. This could be due to dispersion level of layered silicates into polymer matrix. Dispersed particle layers in polymer matrix with the large aspect ratios force permeating molecules to follow more tortuous path. For better understanding of the effect of dispersed layered silicates on barrier performance, aspect ratio of layered silicates was evaluated via various models by fitting to experimental water vapor permeation data. It was found that Cussler

Regular and Random models were the best fitted models in which aspect ratio value of layered silicates was determined as around 160 and 240, respectively.

Significant enhancement in tensile strength, elongation at break and Young's Modulus was obtained by incorporation of layered silicate into polymer matrix. In all nanocomposites, mechanical properties were improved up to a critical limit of Cloisite 10A amount due to the changes in structure of layered silicates in polymer matrix. Most promising improvement was observed in 2%w/w OMMT loaded sample (PHB-S-2) in which tensile strength and strain increased 2 times and 69% relative to virgin PHB-S sample, respectively.

Thermal stability of nanocomposites was investigated via thermogravimetric measurement. The results of TGA analyses showed that the rate of weight loss decreased when the onset temperature of decomposition increased by addition of layered silicates into polymer matrix. This could be due to barrier effect of clay particle which restricts thermal motion of polymer chains. Kinetics of isothermal degradation was evaluated so as to understand the effect of Cloisite 10A addition on thermal stability of nanocomposites. Activation energy of decomposition was evaluated and found that addition of layered silicates increased the activation energy in comparison to pristine polymer. However, at higher clay loaded samples activation energy decreased which can be attributed to intercalated structure of layered silicate in polymer matrix. For better understanding the effect of addition of layered silicates in polymer on crystallization mechanism, DSC analyses were carried out at different cooling rates. Various models were fitted to experimental data and it was observed that exfoliated structure of layered silicate acted as nucleating agent by increasing the crystallization rate constant. Moreover, heterogeneous nucleation took the place of homogenous nucleation by the addition layered silicate.

Biodegradability of prepared nanocomposites was investigated via enzymatic degradation in phosphate buffer medium. Incorporation of even low amount of Cloisite 10A (1%w/w OMMT) increased rate of erosion increased by relative to virgin polymer. However, erosion rate decreased at higher clay loaded samples. Biodegradation rate of the composites is related to morphology of the composites which deals with crystallinity and dispersion level of layered silicates in polymer.

In conclusion, in all nanocomposites, structure of layered silicate in polymer matrix plays a crucial role that affects characteristic properties of nanocomposites. The most significant enhancements were achieved in exfoliated structured nanocomposites.

Addition of layered silicates at low amount enhanced the properties that are necessary to be used in food packaging application.

REFERENCES

- Abe, H. and Y. Doi. Structural effects on enzymatic degradabilities for poly[(R)-3-hydroxybutyric acid] and its copolymers. *International journal of biological macromolecules* 1999 **25**(1–3): 185-192.
- Abou-Zeid, D. M., R. J. Muller and W. D. Deckwer. Degradation of natural and synthetic polyesters under anaerobic conditions. *Journal of biotechnology* 2001 **86**(2): 113-126.
- Achilias, D. S., E. Panayotidou and I. Zuburtikudis. Thermal degradation kinetics and isoconversional analysis of biodegradable poly(3-hydroxybutyrate)/organomodified montmorillonite nanocomposites. *Thermochimica Acta* 2011 **514**(1-2): 58-66.
- Anadao, P., L. F. Sato, H. Wiebeck and F. R. Valenzuela-Diaz. Montmorillonite as a component of polysulfone nanocomposite membranes. *Applied Clay Science* 2010 **48**(1-2): 127-132.
- Bandyopadhyay, J., S. S. Ray and M. Bousmina. Nonisothermal crystallization kinetics of poly(ethylene terephthalate) nanocomposites. *Journal of Nanoscience and Nanotechnology* 2008 **8**(4): 1812-1822.
- Barud, H. S., J. L. Souza, D. B. Santos, M. S. Crespi, C. A. Ribeiro, Y. Messaddeq and S. J. L. Ribeiro. Bacterial cellulose/poly(3-hydroxybutyrate) composite membranes. *Carbohydrate Polymers* 2011 **83**(3): 1279-1284.
- Bharadwaj, R. K. Modeling the Barrier Properties of Polymer-Layered Silicate Nanocomposites. 2001.
- Botana, A., M. Mollo, P. Eisenberg and R. M. Torres Sanchez. Effect of modified montmorillonite on biodegradable PHB nanocomposites. *Applied Clay Science* 2010 **47**(3-4): 263-270.
- Burgentzle, D., J. Duchet, J. F. Gerard, A. Jupin and B. Fillon. Solvent-based nanocomposite coatings I. Dispersion of organophilic montmorillonite in organic solvents. *Journal of Colloid and Interface Science* 2004 **278**(1): 26-39.
- Cervantes-Uc, J. M., J. V. Cauich-Rodríguez, H. Vázquez-Torres, L. F. Garfias-Mesías and D. R. Paul. Thermal degradation of commercially available organoclays studied by TGA–FTIR. *Thermochimica Acta*.2007 **457**: 92-102.

- Chen, D., C. Tang, K. Chan, C. Tsui, P. Yu, M. Leung and P. Uskokovic. Dynamic mechanical properties and in vitro bioactivity of PHBHV/HA nanocomposite. *Composites Science and Technology* 2007 **67**(7-8): 1617-1626.
- Chen, G. X., G. J. Hao, T. Y. Guo, M. D. Song and B. H. Zhang. Crystallization kinetics of poly(3-hydroxybutyrate-co-3-hydroxyvalerate)/clay nanocomposites. *Journal of Applied Polymer Science* 2004 **93**(2): 655-661.
- Cheng, G., Cai, Z., Wang, L. . Biocompatibility and biodegradation of poly(hydroxybutyrate)/poly(ethylene glycol) blend films. *Journal of Materials Science: Materials in Medicine* 2003 **14**: 1973-1978
- Chi, W. S., R. Patel, H. Hwang, Y. G. Shul and J. H. Kim. Preparation of poly(vinylidene fluoride) nanocomposite membranes based on graft polymerization and sol-gel process for polymer electrolyte membrane fuel cells. *Journal of Solid State Electrochemistry* 2012 **16**(4): 1405-1414.
- Choi, W. M., T. W. Kim, o. O. Park, Y. K. Chang and J. W. Lee. Preparation and Characterization of Poly(hydroxybutyrateco-hydroxyvalerate)-Organoclay Nanocomposites. 2003.
- Collier, C. M., X. Jin and J. F. Holzman. Ultrafast Refractometry for Characterization of Nanocomposite Material Systems. *Ieee Photonics Technology Letters* 2012 **24**(7): 590-592.
- Cornwelle, A. J. Barrier Properties of Polymer Nanocomposites. V. Mital. New York, Nova Science Publisher.2009.
- Erceg, M., T. Kovacic and I. Klaric. Thermal degradation and kinetics of poly(3-hydroxybutyrate)/organoclay nanocomposites. *Macromolecular Symposia* 2008 **267**: 57-62.
- Erceg, M., T. Kovacic and S. Perinovic. Isothermal Degradation of Poly(3-hydroxybutyrate)/Organically Modified Montmorillonite Nanocomposites. *Polymer Composites* 2010 **31**(2): 272-278.
- Erceg, M., T. Kovačić and S. Perinović. Isothermal degradation of poly(3-hydroxybutyrate)/organically modified montmorillonite nanocomposites. *Polymer Composites* 2009: NA-NA.
- Fujimori, A., N. Ninomiya and T. Masuko. Structure and mechanical properties in drawn poly(l-lactide)/clay hybrid films. *Polymers for Advanced Technologies* 2008 **19**(12): 1735-1744.

- Garcia-Quesada, J. C., I. Pelaez, O. Akin and I. Kocabas. Processability of PVC plastisols containing a polyhydroxybutyrate-polyhydroxyvalerate copolymer. *Journal of Vinyl and Additive Technology* 2012 **18**(1): 9-16.
- Gatos, K. and J. Kargerkocsis. Effect of the aspect ratio of silicate platelets on the mechanical and barrier properties of hydrogenated acrylonitrile butadiene rubber (HNBR)/layered silicate nanocomposites. *European Polymer Journal* 2007 **43**(4): 1097-1104.
- Gedde, U. W. *Polymer Physics*, Chapman & Hall.1995.
- Grozdanov, A., A. Buzarovska, G. Bogoeva-Gaceva, M. Avella, M. E. Errico and G. Gentile. Nonisothermal crystallization kinetics of kenaf fiber/polypropylene composites. *Polymer Engineering and Science* 2007 **47**(5): 745-749.
- Gunaratne, L. M. W. K. and R. A. Shanks. Melting and thermal history of poly(hydroxybutyrate-co-hydroxyvalerate) using step-scan DSC. *Thermochimica Acta* 2005 **430**(1-2): 183-190.
- Hansen, C. M. (2000). *Hansen Solubility Paramater A User's Handbook*.
- He, J. D., M. K. Cheung, P. H. Yu and G. Q. Chen. Thermal analyses of poly(3-hydroxybutyrate), poly(3-hydroxybutyrate-co-3-hydroxyvalerate), and poly(3-hydroxybutyrate-co-3-hydroxyhexanoate). *Journal of Applied Polymer Science* 2001 **82**(1): 90-98.
- Herrera-Alonso, J. M., E. Marand, J. C. Little and S. S. Cox. Transport properties in polyurethane/clay nanocomposites as barrier materials: Effect of processing conditions. *Journal of Membrane Science* 2009 **337**(1-2): 208-214.
- Hulsmann, P., D. Philipp and M. Kohl. Measuring temperature-dependent water vapor and gas permeation through high barrier films. *Review of Scientific Instruments* 2009 **80**(11): 113901.
- Hwang, J. J., S. M. Huang, H. J. Liu, H. C. Chu, L. H. Lin and C. S. Chung. Crystallization kinetics of poly (L-lactic acid)/montmorillonite nanocomposites under isothermal crystallization condition. *Journal of Applied Polymer Science* 2012 **124**(3): 2216-2226.
- Jaafar, J., A. F. Ismail and T. Matsuura. Effect of dispersion state of Cloisite15A (R) on the performance of SPEEK/Cloisite15A nanocomposite membrane for DMFC application. *Journal of Applied Polymer Science* 2012 **124**(2): 969-977.

- Karbasi, S., H. Hajiali, M. Hosseinalipour and H. R. Rezaie. Preparation of a novel biodegradable nanocomposite scaffold based on poly (3-hydroxybutyrate)/bioglass nanoparticles for bone tissue engineering. *Journal of Materials Science-Materials in Medicine* 2010 **21**(7): 2125-2132.
- Koo, J. H. (2006). *Polymer Nanocomposites Processing, Characterization, Applications*, McGraw-Hill.
- Lagaron, J. M., M. D. Sanchez-Garcia and E. Gimenez. Morphology and barrier properties of nanobiocomposites of poly(3-hydroxybutyrate) and layered silicates. *Journal of Applied Polymer Science* 2008 **108**(5): 2787-2801.
- Liu, L., S. L. Wei and X. J. Lai. In situ synthesis and characterization of polypropylene/polyvinyl acetate-organophilic montmorillonite nanocomposite. *Journal of Applied Polymer Science* 2012 **124**(5): 4107-4113.
- Madison, L. L. and G. W. Huisman. Metabolic engineering of poly(3-hydroxyalkanoates): from DNA to plastic. *Microbiol Mol Biol Rev* 1999 **63**(1): 21-53.
- Mai, Y.-W. and Z.-Z. Yu. *Polymer Nanocomposites*. Cambridge Woodhead Publishing Limited.2006.
- Maiti, P., C. A. Batt and E. P. Giannelis. Biodegradable polyester/layered silicate nanocomposites. *Nanomaterials for Structural Applications* 2003 **740**: 141-145.
- Maiti, P., C. A. Batt and E. P. Giannelis. New biodegradable polyhydroxybutyrate/layered silicate nanocomposites. *Biomacromolecules* 2007 **8**(11): 3393-3400.
- Manikantan, M. R. and N. Varadharaju. Preparation and Properties of Polypropylene-Based Nanocomposite Films for Food Packaging. *Packaging Technology and Science* 2011 **24**(4): 191-209.
- McFerran, N. L. A., C. G. Armstrong and T. McNally. Nonisothermal and isothermal crystallization kinetics of nylon-12. *Journal of Applied Polymer Science* 2008 **110**(2): 1043-1058.
- Miguel, O. I. J. J. Water Transport Properties in Poly (3-hydroxybutyrate) and Poly(3-hydroxybutyrate-co-3-hydroxyvalerate) Biopolymers. *Journal of Applied Polymer Science* 1998 **73**: 455-468.
- Mittal, V. (2010). *Optimization of Polymer Nanocomposite Properties*, WILEY-VCH Verlag GmbH & Co.

- Mubarak, Y., E. M. A. Harkin-Jones, P. J. Martin and M. Ahmad. Modeling of non-isothermal crystallization kinetics of isotactic polypropylene. *Polymer* 2001 **42**(7): 3171-3182.
- Nguyen, Q. T. and D. G. Baird. Preparation of polymer–clay nanocomposites and their properties. *Advances in Polymer Technology* 2006 **25**(4): 270-285.
- Nguyen, T. P., A. Guinault and C. Sollogoub. Miscibility and Morphology of Poly(Lactic Acid)/Poly(B-Hydroxybutyrate) Blends. *International Conference on Advances in Materials and Processing Technologies, Pts One and Two* 2010 **1315**: 173-178.
- Oguzlu, H. and F. Tihminlioglu. Preparation and Barrier Properties of Chitosan-Layered Silicate Nanocomposite Films. *Polychar-18 World Forum on Advanced Materials* 2010 **298**: 91-98.
- Okamoto, M. Biodegradable Polymer Layered silicate Nanocomposites: A Review, American Scientific Publishers.2005 **1**.
- Ozkoc, G. and S. Kemaloglu. Morphology, Biodegradability, Mechanical, and Thermal Properties of Nanocomposite Films Based on PLA and Plasticized PLA. *Journal of Applied Polymer Science* 2009 **114**(4): 2481-2487.
- Panaitescu, D. M., Z. Vuluga, C. Radovici and C. Nicolae. Morphological investigation of PP/nanosilica composites containing SEBS. *Polymer Testing* 2012 **31**(2): 355-365.
- Parulekar, Y., A. K. Mohanty and S. H. Imam. Biodegradable nanocomposites from toughened polyhydroxybutyrate and titanate-modified montmorillonite clay. *Journal of nanoscience and nanotechnology* 2007 **7**(10): 3580-3589.
- Pavlidou, S. and C. D. Papaspyrides. A review on polymer-layered silicate nanocomposites. *Progress in Polymer Science* 2008 **33**(12): 1119-1198.
- Platt, D. K. (2006). *Biodegradable Polymers Market Report*, Smithers Rapra Limited.
- Ratnayake, U. N., B. Haworth and D. J. Hourston. Preparation of Polypropylene-Clay Nanocomposites by the Co-Intercalation of Modified Polypropylene and Short-Chain Amide Molecules. *Journal of Applied Polymer Science* 2009 **112**(1): 320-334.
- Ray, S. S. and M. Bousmina. Biodegradable polymers and their layered silicate nano composites: In greening the 21st century materials world. *Progress in Materials Science* 2005 **50**(8): 962-1079.

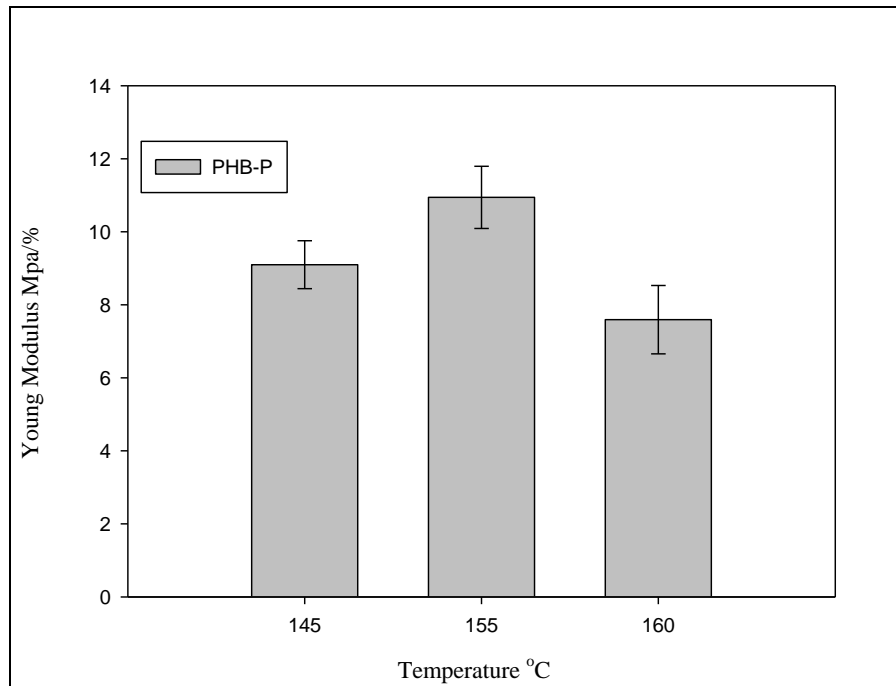
- Reddy, C. S. K. G., R., Rashmi and V. C. Kalia. Polyhydroxyalkanoates: an overview. *Bioresource technology* 2003 (87): 137-146.
- Reddy, S. V., M. Thirumala and S. Mahmood. Production of PHB and P (3HB-co-3HV) biopolymers by *Bacillus megaterium* strain OU303A isolated from municipal sewage sludge. *World Journal of Microbiology & Biotechnology* 2009 **25**(3): 391-397.
- Sanchez-Garcia, M. D., E. Gimenez and J. M. Lagaron. Morphology and barrier properties of nanobiocomposites of poly(3-hydroxybutyrate) and layered silicates. *Journal of Applied Polymer Science* 2008 **108**(5): 2787-2801.
- Sato, H., Y. Ando, H. Mitomo and Y. Ozaki. Infrared Spectroscopy and X-ray Diffraction Studies of Thermal Behavior and Lamella Structures of Poly(3-hydroxybutyrate-co-3-hydroxyvalerate) (P(HB-co-HV)) with PHB-Type Crystal Structure and PHV-Type Crystal Structure. *Macromolecules* 2011 **44**(8): 2829-2837.
- Shen, L., J. Haufe and M. K. Patel. Product Overview and Market Projection of Emerging Bio-based Plastics, European Bioplastics.2009.
- Shishatskaya, E. I., T. G. Volova, S. A. Gordeev and A. P. Puzyr. Degradation of P(3HB) and P(3HB-co-3HV) in biological media. *Journal of biomaterials science. Polymer edition* 2005 **16**(5): 643-657.
- Sinha Ray, S. and M. Okamoto. Polymer/layered silicate nanocomposites: a review from preparation to processing. *Progress in Polymer Science* 2003 **28**(11): 1539-1641.
- Siracusa, V., P. Rocculi, S. Romani and M. D. Rosa. Biodegradable polymers for food packaging: a review. *Trends in Food Science & Technology* 2008 **19**(12): 634-643.
- Smith, K. W., F. W. Cain and G. Talbot. Kinetic analysis of nonisothermal differential scanning calorimetry of 1,3-dipalmitoyl-2-oleoylglycerol. *J Agric Food Chem* 2005 **53**(8): 3031-3040.
- Someya, Y., N. Kondo and M. Shibata. Biodegradation of poly(butylene adipate-co-butylene terephthalate)/Layered-Silicate nanocomposites. *Journal of Applied Polymer Science* 2007 **106**(2): 730-736.
- Stephen, Z. D. and Cheng. Handbook of Thermal Analysis and Calorimetry: Applications to Polymers and Plastics. S. Z. D. Cheng, Elsevier.2002 **3**.

- Sun, L., W. J. Boo, A. Clearfield, H. J. Sue and H. Q. Pham. Barrier properties of model epoxy nanocomposites. *Journal of Membrane Science* 2008 **318**(1–2): 129-136.
- Terada, M. and R. H. Marchessault. Determination of solubility parameters for poly(3-hydroxyalkanoates). *International Journal of Biological Macromolecules* 1999 **25**(1-3): 207-215.
- Thellen, C., C. Orroth, D. Froio, D. Ziegler, J. Lucciarini, R. Farrell, N. A. D'Souza and J. A. Ratto. Influence of montmorillonite layered silicate on plasticized poly(L-lactide) blown films. *Polymer* 2005 **46**(25): 11716-11727.
- Tjong, S. C. Structural and mechanical properties of polymer nanocomposites. *Materials Science and Engineering: R: Reports* 2006 **53**(3–4): 73-197.
- van Krevelen, D. W. and P. J. Hoftyzer. Properties of polymers: their estimation and correlation with chemical structure. Amsterdam, Elsevier.1990.
- Verhoogt, H., B. A. Ramsay and B. D. Favis. Polymer Blends Containing Poly(3-Hydroxyalkanoate)S. *Polymer* 1994 **35**(24): 5155-5169.
- Wang, S., L. Shen, Y. Tong, L. Chen, I. Phang, P. Lim and T. Liu. Biopolymer chitosan/montmorillonite nanocomposites: Preparation and characterization. *Polymer Degradation and Stability* 2005 **90**(1): 123-131.
- Wang, S., C. Song, G. Chen, T. Guo, J. Liu, B. Zhang and S. Takeuchi. Characteristics and biodegradation properties of poly(3-hydroxybutyrate--3-hydroxyvalerate)/organophilic montmorillonite (PHBV/OMMT) nanocomposite. *Polymer Degradation and Stability* 2005 **87**(1): 69-76.
- Weber, C. J. (2000). Biobased Packaging Materials for the Food Industry: Status and Prospectives, KVL.
- Won Mook Choi, T. W. K., O Ok Park, Yong Keun Chang, Jin Woo Lee. Preparation and Characterization of Poly(hydroxybutyrateco-hydroxyvalerate)–Organoclay Nanocomposites. *Journal of Applied Polymer Science* 2003 **90**: 525-529.
- Wu, T. M., S. F. Hsu and C. S. Liao. Nonisothermal crystallization behavior and crystalline structure of poly(3-hydroxybutyrate)/layered double hydroxide nanocomposites. *Journal of Polymer Science Part B-Polymer Physics* 2007 **45**(9): 995-1002.
- Xu, W., M. Ge and P. He. Nonisothermal crystallization kinetics of polyoxymethylene/montmorillonite nanocomposite. *Journal of Applied Polymer Science* 2001 **82**(9): 2281-2289.

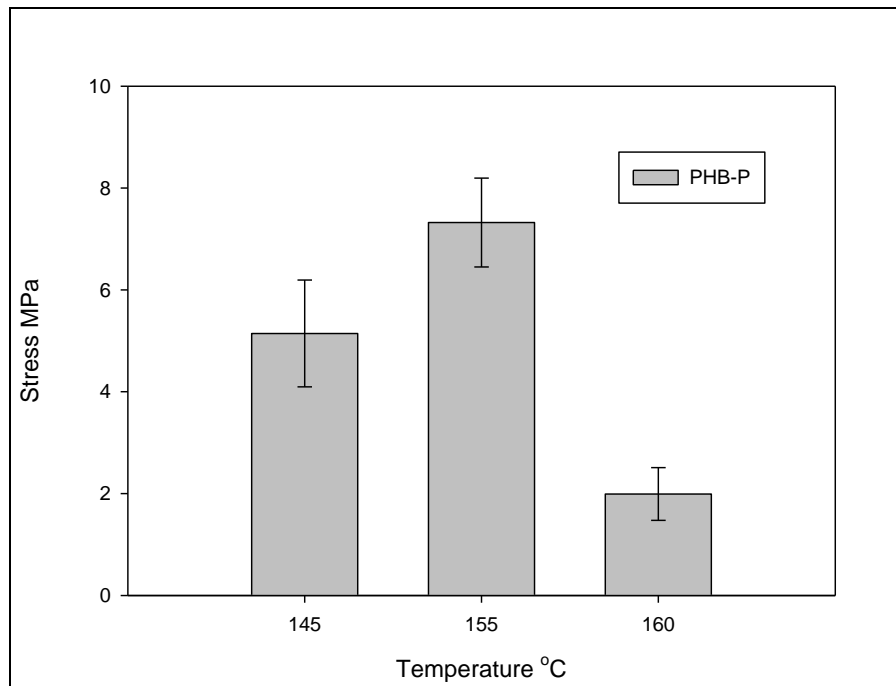
- Xu, W. B., G. D. Liang, H. B. Zhai, S. P. Tang, G. P. Hang and W. P. Pan. Preparation and crystallization behaviour of PP/PP-g-MAH/Org-MMT nanocomposite. *European Polymer Journal* 2003 **39**(7): 1467-1474.
- Yeo, S. Y., W. L. Tan, M. Abu Bakar and J. Ismail. Silver sulfide/poly(3-hydroxybutyrate) nanocomposites: Thermal stability and kinetic analysis of thermal degradation. *Polymer Degradation and Stability* 2010 **95**(8): 1299-1304.
- Yu, L. Biodegradable Polymer Blends and Composites. New Jersey, John Wiley & Sons.2009.
- Zhang, J. W., J. Qian, L. Y. Zhu and R. S. Whitehouse. Comparison of different nucleating agents on crystallization of poly(3-hydroxybutyrate-co-3-hydroxyvalerates). *Journal of Polymer Science Part B-Polymer Physics* 2007 **45**(13): 1564-1577.
- Zhang, M. and N. L. Thomas. Blending Polylactic Acid with Polyhydroxybutyrate: The Effect on Thermal, Mechanical, and Biodegradation Properties. *Advances in Polymer Technology* 2011 **30**(2): 67-79.
- Zhang, X. J., G. Lin, R. Abou-Hussein, M. K. Hassan, I. Noda and J. E. Mark. Some novel layered-silicate nanocomposites based on a biodegradable hydroxybutyrate copolymer. *European Polymer Journal* 2007 **43**(8): 3128-3135.
- Zhou, W. Y., B. Duan, M. Wang and W. L. Cheung. Crystallization Kinetics of Poly(L-Lactide)/Carbonated Hydroxyapatite Nanocomposite Microspheres. *Journal of Applied Polymer Science* 2009 **113**(6): 4100-4115.
- Zulfiqar, S., Z. Ahmad and M. I. Sarwar. Preparation and properties of aramid/layered silicate nanocomposites by solution intercalation technique. *Polymers for Advanced Technologies* 2008 **19**(12): 1720-1728.

APPENDIX A

CHARACTERIZATION OF PHB AND PHBV NANOCOMPOSITE FILMS

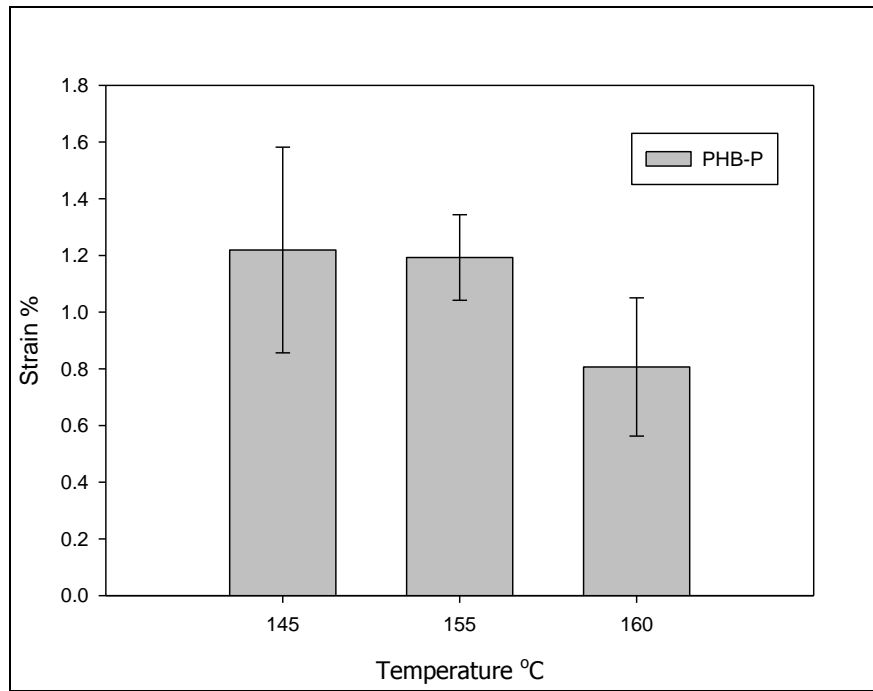


a)



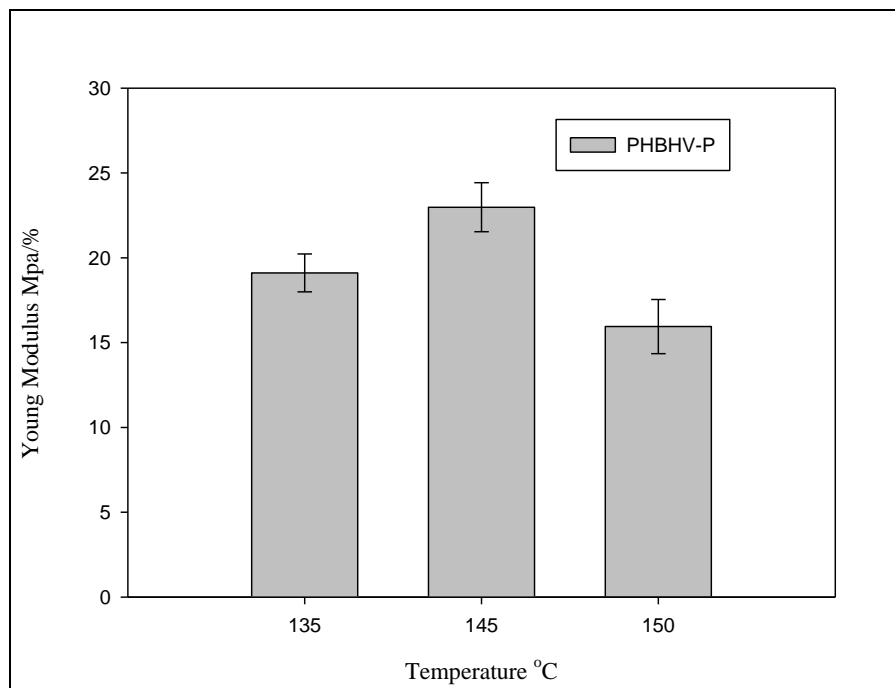
b)

Figure A.1. a) Young Modulus b) Tensile Strength and c) Strain of PHB-P at 145,155, and 160 C (cont. on next page)



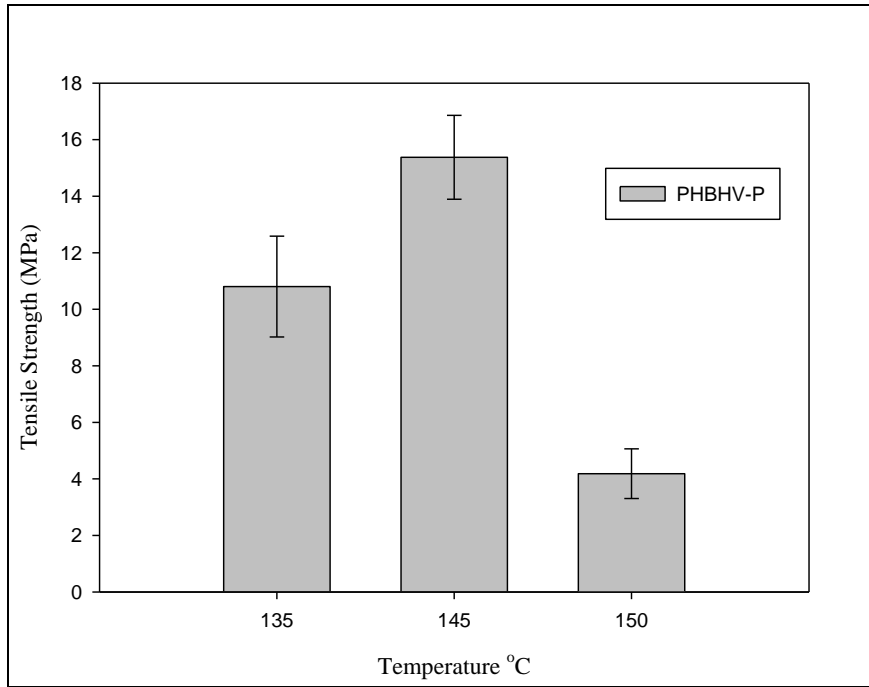
(Figure A.1. cont.)

c)

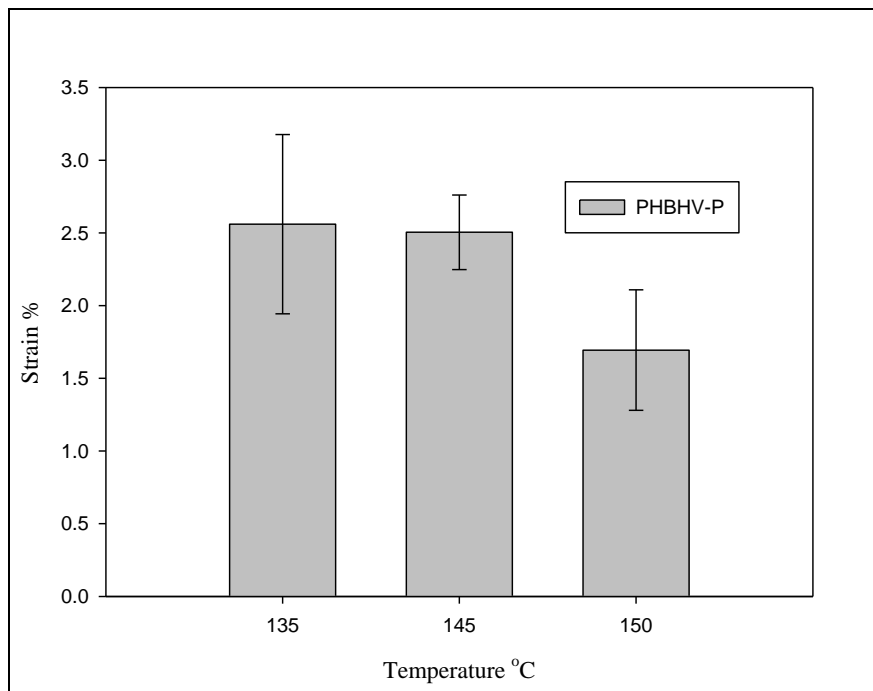


a)

Figure A.2. -a) Young Modulus b) Tensile Strength and c) Strain of PHB-P at 145,155, and 160 C (cont. on next page)



b)



c)

(Figure A.2. cont.)

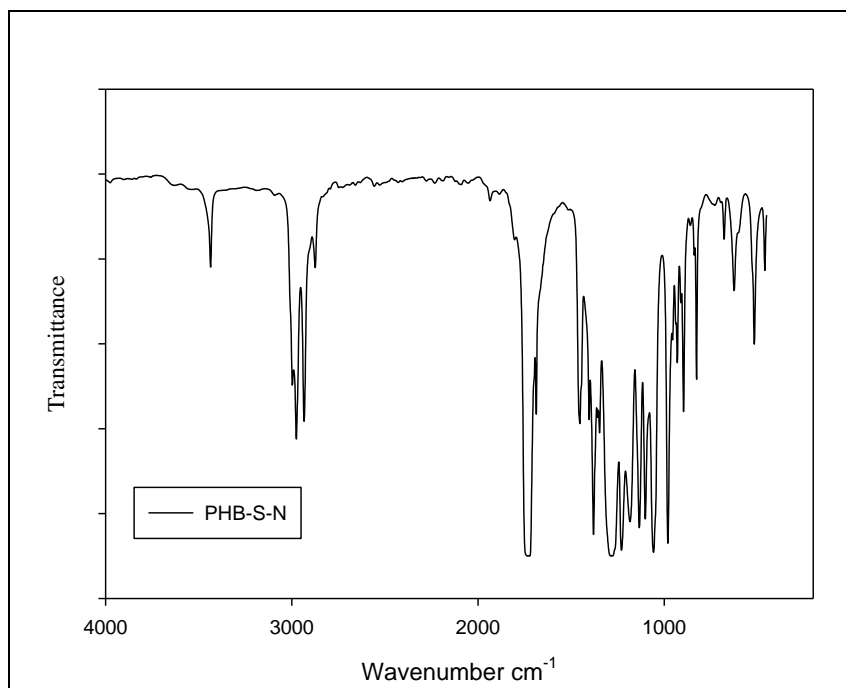


Figure A.3. FTIR spectrum of PHB-S-N

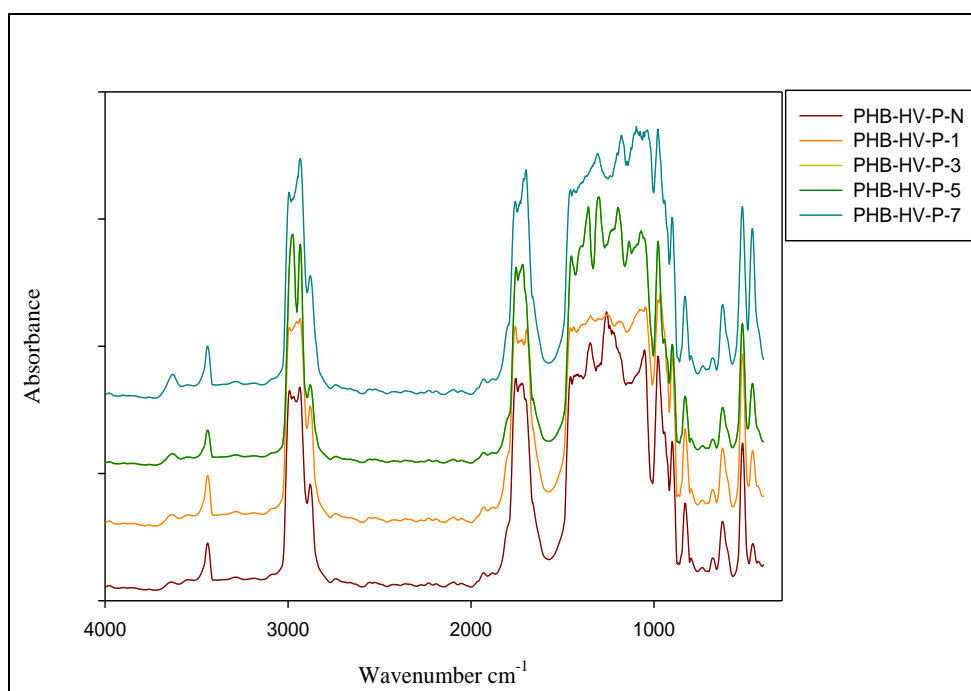


Figure A.4. FTIR Spectrum of PHBHV-P nanocomposite films

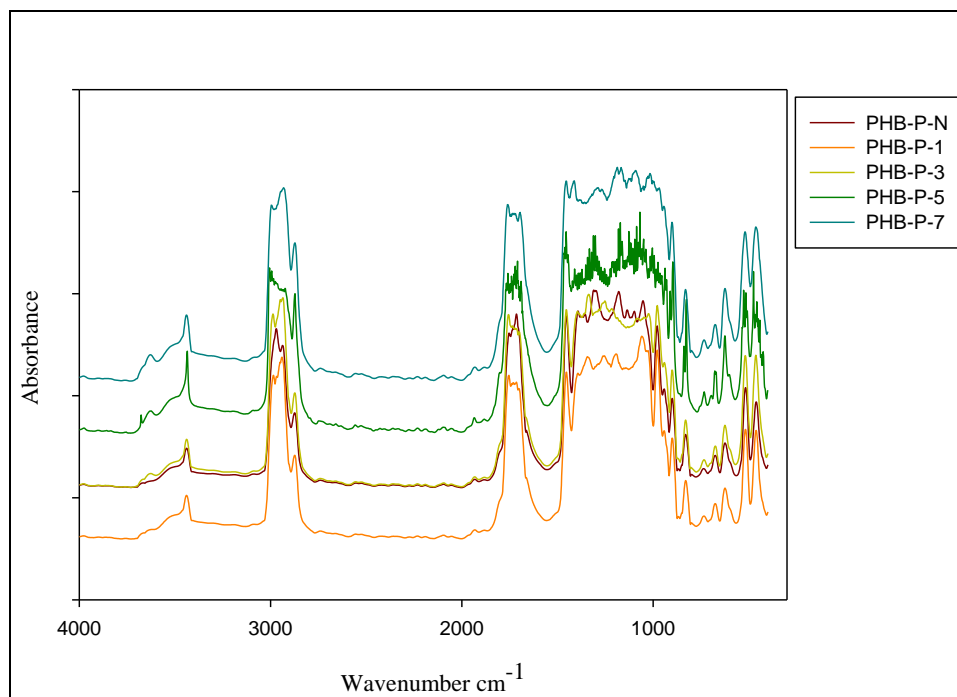


Figure A.5. FTIR Spectrum of PHB-P nanocomposite films

Table A.1. WVPs of PHB and PHBHV nanocomposites films

Sample Code	Cloisite 10A Concentration (%w/w)	WVP of Nanocomposite Films ($\times 10^{-2}$ g mm / m ² day mmHg)
PHB-S-N	-	3.60±0.57
PHB-S-1	1	2.45±0.45
PHB-S-2	2	2.12±0.33
PHB-S-3	3	2.30±0.24
PHB-S-5	5	24.8±1.75
PHB-S-7	7	-
PHBHV-S-N	-	2.03±0.19
PHBHV-S-1	1	1.59±0.35
PHBHV-S-3	3	1.64±0.38
PHBHV-S-5	5	2.94±0.35
PHBHV-S-7	7	-
PHB-P-N	-	3.04±0.05
PHB-P-1	1	2.84±0.06
PHB-P-3	3	4.18±0.27
PHB-P-5	5	-
PHB-P-7	7	-
PHBHV-P-N	-	3.24±0.048
PHBHV-P-1	1	3.15±0.18
PHBHV-P-3	3	3.04±0.15
PHBHV-P-5	5	3.83±0.22
PHBHV-P-7	7	-

Table A.5. Evaluated Aspect Ratios and Errors of Permeability Models for PHB-S Nanocomposite Films

Models	Aspect Ratio	Error
Nielsen	7600	0.74
Cussler Regular	160	4.15E-05
Cussler Random	240	4.15E-05
Bharadwaj (-0.5)	92	0.0095
Bharadwaj (1)	13	0.0095
Bhardwaj (0)	2324	0.0095

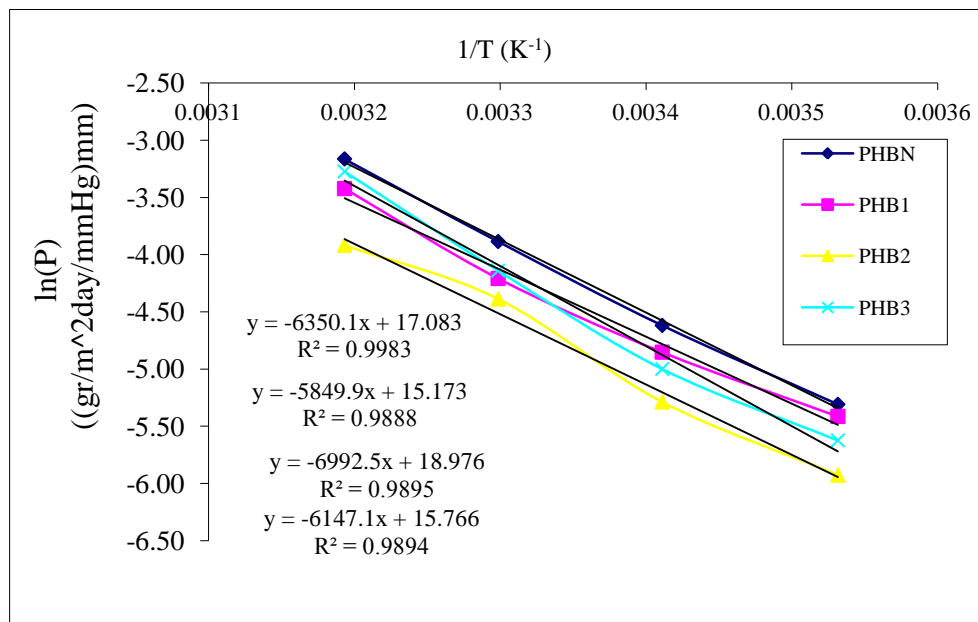


Figure A.6. Arrhenius plot of WVPs for PHB-S nanocomposite films

Table A.6. WVPs of PHB-S nanocomposites at different temperatures

Sample /Temperature °C/	WVP ((gr/m ² day/mm Hg)mm)			
	10	20	30	40
PHB-S-N	0.0049	0.0099	0.0205	0.0422
PHB-S-1	0.0045	0.0078	0.0149	0.0326
PHB-S-2	0.0027	0.0050	0.0124	0.0199
PHB-S-3	0.0036	0.0067	0.0159	0.0378
PHB-S-5	0.0669	0.1316	0.0201	0.0432

Table A.7. WVPs of PHBHV-S nanocomposites at different temperatures

Sample /Temperature °C/	WVP ((gr/m ² day/mm Hg)mm)			
	10	20	30	40
PHBHV-S-N	0.0033	0.0063	0.0177	0.0228
PHBHV-S-1	0.0030	0.0046	0.0076	0.0182
PHBHV-S-3	0.0036	0.0066	0.0119	0.0235
PHBHV-S-5	0.0046	0.0080	0.0156	0.0330

Table A.8. Mechanical Properties of PHB and PHBHV nanocomposites

Sample	Tensile Strength (MPa)	Elongation @ break (%)	Young's Modulus
PHB-S-N	11.6040±2.1937	0.4284±0.0887	24.7003±2.8359
PHB-S-1	29.7100±3.9643	0.8147 ±0.1096	37.2530±2.3963
PHB-S-2	36.5155±2.0776	0.7152±0.0358	27.8700±0.9107
PHB-S-3	29.2720±3.3881	0.7628±0.0743	39.4590±1.4544
PHB-S-5	23.3100±1.1521	0.6285±0.0480	35.4027±0.6747
PHB-S-7	19.9500±2.7925	0.5525±0.0844	33.0142±2.2669
PHBHV-S-N	6.9324±1.4570	0.6874±0.1927	11.7064±1.3119
PHBHV-S-1	12.8822±2.4274	0.6462±0.0977	22.6213±2.6312
PHBHV-S-3	12.0049±1.9281	0.8083±0.1561	18.2316±1.3594
PHBHV-S-5	9.2246±1.3799	0.7300±0.0802	14.0080±0.9717
PHB-P-N	7.7420±0.2100	0.5289±2.7118	16.5517±0.5220
PHB-P-1	9.6946±0.0793	0.6988±0.5090	15.9012±0.3702
PHB-P-3	10.0689±0.1757	0.7851±1.9201	15.4061±0.2531
PHB-P-5	9.4582±0.0707	0.6919±0.7178	15.2353±0.4283
PHB-P-7	7.5956±0.1323	0.5418±1.8776	15.1160±0.7808
PHBHV-P-N	16.9968±0.5225	2.3936±2.2544	12.6566±0.3793
PHBHV-P-1	16.0153±0.5974	2.0903±2.4942	13.6554±0.4199
PHBHV-P-3	11.9974±0.2782	1.1564±1.5831	13.4316±0.6797
PHBHV-P-5	11.4998±0.3989	1.0288±4.0344	13.6662±0.6874
PHBHV-P-7	9.6391±0.0247	0.8491±0.4709	14.5982±0.5926

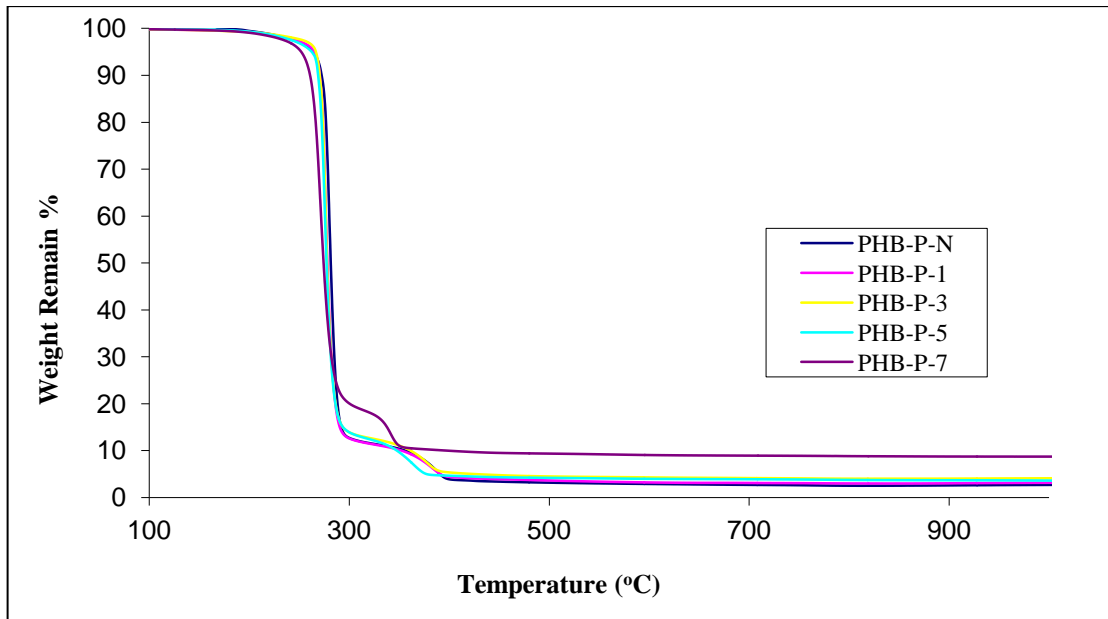


Figure A.7. TGA curves of PHB-P nanocomposites

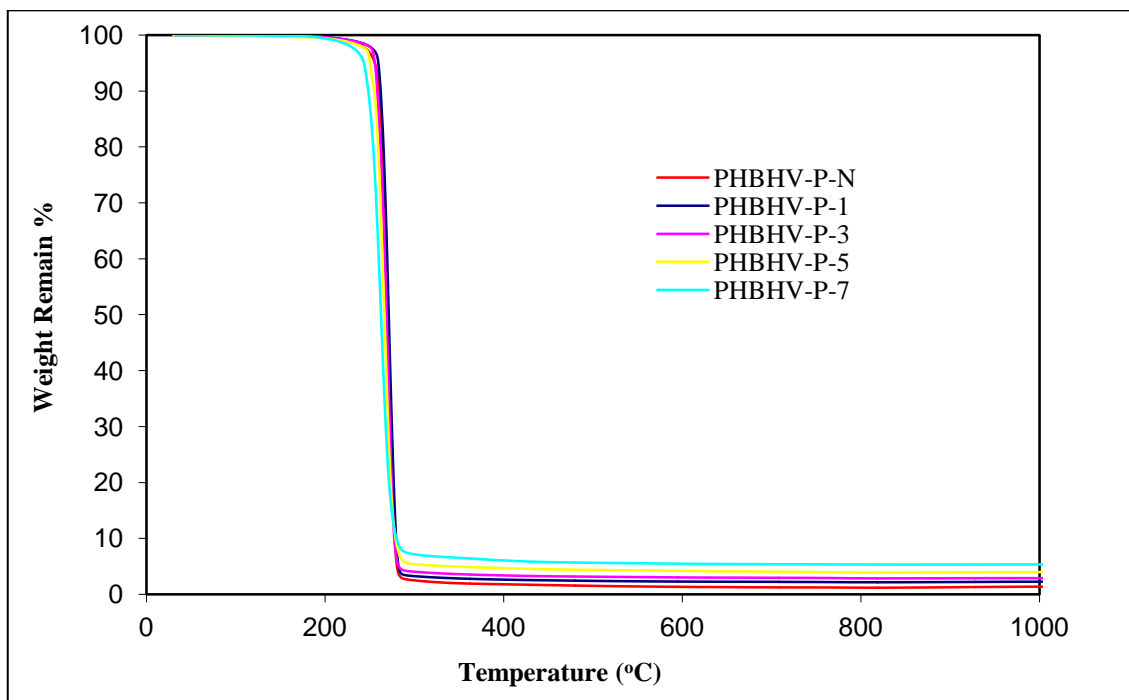


Figure A.8. TGA curves of PHBHV-P nanocomposites

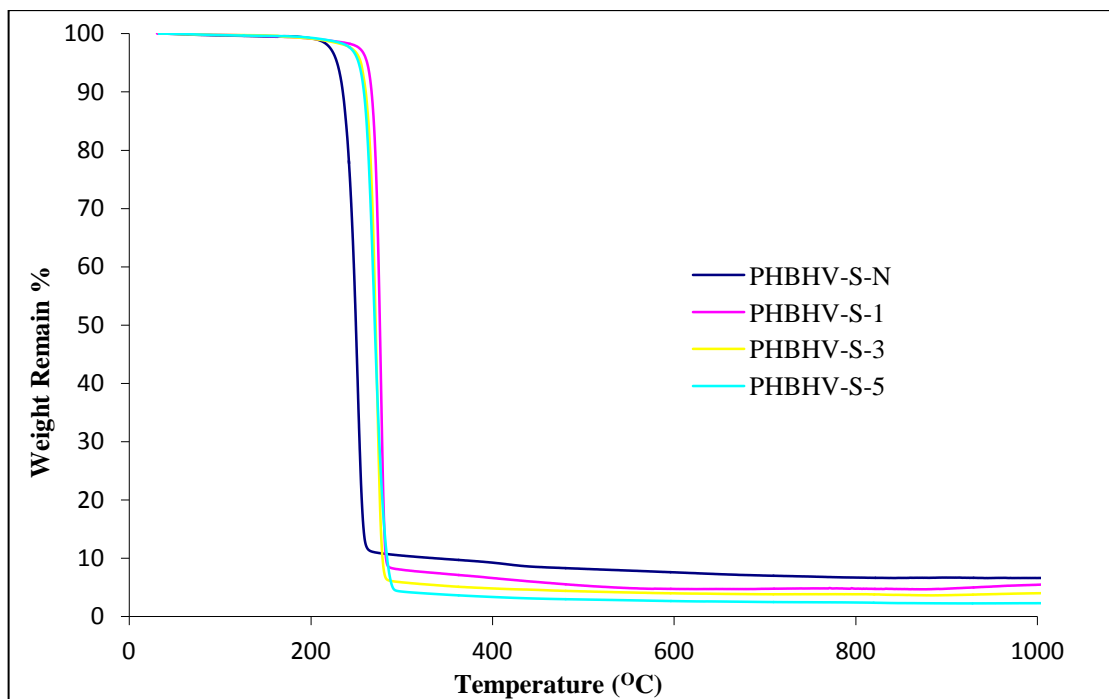


Figure A.9. TGA curves of PHB-P nanocomposites

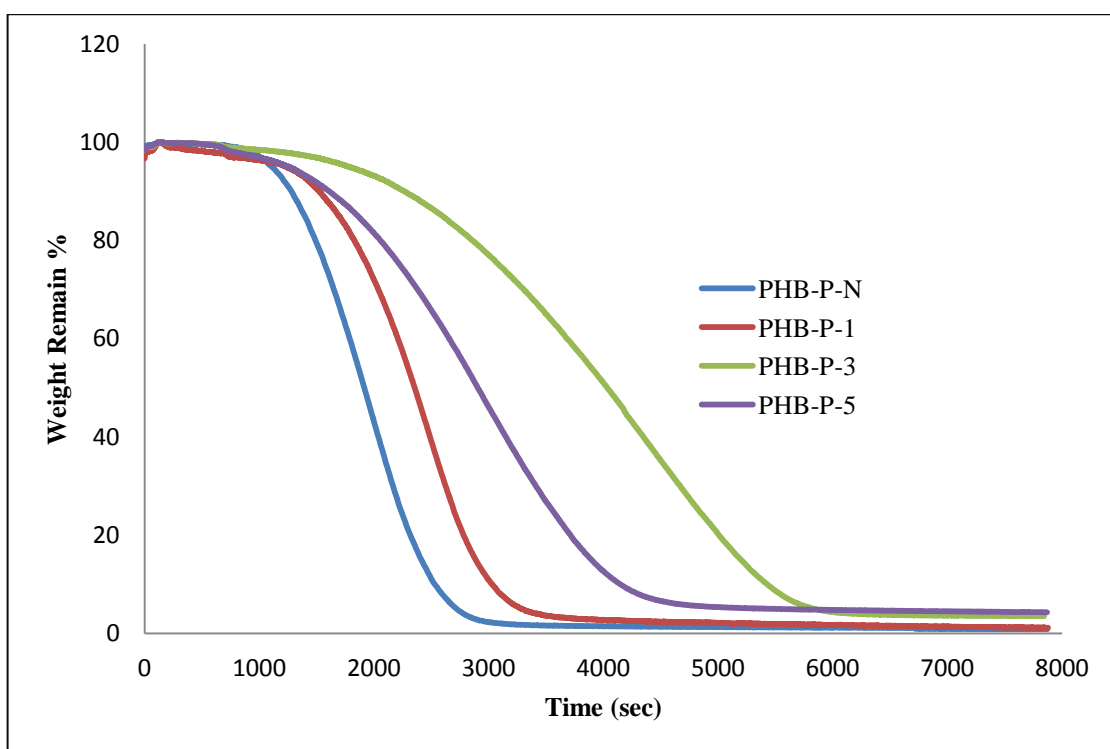


Figure A.10. Isothermal TGA curves of PHB-P nanocomposites at 230 °C

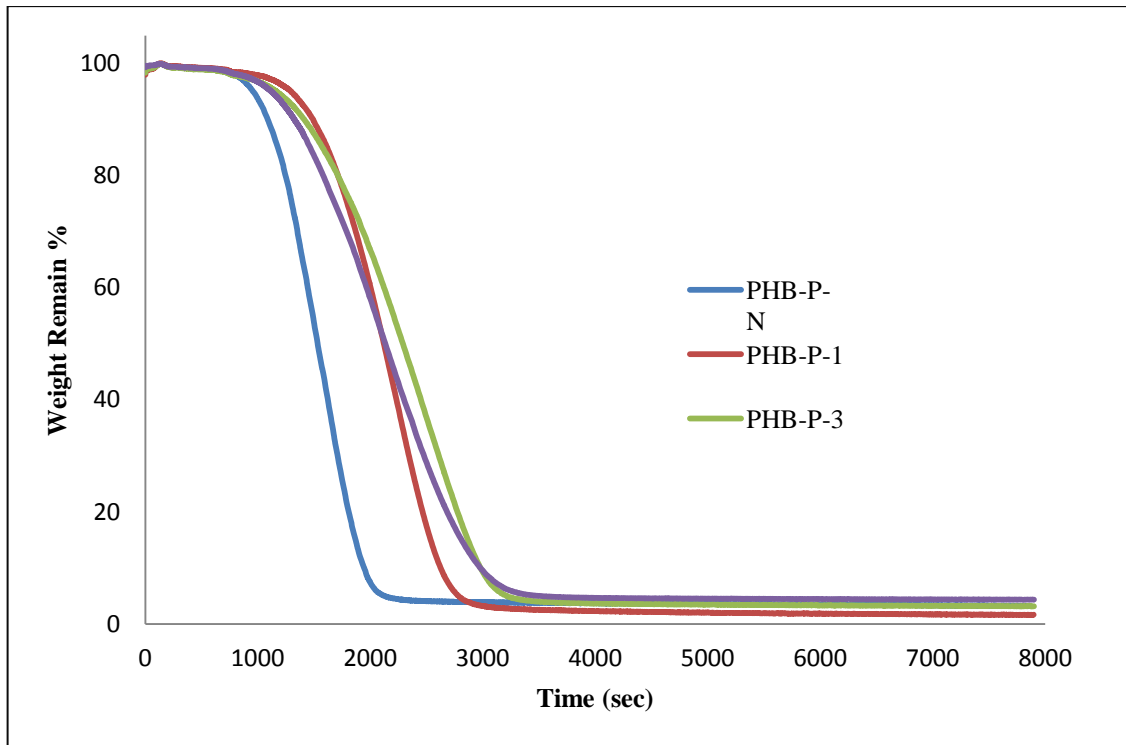


Figure A.11. Isothermal TGA curves of PHB-P nanocomposites at 240 °C

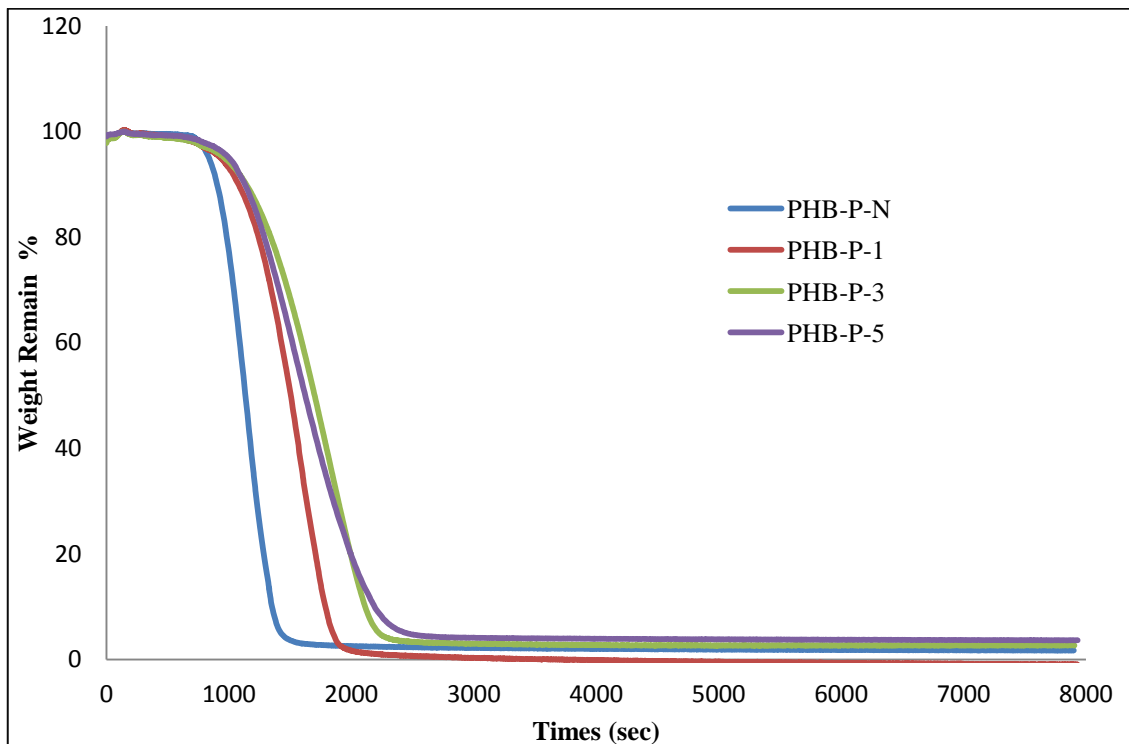


Figure A.12. Isothermal TGA curves of PHB-P nanocomposites at 250 °C

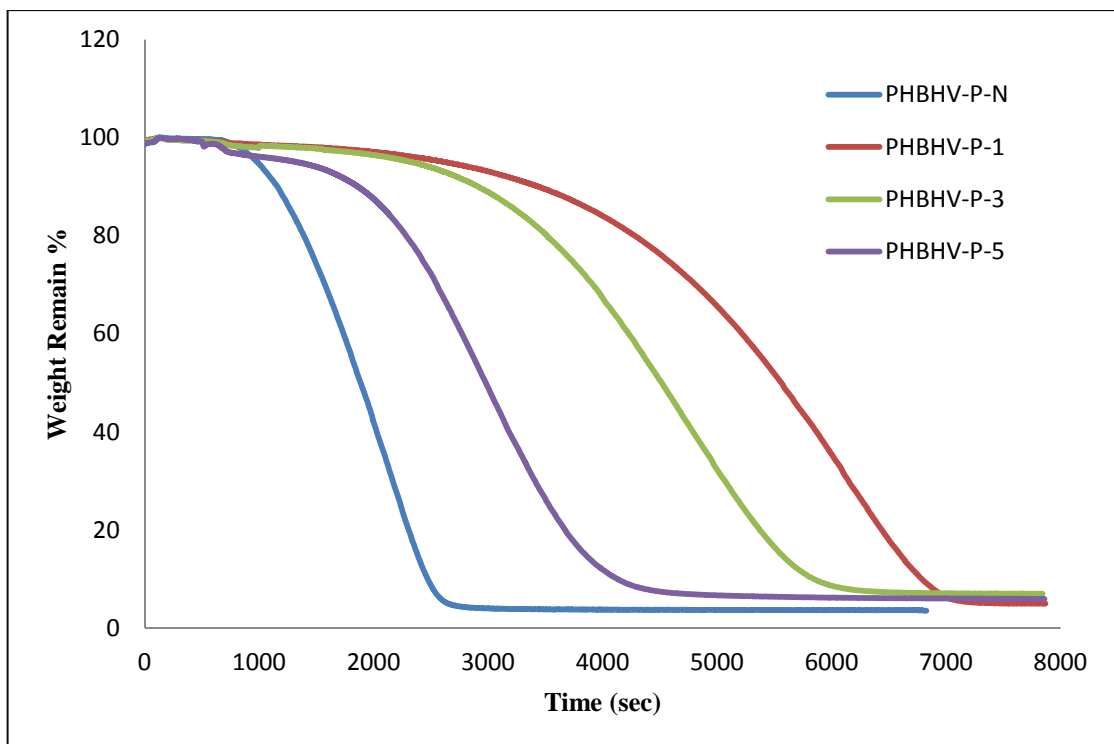


Figure A.13. Isothermal TGA curves of PHBHV-P nanocomposites at 230 °C

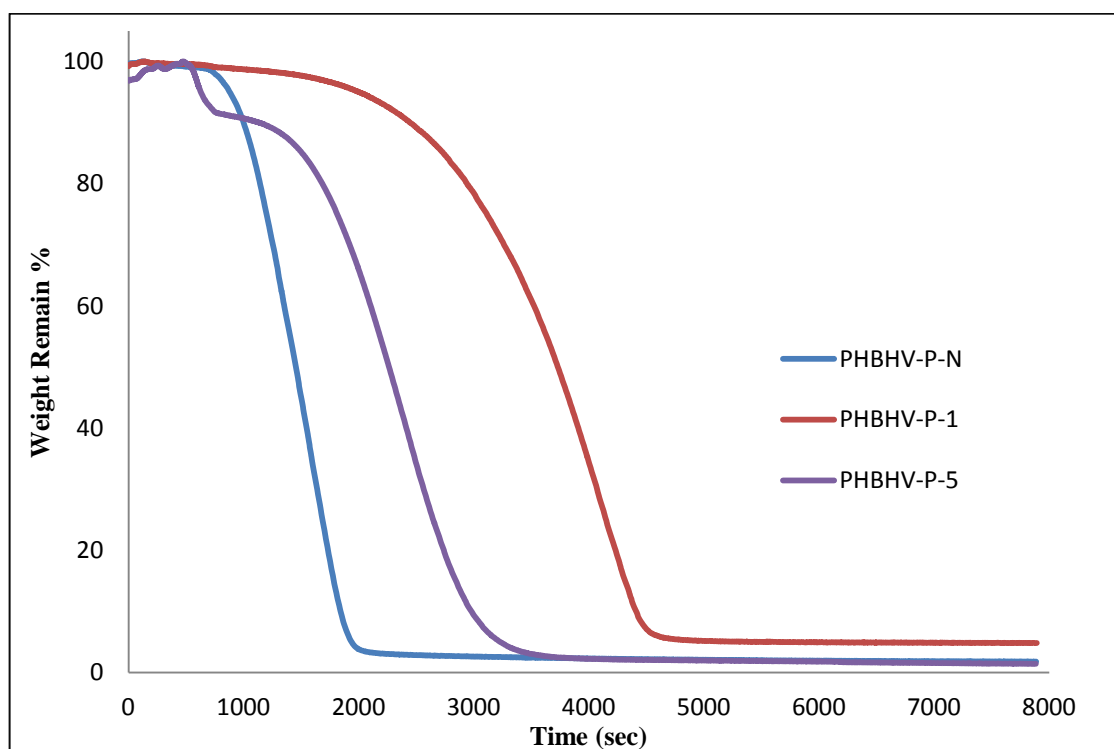


Figure A.14. Isothermal TGA curves of PHBHV-P nanocomposites at 240 °C

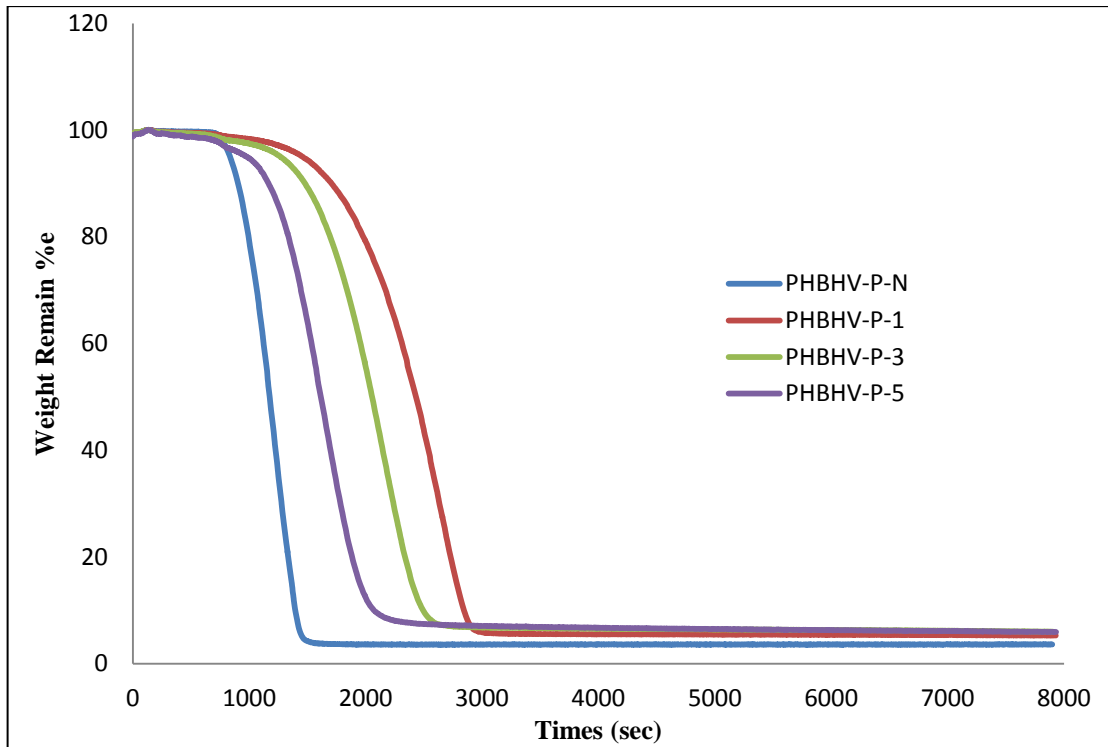


Figure A.15. Isothermal TGA curves of PHBHV-P nanocomposites at 250 °C

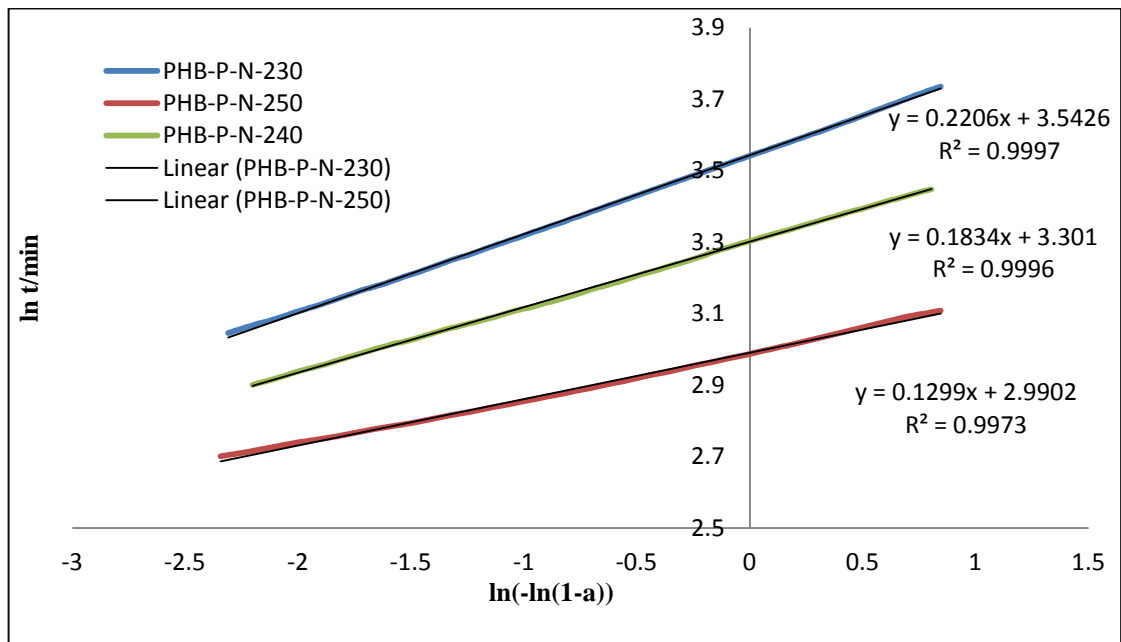


Figure A.16. $\ln t$ vs $\ln [-\ln(1 - \alpha)]$ plots for the isothermal degradation of PHB-P-N nanocomposite

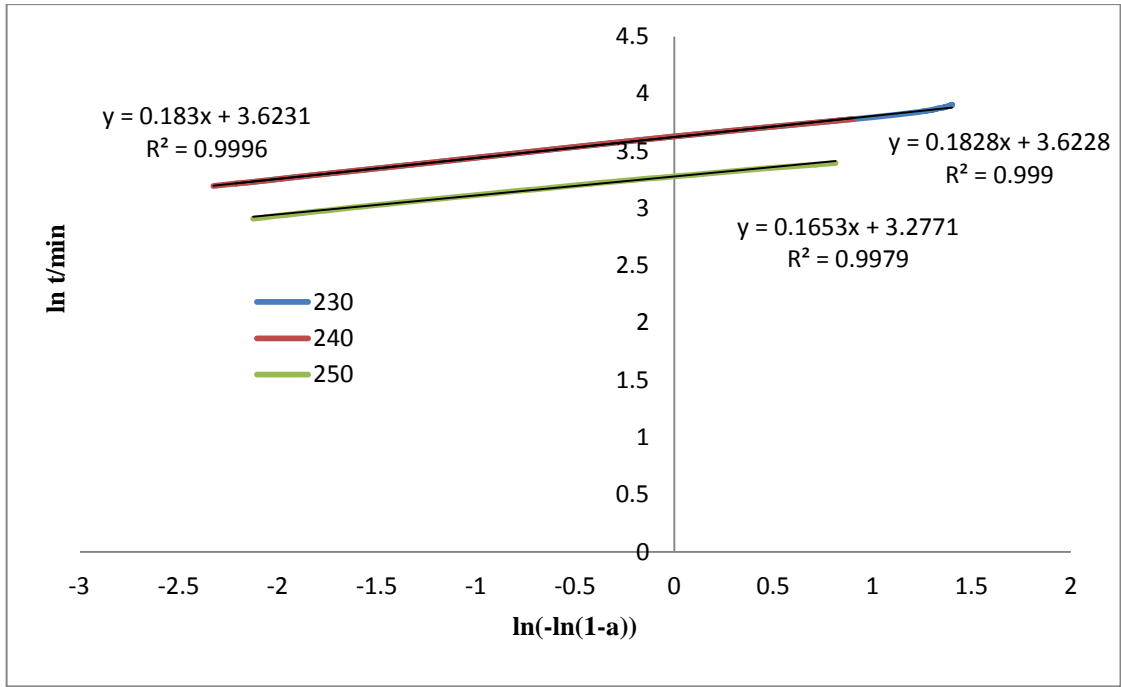


Figure A.17. $\ln t$ vs $\ln[-\ln(1-\alpha)]$ plots for the isothermal degradation of PHB-P-1 nanocomposite

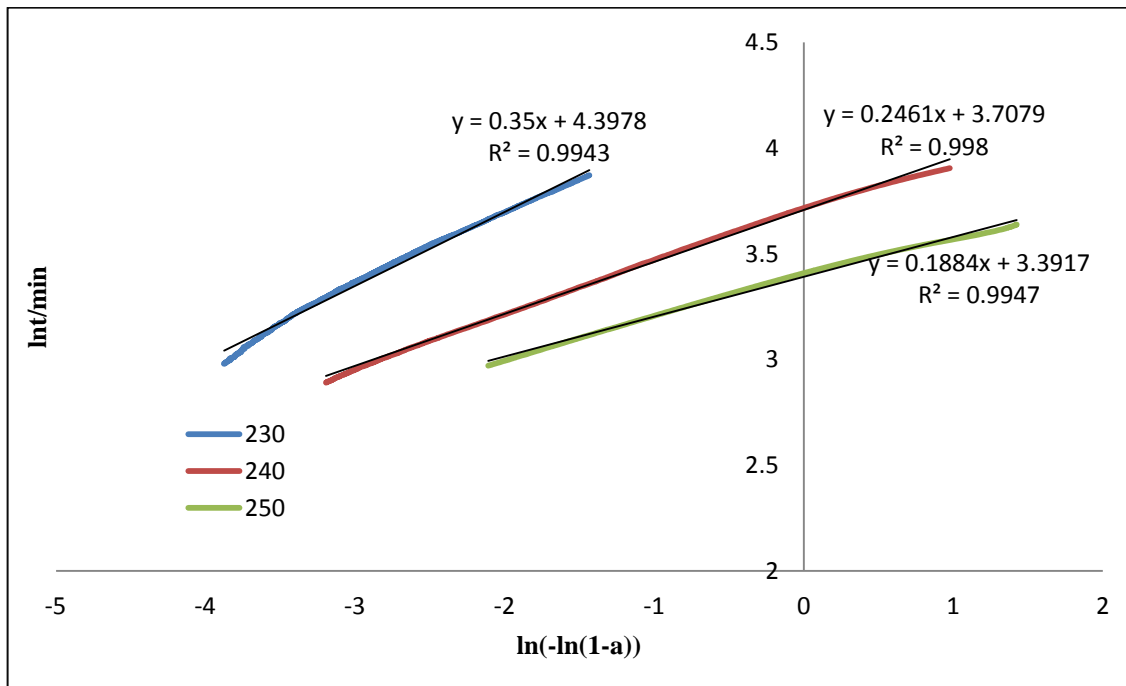


Figure A.18. $\ln t$ vs $\ln[-\ln(1-\alpha)]$ plots for the isothermal degradation of PHB-P-3 nanocomposite

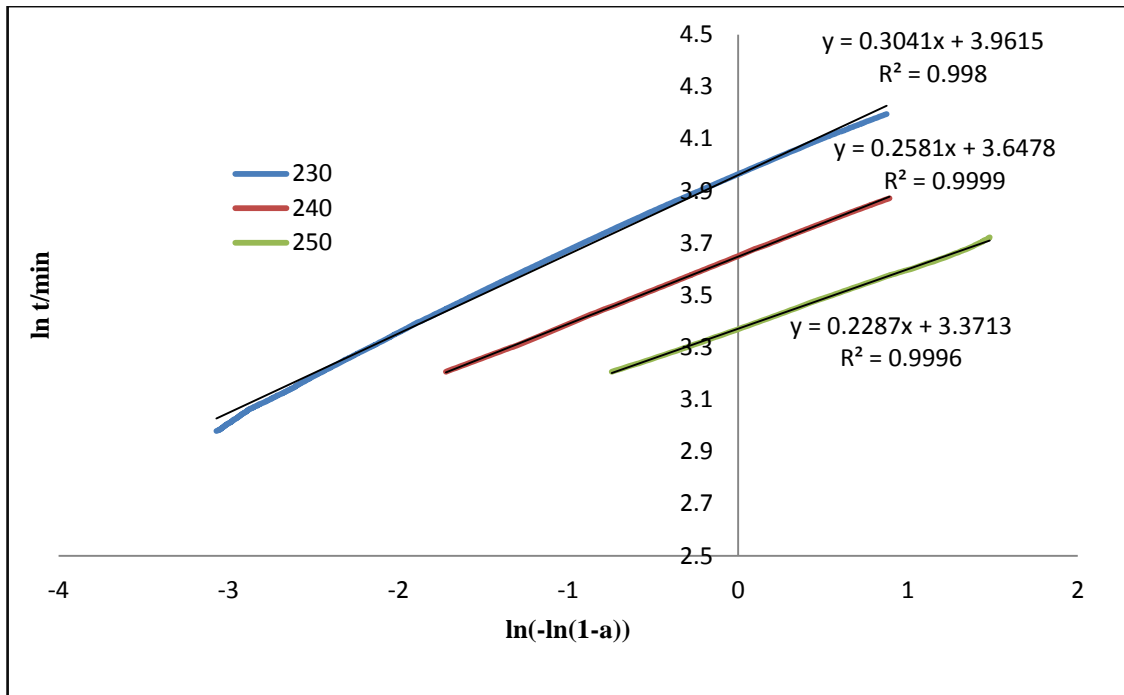


Figure A.19. $\ln t$ vs $\ln [-\ln(1 - \alpha)]$ plots for the isothermal degradation of PHB-P-5 nanocomposite

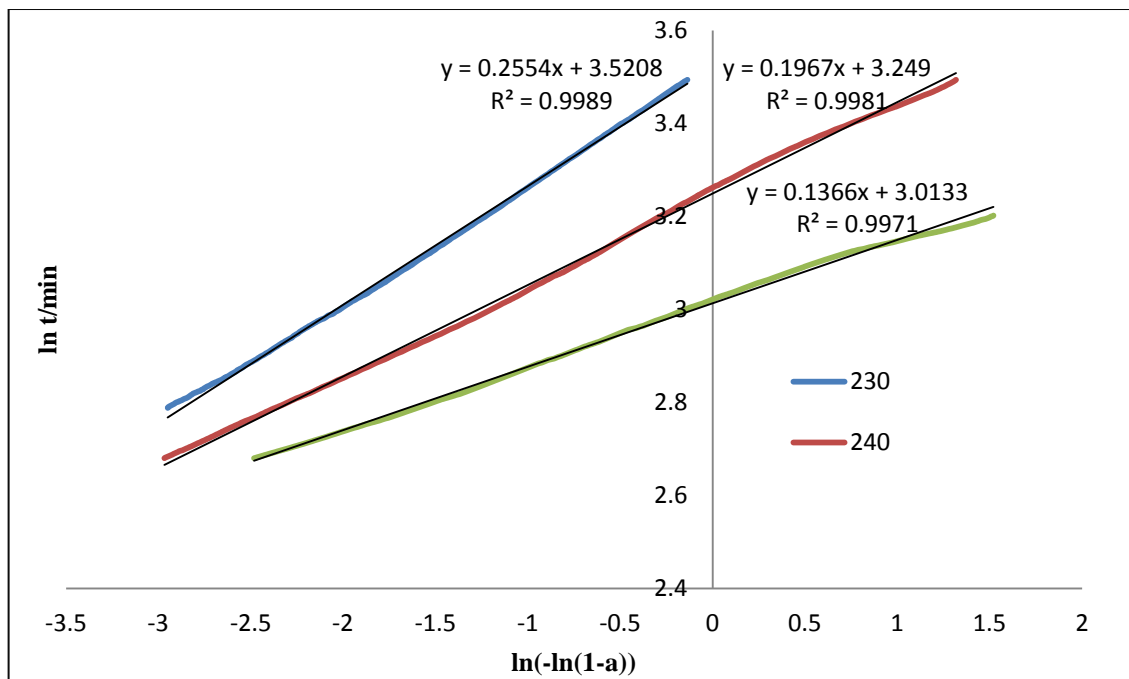


Figure A.20. $\ln t$ vs $\ln [-\ln(1 - \alpha)]$ plots for the isothermal degradation of PHBHV-P-N nanocomposite

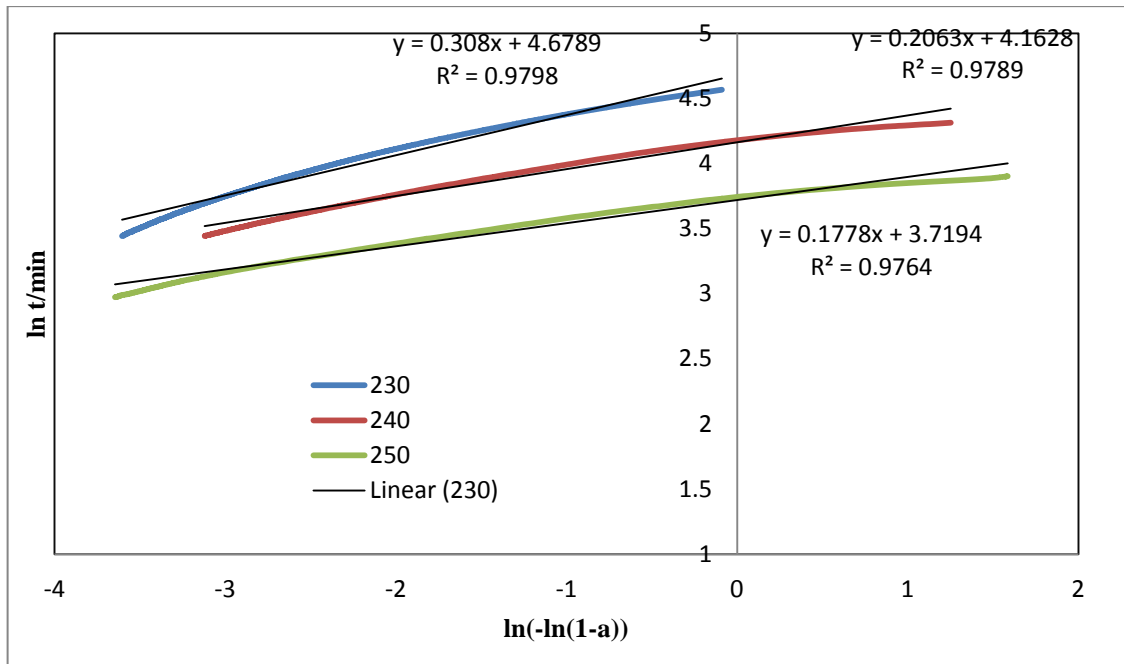


Figure A.21. $\ln t$ vs $\ln [-\ln(1 - \alpha)]$ plots for the isothermal degradation of PHBHV-P-1 nanocomposite

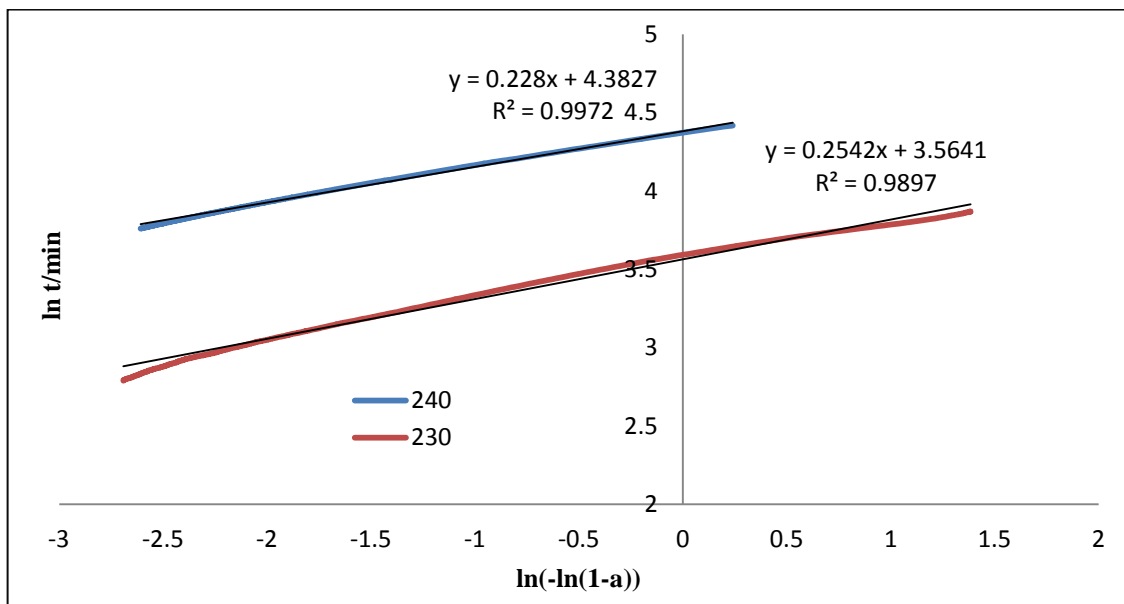


Figure A.22. $\ln t$ vs $\ln [-\ln(1 - \alpha)]$ plots for the isothermal degradation of PHBHV-P-3 nanocomposite

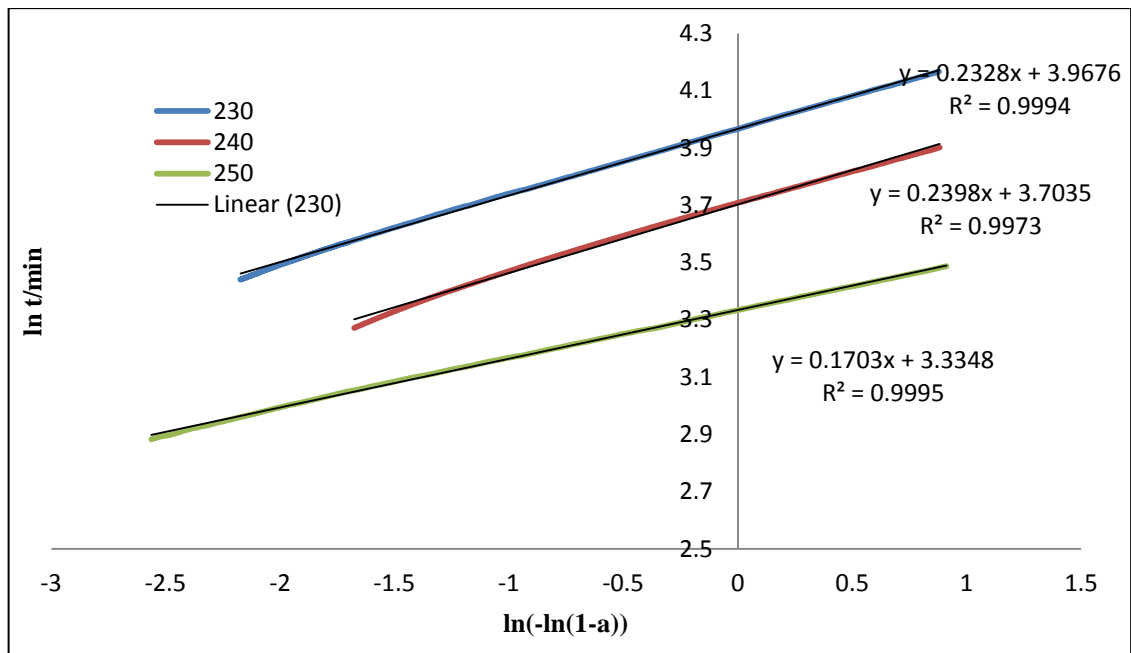


Figure A.23. $\ln t$ vs $\ln [-\ln(1 - \alpha)]$ plots for the isothermal degradation of PHBHV-P-5 nanocomposite

APPENDIX B

THERMAL ANALYSES OF PHB AND PHBV NANOCOMPOSITE FILMS

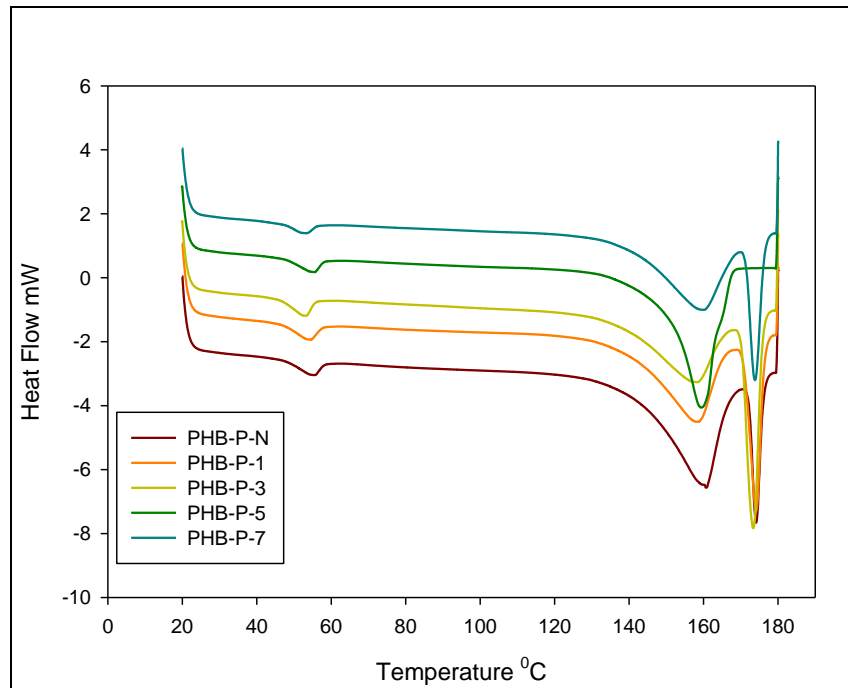


Figure B.1. First heating run of DSC analysis of PHB-P nanocomposites

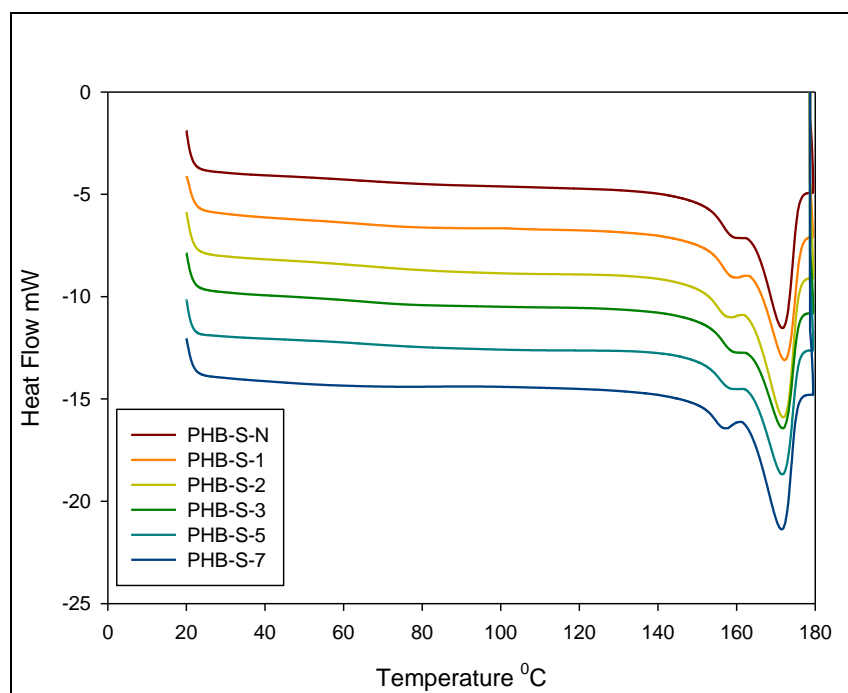


Figure B.2. First heating run of DSC analysis of PHB-S nanocomposites

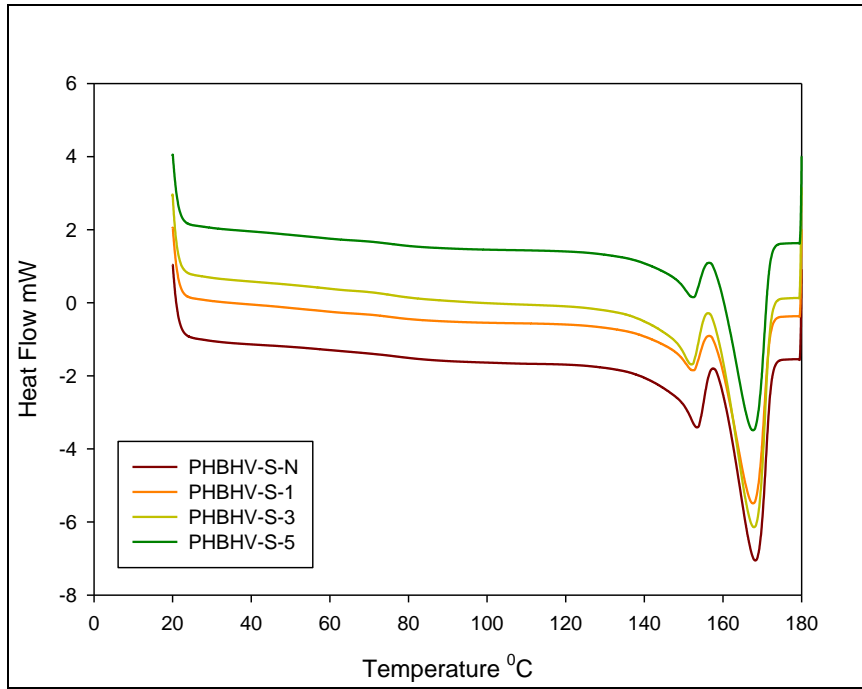


Figure B.3. First heating run of DSC analysis of PHBHV-S nanocomposites

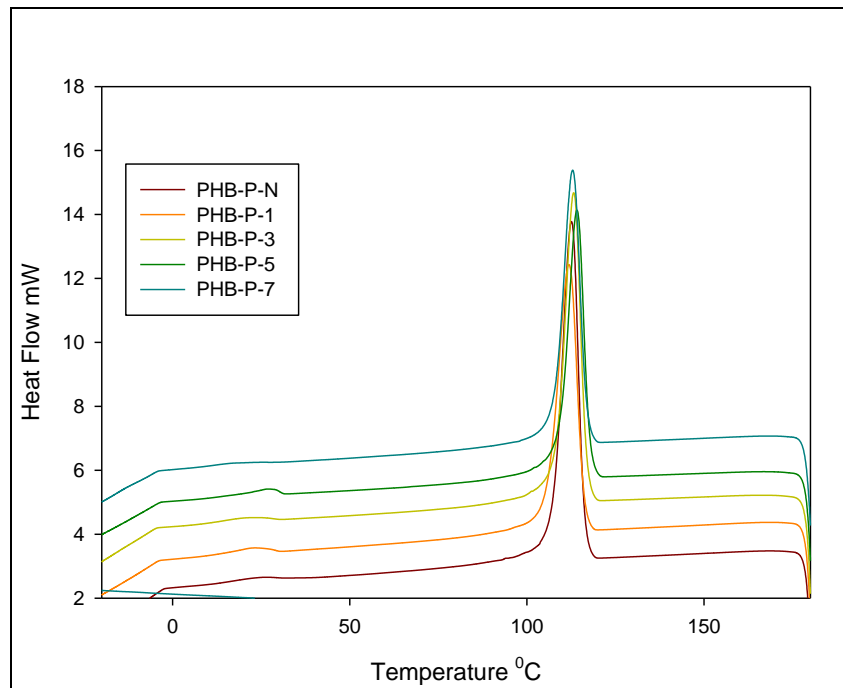


Figure B.4. First cooling run of DSC analysis of PHB-P nanocomposites

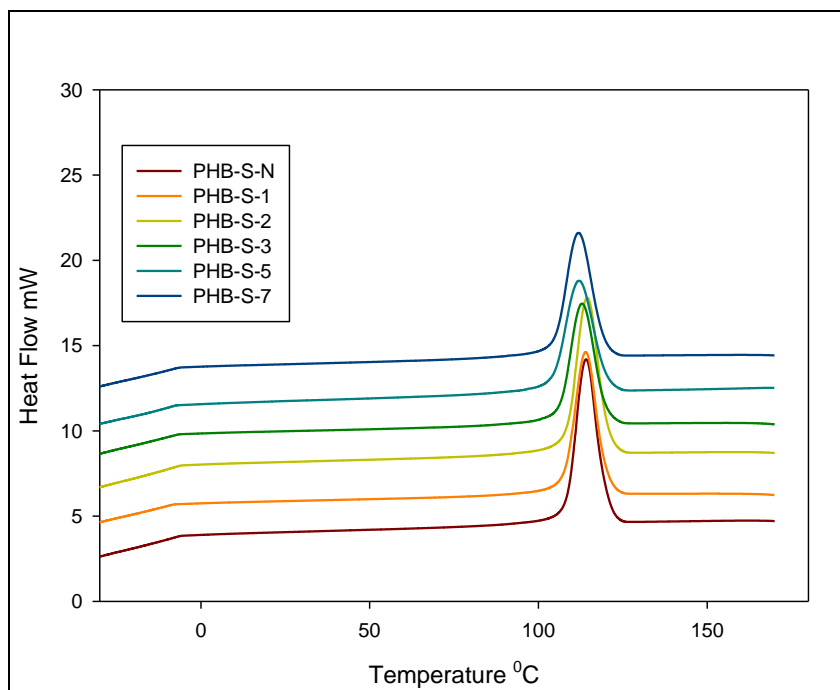


Figure B5 First cooling run of DSC analysis of PHB-S nanocomposites

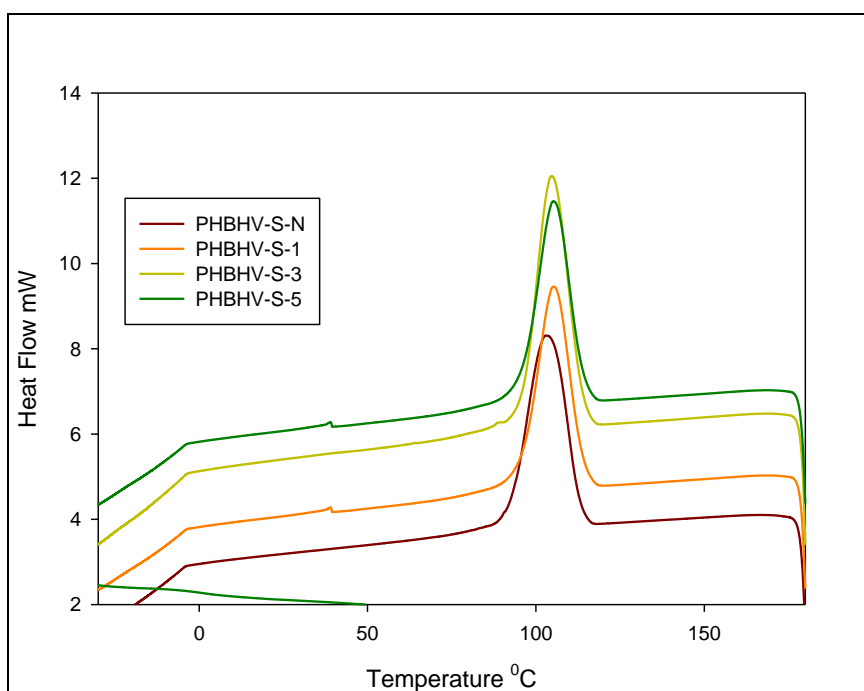


Figure B.6. First cooling run of DSC analysis of PHBHV-S nanocomposites

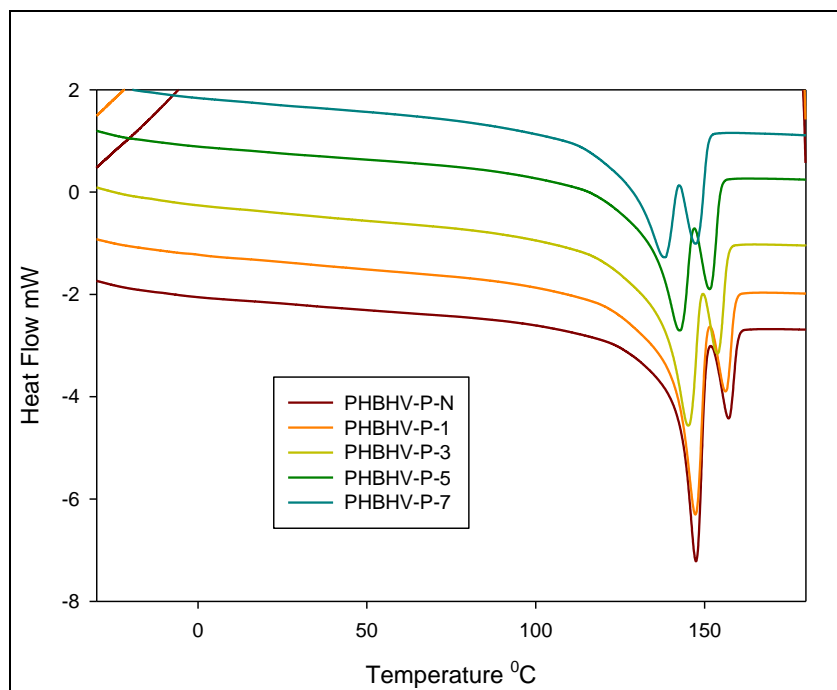


Figure B.7. Second heating run of DSC analysis of PHBHV-P nanocomposites

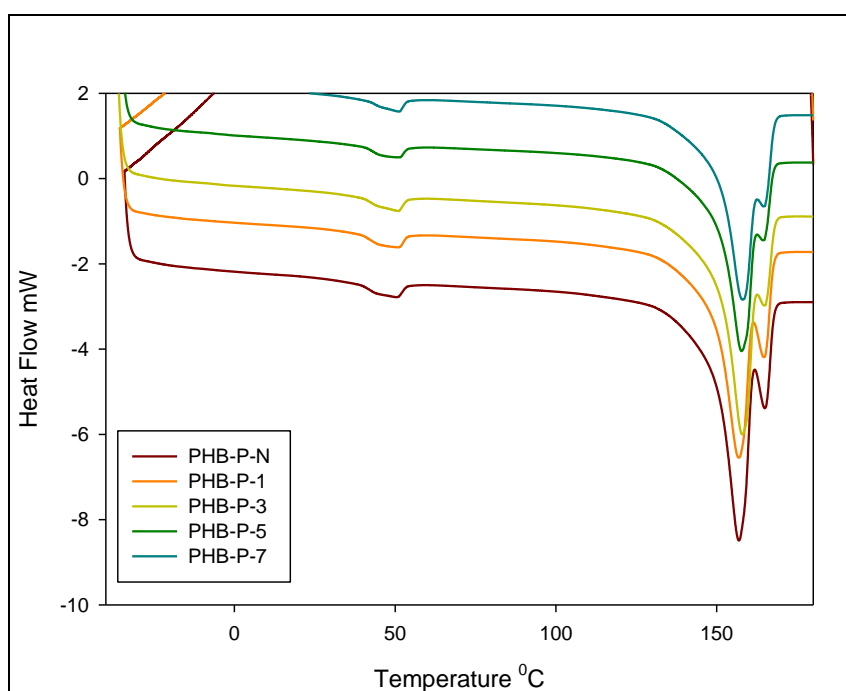


Figure B.8. Second heating run of DSC analysis of PHB-P nanocomposites

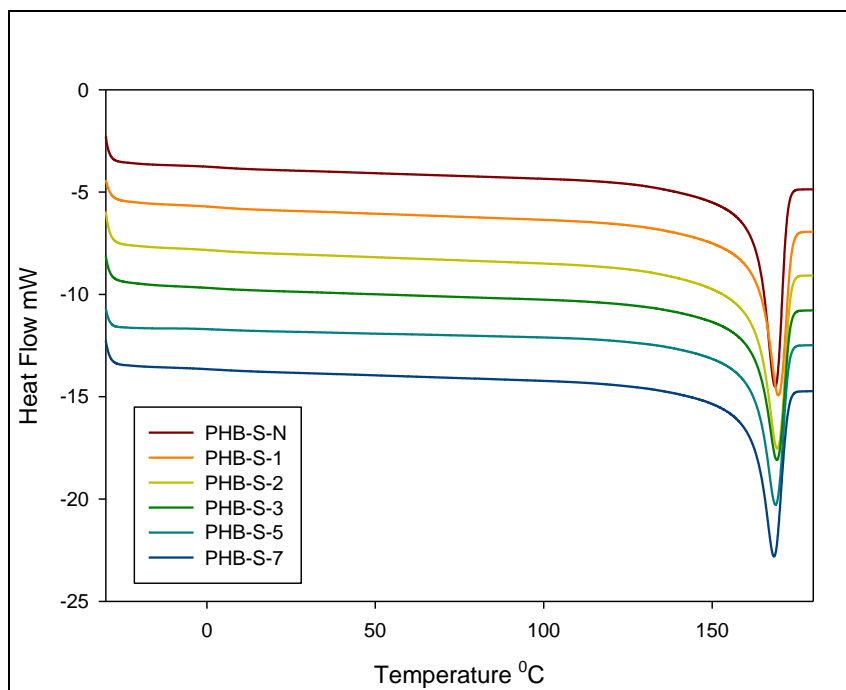


Figure B.9. Second heating run of DSC analysis of PHB-S nanocomposites

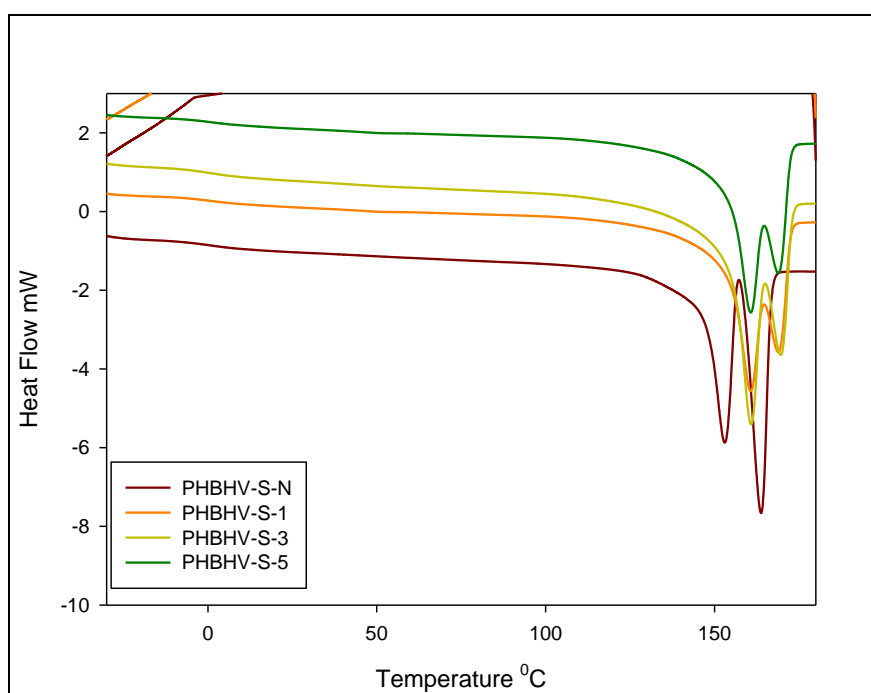


Figure B.10. Second heating run of DSC analysis of PHBHV-S nanocomposites

APPENDIX C

CRYSTALLIZATION KINETIC OF PHB NANOCOMPOSITE FILMS

Table C.1. DSC measurement of PHB-P nanocomposite at different cooling rates

	$\phi(^{\circ}\text{C}/\text{min.})$			Non -Isothermal Crystallization				
	5	10	20	1 st Melting		2 nd Melting		T_c
				T_m	Relative Crystallinity % DSC	T_m	Relative Crystallinity % DSC	
PHB-P-N	X			159.61	49.81	156.61	28.70	117.91
		X		159.94	54.79	155.56	30.27	112.56
			X	158.89	49.46	154.63	46.27	105.4
PHB-P-1	X			159.97	26.71	157.34	17.81	117.85
		X		156.22	43.84	157.11	27.40	112.61
			X	154.39	47.26	155.86	47.26	105.39
PHB-P-3	X			160.42	39.04	157.79	30.14	118.63
		X		157.2	34.93	157.16	27.40	113.42
			X	153.81	36.30	148.47	26.71	96.22

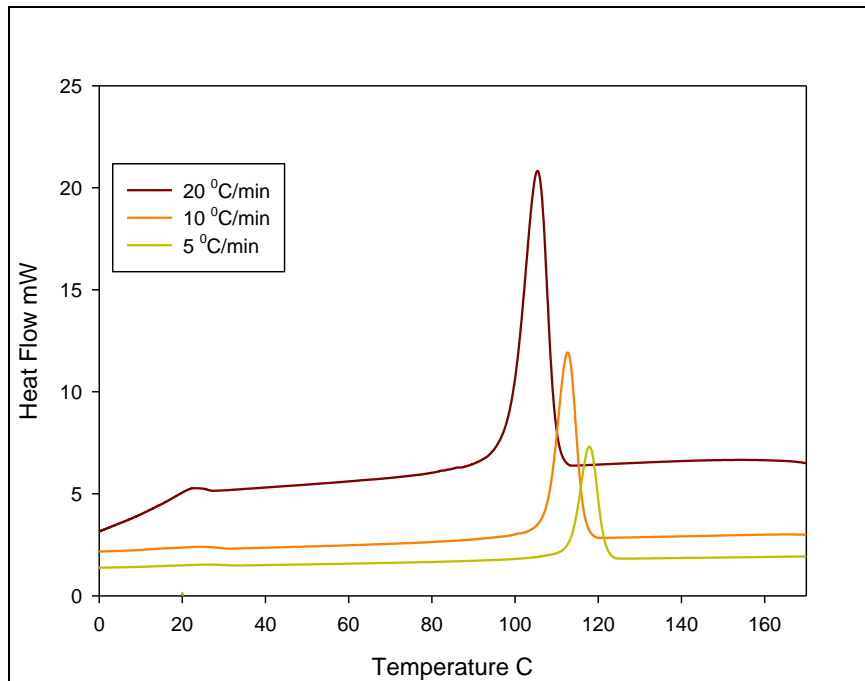


Figure C.1. Cold crystallization (T_c) peaks of PHB-P-N at different cooling rates

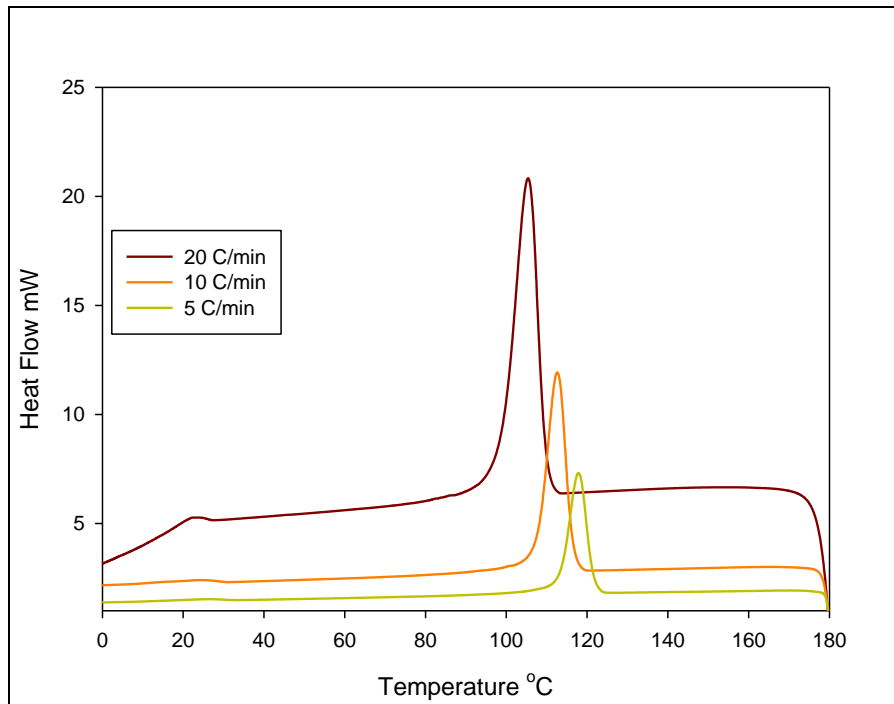


Figure C.2. Cold crystallization (T_c) peaks of PHB-P-1 at different cooling rates

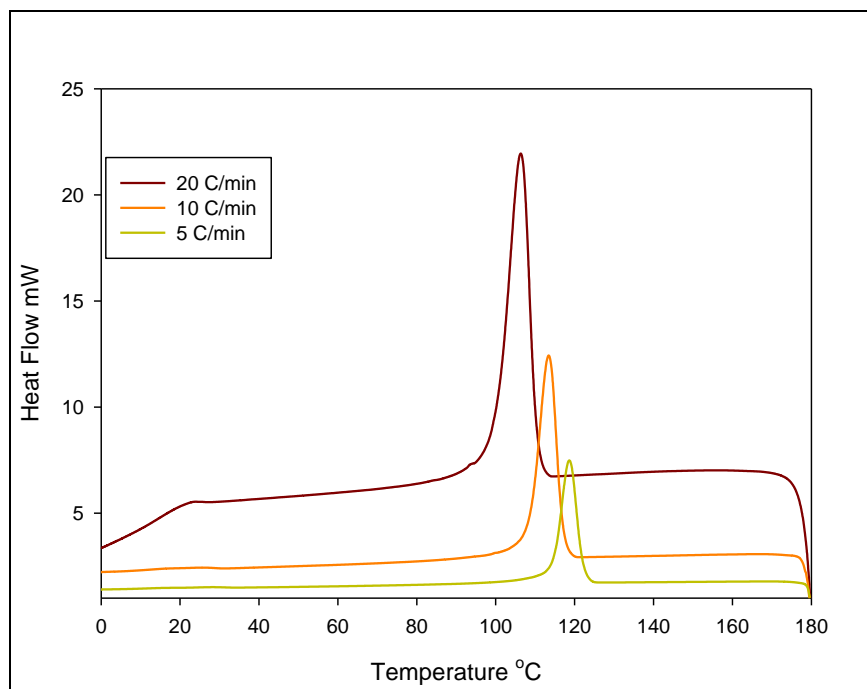


Figure C.3. Cold crystallization (T_c) peaks of PHB-P-3 at different cooling rates

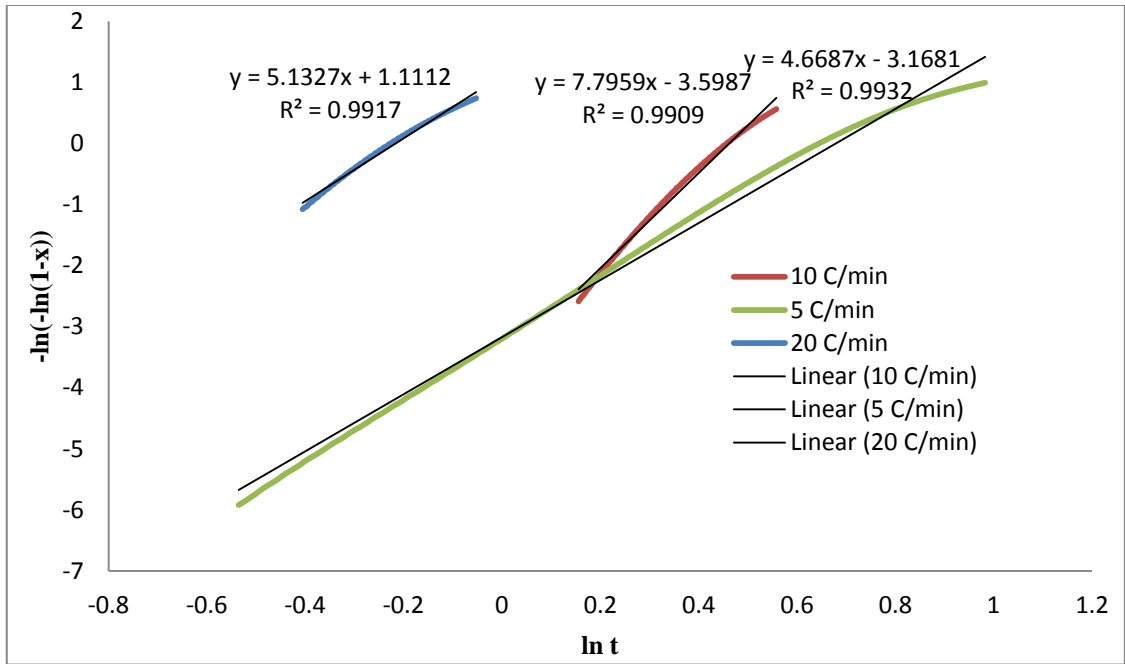


Figure C.4. Avrami plots of PHB-P-N at different cooling rates

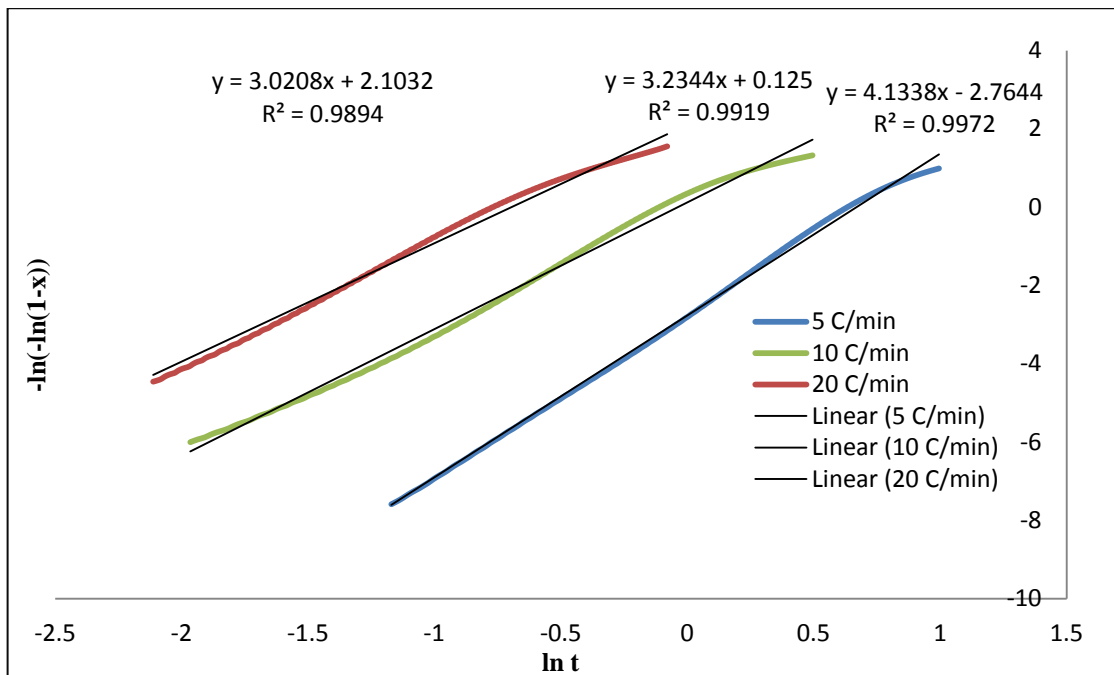


Figure C.5. Avrami plots of PHB-P-1 at different cooling rates

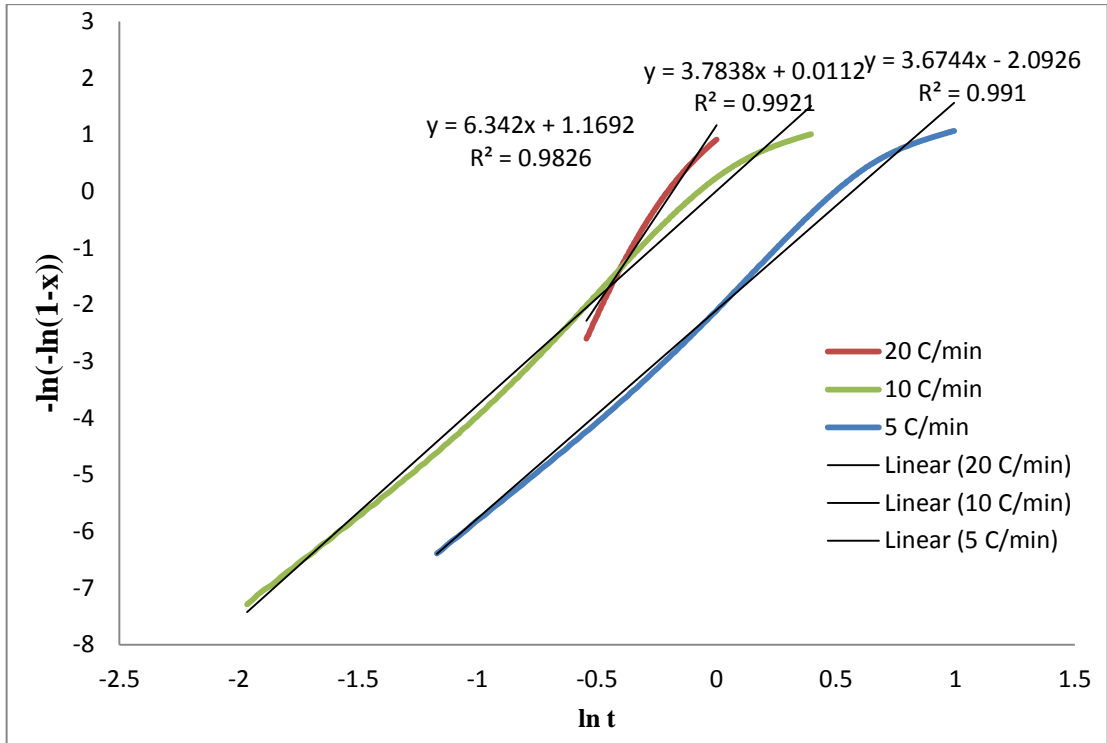


Figure C.6. Avrami plots of PHB-P-3 at different cooling rates

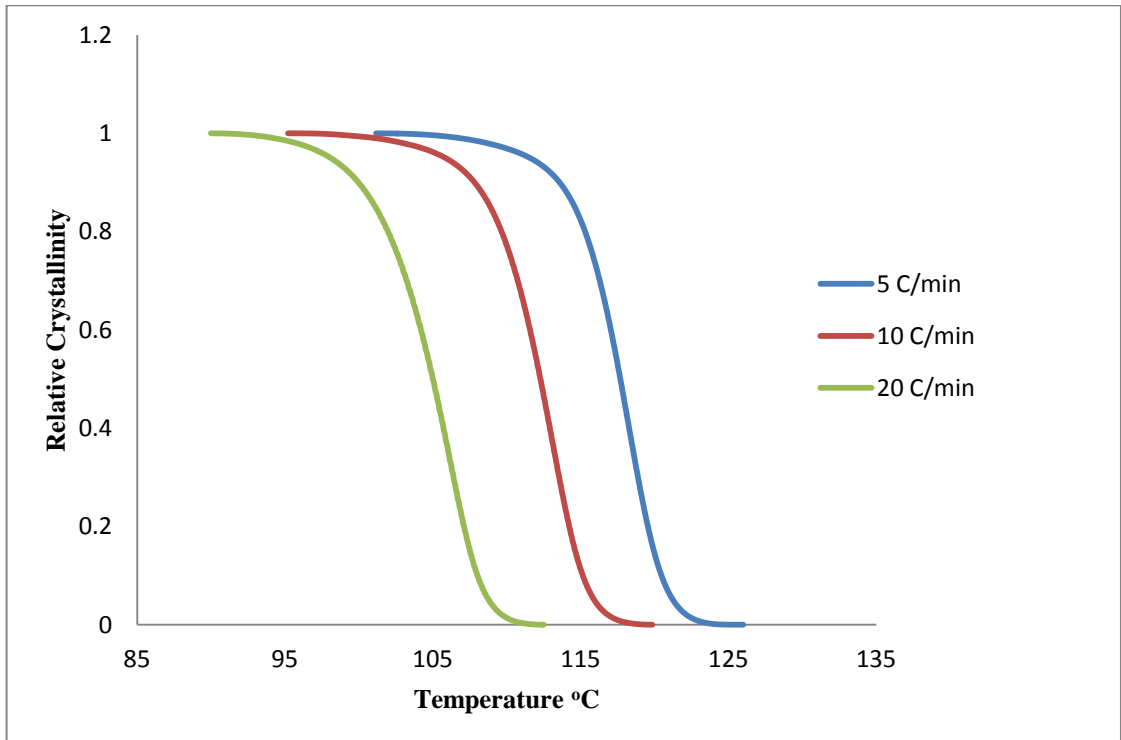


Figure C.7. Relative Crystallinity curves of PHB-P-N at different cooling rates

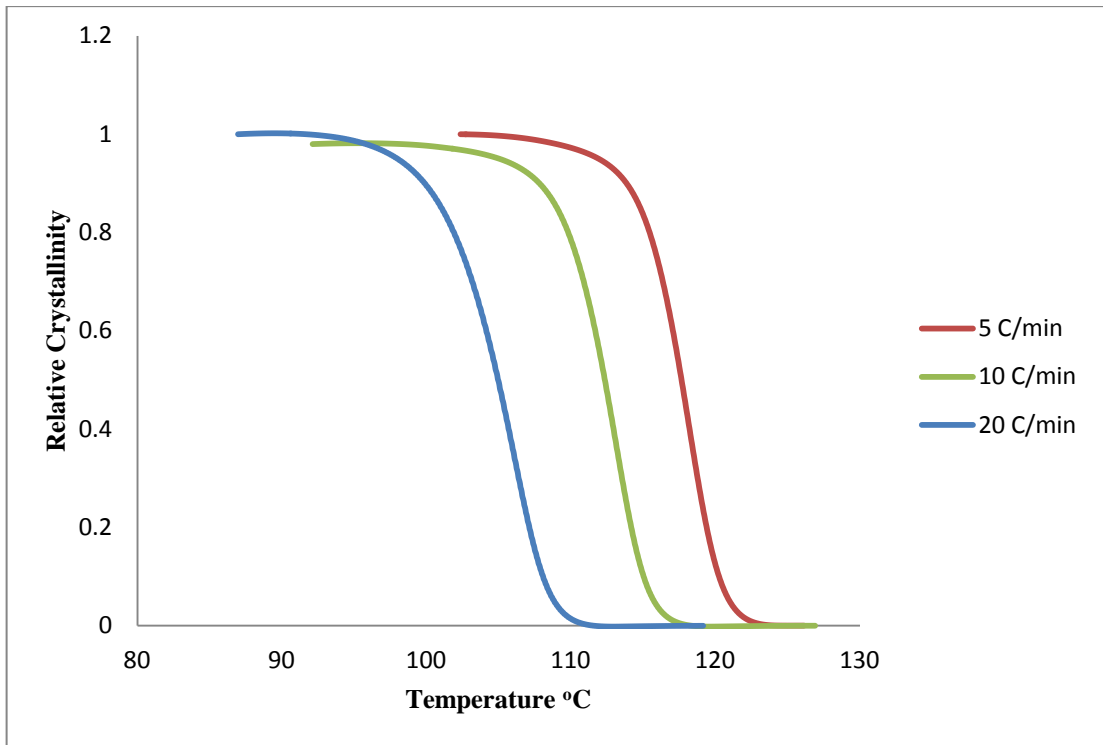


Figure C.8. Relative Crystallinity curves of PHB-P-3 at different cooling rate

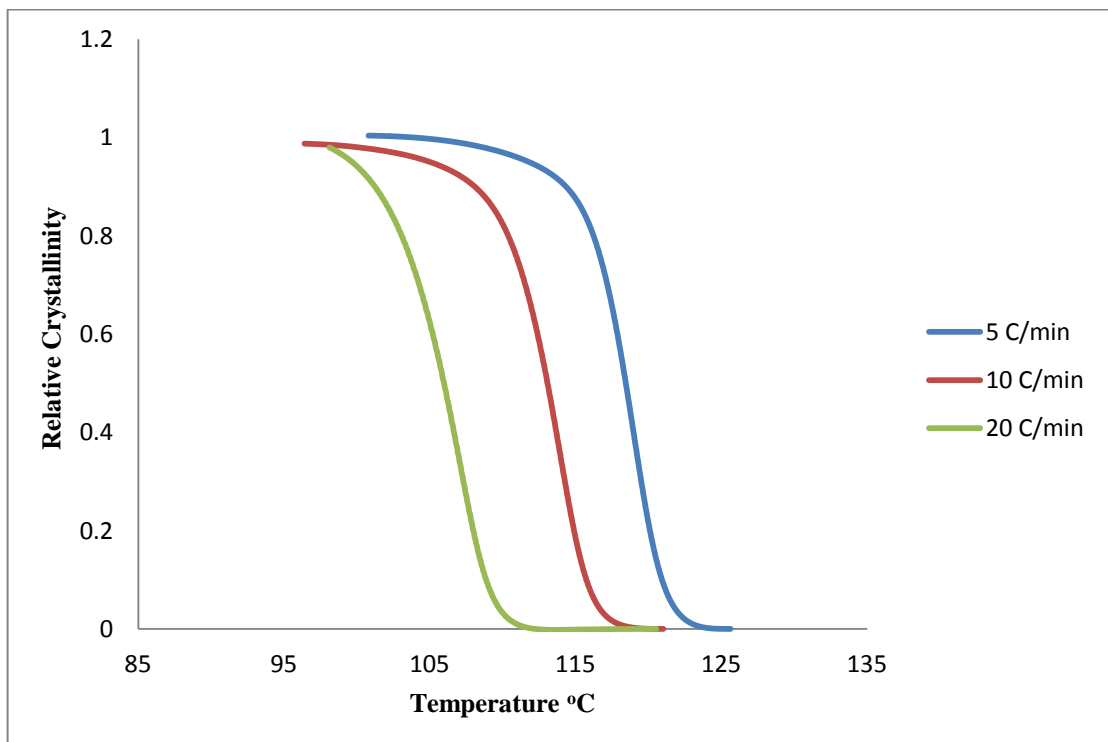


Figure C.9. Relative Crystallinity curves of PHB-P-3 at different cooling rates

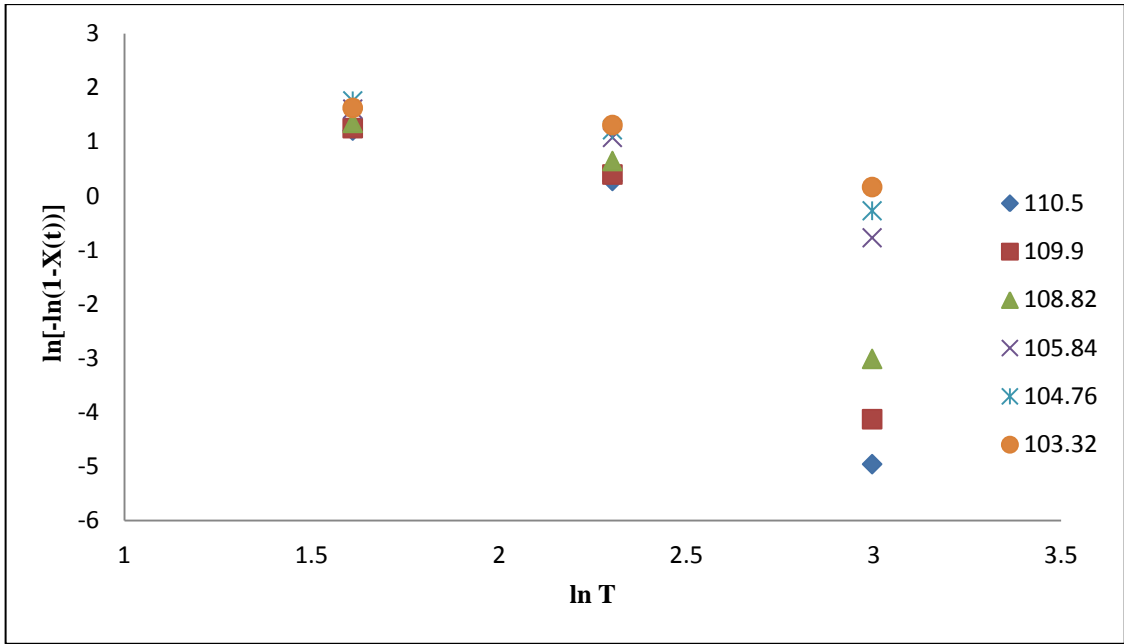


Figure C.10. Ozawa curves of PHB-P-N at different temperatures

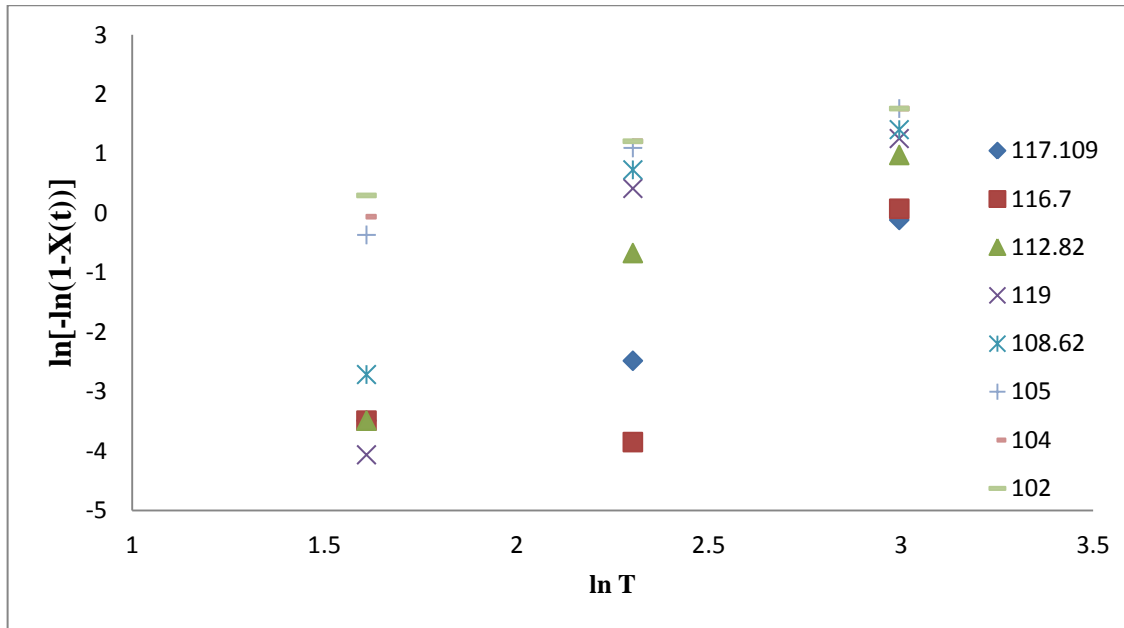


Figure C.11. Ozawa curves of PHB-P-1 at different temperatures

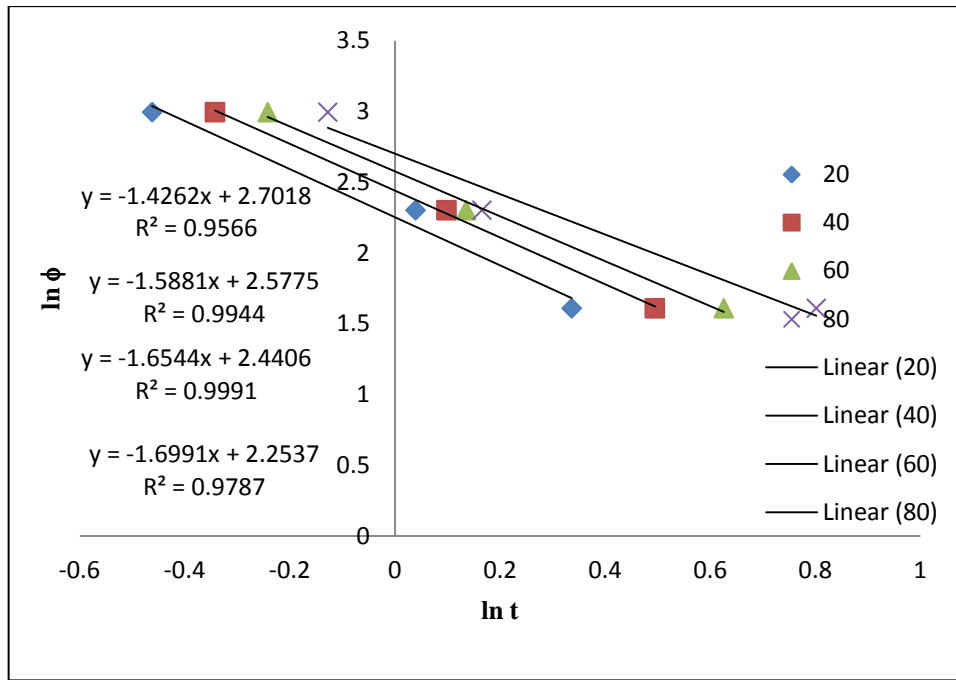


Figure C.12. Lui Mo plot of PHB-P-N at different relative crystallinities

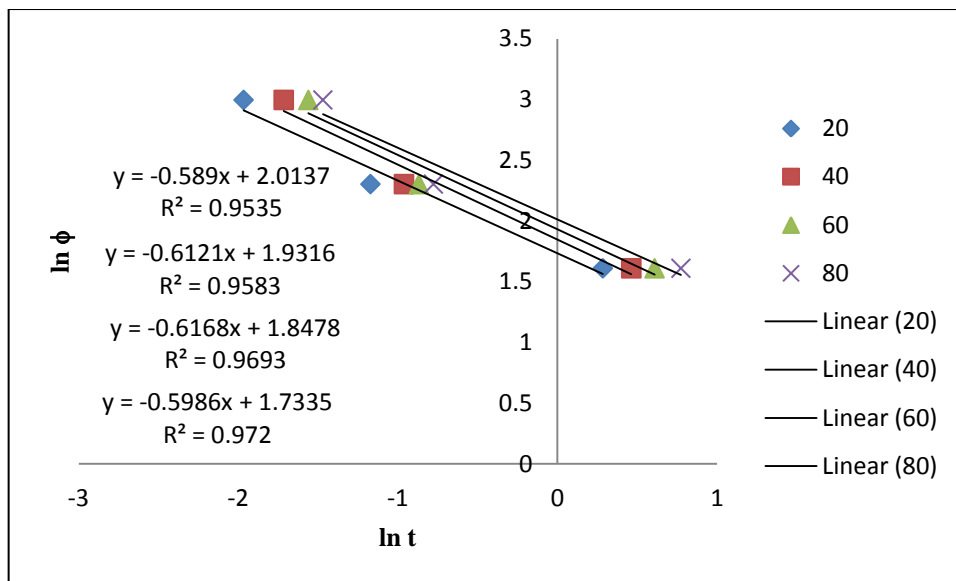


Figure C.13. Lui Mo plot of PHB-P-1 at different relative crystallinities

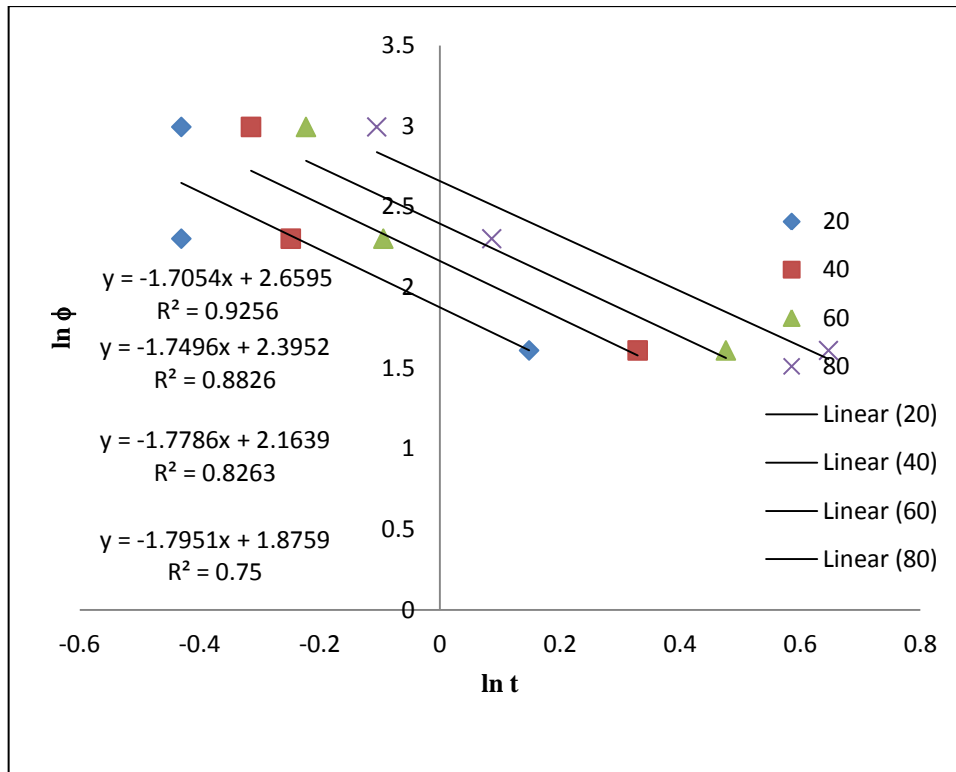


Figure C.14. Lui Mo plot of PHB-P-3 at different relative crystallinities

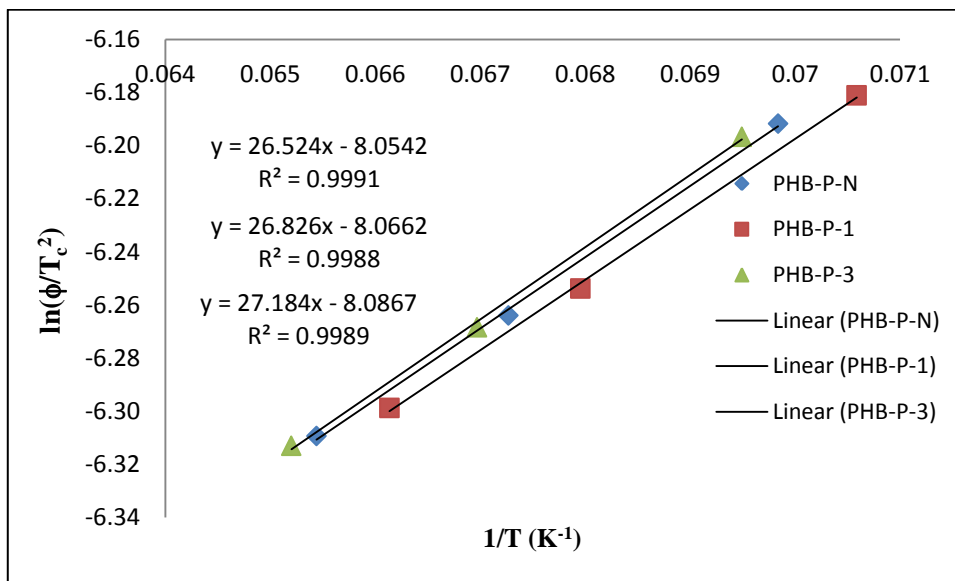


Figure C.15. Kissinger plot of PHB-P nanocomposites at different cooling rates